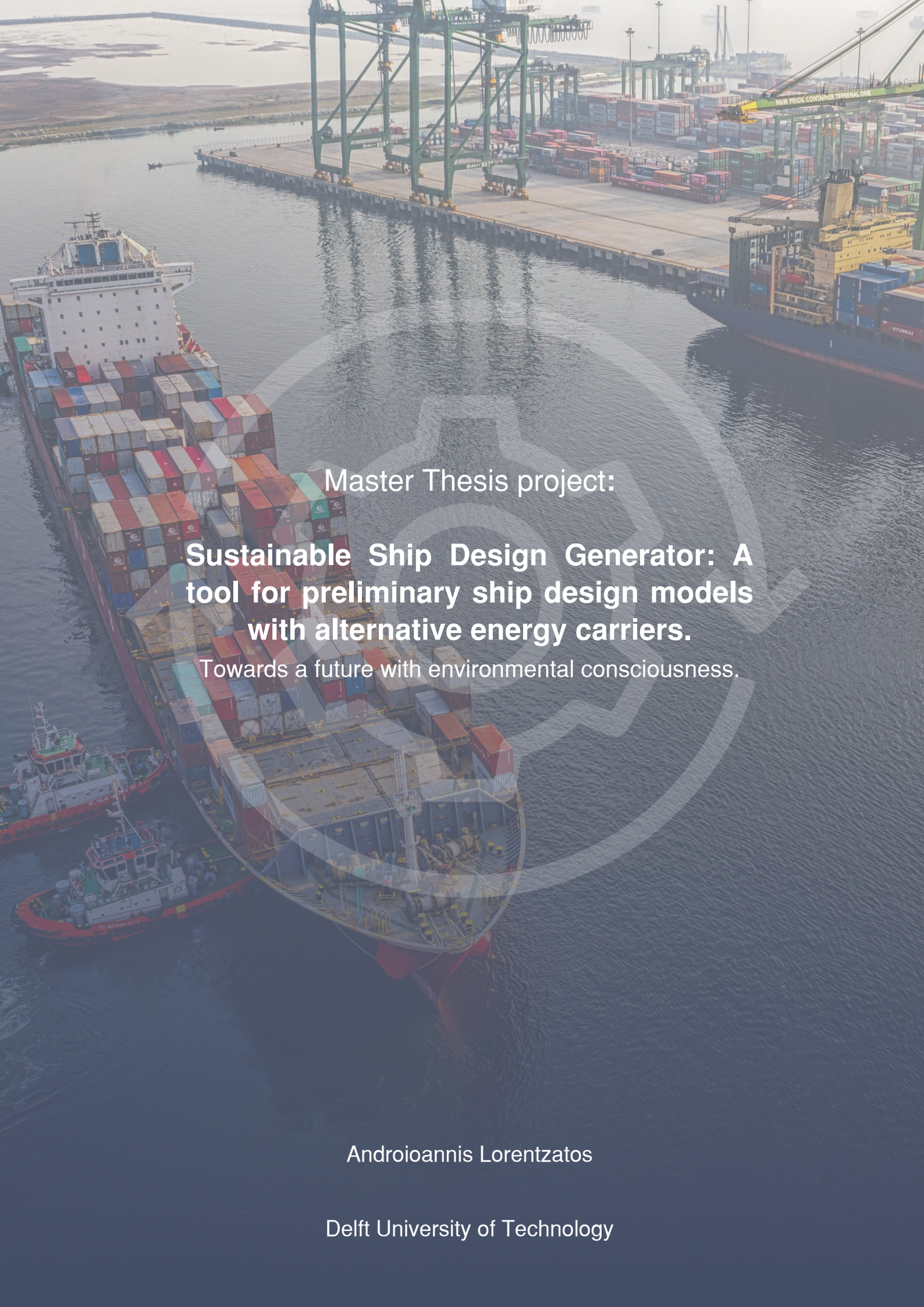

Master Thesis project:

Sustainable Ship Design Generator: A tool for preliminary ship design models with alternative energy carriers.

Towards a future with environmental consciousness.

Androioannis Lorentzatos

Delft University of Technology

Sustainable Ship Design Generator: A tool for preliminary ship design models with alternative energy carriers

by

Androioannis Lorentzatos

Performed at

C-Job Naval Architects

to obtain the degree of Master of Science in Marine technology
in the specializations of Ship Design and Marine Engineering
at the Delft University of Technology.

Student number:	5600138	
Project duration:	Nov. 15, 2022 - Sept. 27, 2023	
Thesis number:	MT.23/24.048.M	
Thesis Committee:	dr. Austin A. Kana,	TU Delft supervisor, committee chairman
	ir. Nicole Charisi,	TU Delft supervisor
	dr. ir. Lindert van Biert	TU Delft
	ir. Niels de Vries,	C-Job Naval Architects, supervisor
	Roy de Winter M.Sc.,	C-Job Naval Architects, supervisor

An electronic version of this thesis is available at http://repository.tudelft.nl/.

TU Delft Delft University of Technology

C-JOB DEDICATED NAVAL ARCHITECTS

PREFACE

The moment I realised that through engineering I could become part of the change that I would like to witness towards protecting the environment, then it became clear to me. I have since been determined to contribute in any way possible, starting with my thesis project. For this reason, I chose to get in touch with C-Job and discuss the possibility of working on a project focusing on alternative energy carriers. The discussed project was exactly what I would expect to match my aspiration. Therefore, I would like to thank Niels de Vries and Roy de Winter for their recommendation of the subject, as well as their support and the valuable knowledge that they were each able to provide me with throughout the course of this project.

I would also like to thank Austin Kana for accepting the supervision of this project, as well as for his support, feedback and ideas that were offered to me. Also, special thanks to my daily TU Delft supervisor, Nicole Charisi. She was always eager to help me and was at times even more stressed than I was about the quality of the project, and I am more than thankful and grateful for that.

Finally, I would like to thank my friends and coursemates for the help that they offered whenever I troubled them with my silly questions. And of course, my most sincere thanks to my family for supporting me all these years from the beginning till the end of my studying years.

Androioannis Lorentzatos
Delft, September 2023

SUMMARY

The urge to protect the environment from the footprint of the shipping industry has spiked during the past few years with the demanding short- and long-term goals of IMO. These relate to limiting greenhouse gas emissions, which has forced the shipowners to implement drastic measures towards becoming sustainable. The current study is targeted to contribute to the sustainable improvement of the industry by aiming to automate the feasibility study process in early-stage design. This is made relevant by integrating a pre-selection of alternative energy carriers, including batteries, hydrogen, ammonia and methanol. The challenging part of this that is missing from relevant existing design generators relates to the independent creation of different design spaces corresponding to each energy carrier, prior to comparing their optimal designs in a consistent manner.

For these reasons, this study presents a method and its respective tool that address the automation of early-stage feasibility studies for alternative energy carriers. The mentioned energy carrier pre-selection is investigated through the aspects of energy density, storage (conditions and tank type), regulations, power generation and engine and tank rooms. These were determined in order to address the considerations applicable to the early-stage design level for the development of a general arrangement and a parametric model. The literature study is concluded with the exploration of state-of-the-art relevant ship design generators, where it was confirmed that none of them has explicitly addressed the implementation of the chosen energy carriers.

The key takeaways from the studies on energy carriers and ship design generators are finally brought together, towards the development of the proposed approach to address the said research gap. The creation of the said tool was completed successfully, as it generates reasonable results that confirm the performance expectations. More specifically, methanol dominates the other options in terms of achieving the requested inputs of speed and autonomy with lower LSW and total resistance. Ammonia comes second, and hydrogen and batteries follow in this order. It was, however, found that in the current version of the tool, there are discrepancies that deviate the tool from reality. The methanol solutions appear more efficient than the original case vessel running on diesel. This can be explained by the consistent underestimation that was observed for the LSW calculation. Moreover, the vessels generated models are optimised for only three main blocks (power generation, energy storage and cargo hold rooms), whereas the case vessel includes a series of systems and components that are currently not being considered in the proposed tool. These observations were consistent for all five tested case studies, in which different types of cargo vessels were tested each time.

Regarding the relative performance of the energy carriers, the difference between them increases exponentially when the inputs of speed and autonomy are highly demanding. However, there are ranges where the design spaces are closer and the relative performance could be adjusted and argued, should more performance indicators be considered.

In terms of validation, the tool was tested for the accuracy level of the LSW and total resistance estimations, with average respective deviations of 20 and 11.3%. Beyond that, it was validated by the tested case studies, as the results were also analysed for consistency and how reasonable they appear. The overall design method was explored for its validity by following a "Relativist validation" approach, that breaks down the process into a series of steps with the aim of building confidence in their credibility.

The concluding recommendations mostly revolve around the functionality improvement of the tool, in order to increase its quality and generate models of higher accuracy. These relate to improving the LSW estimation method, including all the systems/components that are essential for the operation of the vessel, or properly defining a ballast system. Additionally, it is recommended to integrate a 3D-modelling generator to aid the decision-making of the user by completing the perspective of the relative performances.

CONTENTS

NOMENCLATURE

CH_2	Compressed hydrogen
LH_2	Liquid hydrogen
∇	Volumetric Displacement
ABS	American Bureau of Shipping
AC	Alternating Current
B	Breadth
BMS	Battery Management System
CH_4	Methane
CI	Compression Ignition
CL	Centerline
CO	Carbon Monoxide
CoB	Centre of Buoyancy
CoG	Centre of Gravity
D	Depth
DBB	Design Building Block
DC	Direct Current
DDSD	Data Driven Ship Design
DEE	Design and Engineering Engine
DF	Dual Fuel
DI	Direct Injection
DoD	Depth of Discharge
DWT	Deadweight
EGR	Exhaust Gas Recirculation
EM	Entities Model
EMS	Energy Management System
EPS	Energy Power System
GHG	Greenhouse Gas
GM	Metacentric height
HC	Hydrocarbons
HFO	Heavy Fuel Oil
HHV	Higher Heating Value
HLP	High Level Primitive
I_T	Transverse moment of inertia
IC	Internal Combustion
ICE	Internal Combustion Engine
JS	JavaScript
KBE	Knowledge-Based Engineering
KPI	Key Performance Indicator
KR	Korean Register
L	Length
LA	Lead-Acid
LHV	Lower Heating Value
$Li-ion$	Lithium-Ion
LIB	Lithium Ion Battery
LNG	Liquid Natural Gas
LOA	Length Over All
LSW	Lightship Weight
MGO	Marine Gas Oil
ML	Machine Learning
MMG	Multi Model Generator
NaS	Sodium-Sulphur
NH_3	Ammonia
$Ni-Cd$	Nickel-Cadmium
NMC	Nickel Manganese Cobalt oxide
OPEX	Operating Expenses
OSV	Offshore Support Vessel
PEMFC	Proton Exchange Membrane Fuel Cell
PM	Particulate Matter
PTO	Power Take-Off
r_{bilge}	Bilge radius
R_t	Total Resistance
SBD	Simulation Based Design

SBSD	System Based Ship Design
SFC	Specific Fuel Consumption
SI	Spark Ignition
SM	States Model
SoC	State of Charge
SOFC	Solid Oxide Fuel Cell
SSDG	Sustainable Ship Design Generator
T	Draught
TDI	Turbocharged Direct Injection
TRL	Technology Readiness Level
ZnBr	Lead-Acid

1

INTRODUCTION

This graduation research assignment presents the development of a method and the respective tool for the generation of early-stage models with alternative energy carriers. The present chapter introduces the reader to the research problem, starting with the problem background, before linking it with the identified research gap and the derived research objective. Lastly, the overall layout of the assignment is presented.

1.1 BACKGROUND

Sustainability has arguably become one of the main goals of the shipping industry, in the efforts of reducing Greenhouse Gas (GHG) emissions. The International Maritime Organisation (IMO) has set the goal of reducing the total GHG emissions by 50% by 2050. In the short-term, IMO is aiming to achieve a 40% reduction of CO_2 emissions per transport work on average compared to 2008 [1, 2]. To achieve this, energy saving alone is insufficient, and thus, alternative energy storage and power generation are required. Fortunately, during the past few years, the attempts to establish alternative fuels in the maritime industry have been intensified, and solutions such as batteries, hydrogen, ammonia, and methanol have a matured application potential.

Compared to the currently used fuels, the alternative options have different energy densities, as well as different application requirements, including storage and hazard prevention. These are issues that directly affect the space occupation of the engine room and the fuel tanks, on top of the vessel's autonomy and other indirect implications on the ship's layout. This diversity of fuel solutions, however, has increased the complexity of ship design since there are different obstacles to overcome for each fuel. This demands that beyond the research on improving their application, it would be useful to have a means of speeding up the feasibility and performance evaluation of the alternative energy carriers.

In early-stage design, this would focus on the main particulars and the general arrangement of the ship. A potential future-proof solution to this quest could be the implementation of machine learning algorithms, that could learn from the optimisation that they perform. As some aspects of the alternative fuels are still under research, it is understandable that a proper database of *sustainable ships* and their specifications, is nonexistent. In this way, an algorithm could learn using the early-stage decisions of a designer, by storing historical data when generating preliminary designs with alternative fuels using a relevant tool.

1.2 STAGES OF SHIP DESIGN

It is necessary to obtain a deeper understanding of the targeted early-stage level of this research, before further diving into its objectives. This is useful in order to fully comprehend the perspective on the identified research gap, as well as the approach that will be followed in tackling this study.

The term "*Ship Design*" is used to describe the full designing process from the owner's demands up to the final plans that are handed to the shipyards for construction. For this reason, ship design can be organised into four main stages [3]:

- Concept design/ Feasibility study
- Preliminary design
- Contract design
- Detailed design

The concept design phase focuses on converting the mission or owner's requirements into the technical characteristics of a ship. It is essentially a feasibility study that investigates the extent to which the said requirements can be satisfied in the naval architectural and marine engineering frameworks in a first draft. Then, the preliminary design suggests a more thorough analysis and definition of the ship's major characteristics that are briefly addressed during the concept design. The goal of this stage is to satisfy the requirements while simultaneously converging towards an optimal solution using a determined cost-driven filter. These first two phases can be combined under the term "*basic design*". The rest of the stages revolve around refining the model by adding higher detail in the systems and their arrangement, and level of accuracy on the performance computations [3]. However, the focus of this study lies between concept and preliminary design, since the primary target is the feasibility study based on the operational profile of the vessel. At the same time, it is desired to initiate building the foundation for comparing the solutions for the different energy carriers based on cost, without further refining the ship's major characteristics.

1.3 RESEARCH GAP

The identified research gap is primarily related to the fact that it is highly time-consuming to derive preliminary designs with alternative energy carriers. Consequently, this affects the time efficiency and the effectiveness of comparing the available options in a consistent manner. Therefore, the gap can be scoped down to researching the automation of the refining iterations of a designer when translating the operational profile to the early-stage design solution for each energy carrier. The consistency of detail among the included fuel options can then lead to more objective comparisons between them, and significantly reduce the time of doing so. The challenging part of this gap is that currently there is no existing tool that generates different design spaces independently for the different integrated alternative energy carriers, in order to study the early-stage feasibility of each option prior to comparing them.

C-Job Naval Architects has recently initialised a quest for the development of a tool that will automate the development of early-stage designs, including the integration of a variety of alternative fuel options. At the same time, the company has already developed optimisation algorithms, which are currently lacking the essential learning material for the machine learning algorithm to provide educated solutions. The challenging proportion of the latter, involves the translation, of newly generated solutions, into mathematical blocks, in order for the algorithm to be able to process them. Therefore, the gap that this project will attempt to fill aligns with the current goals of C-Job Naval Architects; thus the company will mentor and support the completion of this study.

1.4 RESEARCH OBJECTIVE

This graduation project aims to develop a methodology and its respective *Sustainable Ship Design Generator* (SSDG) tool for studying the feasibility of early-stage designs of a set of alternative energy carriers. This will target to increase the time efficiency, as well as the optimisation of the initial starting point ensuring consistent comparisons between the included fuel options. Furthermore, it is desired to study the energy carriers in different cases and identify trends relating to the energy carriers, and their different properties, with the variation of input variables.

The fuel options are limited to batteries, hydrogen, ammonia and methanol as these have been identified as the options with higher potential. It is important to highlight that the identified gap addresses the entirety of the shipping industry, and it is desired that the SSDG will be suitable for all ship types. However, for the purposes of this research assignment applicability will be limited to case studies on cargo vessels in order to prove the functionality of the tool, before expanding it in the future.

Additionally, the research questions are defined below with the hope of guiding the research in the desired direction. They are, also, expected to be vital for ensuring a smooth workflow and completion of the project within the defined timeline.

1. Which are the state-of-the-art advancements in batteries, hydrogen, ammonia and methanol?
   (a) What are the properties of these fuels regarding energy density, energy storage, and power generation?
   (b) What are the requirements for these fuels to be implemented on a ship?
2. What are the state-of-the-art advancements in ship design generators?
   (a) How have alternative fuels been addressed in early-stage design so far?
3. Which will the overall architecture of the tool be?
   (a) Which will the input variables be?
   (b) Which will the outputs be?
   (c) Which will the main analysis blocks and their general arrangement be?
4. How will the design space be constrained and evaluated?
5. What are the optimisation objective/-s and how are the optimal solutions determined?
6. How is the tool and the design method tested and validated?
7. What trends can be identified for the relation between the chosen energy carriers and the input variables for the chosen case studies?

1.5 THESIS LAYOUT

- Chapter 2: Alternative Energy Carriers

  This chapter provides a general background of the chosen energy carriers (batteries, hydrogen, ammonia and methanol) and highlights the qualities that are most relevant for early-stage design. It also includes a brief overview of the selected carriers as well as the other relevant options in order to contextualise the pre-selection.

- Chapter 3: Ship Design Generators

  Provides state-of-the-art advancements of ship design generators in order to offer relevant background. Additionally, the most relevant elements are highlighted, which can potentially aid the development of the SSDG.

- Chapter 4: Proposed Method & Tool

  The major findings of Chapters 2 and 3 are brought together and a design method for solving this problem is proposed. Additionally, the architecture of the developed tool and its detailed functionality are thoroughly explained. The chapter is divided into the specific requirements for the SSDG, the derived generalised steps that are followed to build the framework, the analysis of the design blocks' definition, the technical feasibility, and the performed optimisation.

- Chapter 5: Performance & Validation of SSDG

  This chapter explores the performance and validation of the SSDG and the design method. The first section focuses on the validation of the estimations for LSW and R_t by comparing actual and estimated values for ten existing vessels. Following that, there are the results of the first case study for a tanker vessel. This section is further split into two parts, in which the first presents the results of running the SSDG with the exact same inputs as the case vessel, while the second the outcome of varying the inputs of speed and autonomy. The chapter is completed with the theoretical validation of the design method, by following a series of steps that build confidence in the process of developing the method.

2

ALTERNATIVE ENERGY CARRIERS

This chapter will explore the properties of alternative energy carriers that are most useful for the concept design stage of ships. A pre-selection of options was determined after following the industry trends and consulting with C-Job Naval Architects, with the final choices consisting of batteries, ammonia, hydrogen and methanol. The chapter starts with a brief comparison of the chosen carriers with the rest of the available options. This is followed by the exploration of each option in the aspects of their properties, energy production, implementation requirements, and power generation. At the end of the chapter, the overview of the concluded decisions is provided.

2.1 JUSTIFICATION OF PRE-SELECTED CARRIERS

This section provides a short overview of how the selected carriers compare with each other and with the rest of the options in this industry. A range of sustainable options is chosen, along with Marine Gas Oil (MGO) that is used as a comparison baseline. The major properties of interest for these fuels are tabulated below. Beyond the energy densities and storage conditions, the renewable synthetic production cost is included, which measures how much renewable energy is required to produce 1 MJ of the fuel.

Energy Carrier	Energy density LHV[1] [MJ/kg]	Volumetric energy density [MJ/litre]	Volumetric energy density (fuel + tank) [MJ/litre]	Renewable synthetic production cost [MJ/MJ]	Storage temperature [°C]	Storage pressure [bar]
MGO	42.7	36.7	36.0	-	20	1
Ethanol	26.7	21.1	20.7	> 3.0	20	1
Methanol	19.9	15.8	15.5	2.4	20	1
Methane[2]	50.0	23.4	9.9	2.3	-162	1
Ammonia[2]	18.6	12.7	6.6	1.8	-34/ 20	1/ 10
Hydrogen[2]	120.0	8.5	3.4	1.8	-253	1
Batteries (Li-ion)	-	0.44	-	-	20	1

Table 1: Energy density and storage properties of a selection of marine energy carriers [4, 5, 6].

Note that methane, ammonia, and hydrogen properties correspond to their liquid state to have a standard point of reference between them. Additionally, the set of values that are indicated for ammonia's storage temperature and pressure correspond to the two options for storing liquid ammonia.

Hydrogen has by far the highest LHV (almost three times higher than MGO), but in terms of volumetric energy density, it ranks lowest excluding the batteries. Hydrogen also has the lowest

[1] Lower Heating Value: The heating value of a substance measures the released heat upon combustion of the substance, and in this case, LHV is chosen over the Higher Heating Value (HHV). The difference between HHV and LHV is that the latter excludes the latent heat of vaporisation of the water that is released during combustion which is more realistic in practice.

[2] The *fuel + tank* energy density of these fuels is estimated for cylindrical Type C tanks.

renewable synthetic production cost, but it does, however, require extreme storage conditions with the cryogenic storage of its liquid state. Methanol, on the other hand, is the ideal option in terms of storage, as it is in a liquid state in ambient conditions. At the same time, it offers energy density comparable to MGO, and it is only lower than the density of ethanol when the tank implications are included. On the downside, it has a synthetic production cost higher than both hydrogen and ammonia. Lastly, ammonia is the intermediate solution with energy densities and storage conditions lying between those of methanol and ammonia, while also having the lowest synthetic production cost (together with hydrogen).

Regarding the two discarded options of ethanol and methane, the justification is found in their emissions and production. Methane as a fuel alone has a higher volumetric energy density than methanol; however, once the consequences of the tank (with storage at -162 °C) are taken into account then it is substantially less energy dense than methanol. Furthermore, methane slip is a serious issue as it is a strong GHG. Mitigating methane slip is still a huge challenge for both tank-to-propeller on the vessel and wake-to-tank within the respective supply chain infrastructure. The combination of those primary reasons is why methane is excluded [7].

Lastly, ethanol can be stored in ambient conditions and has a higher energy density than methanol. However, ethanol has the highest renewable synthetic production cost, making it more demanding to produce for a relatively small gain in energy density [8].

In addition, a hazard risk comparison between the energy carriers (plus Liquefied Petroleum Gas (LPG) and Liquefied Natural Gas (LNG)) is tabulated below, as provided by the US National Fire Protection Association (NFPA).

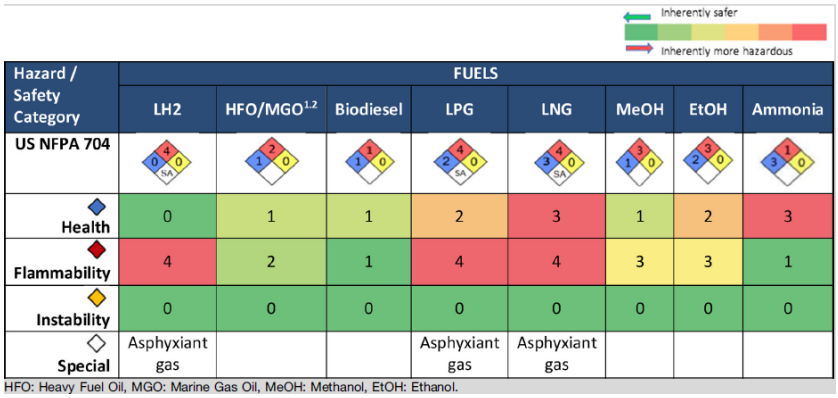

Hazard / Safety Category	FUELS							
	LH2	HFO/MGO[1,2]	Biodiesel	LPG	LNG	MeOH	EtOH	Ammonia
US NFPA 704								
Health	0	1	1	2	3	1	2	3
Flammability	4	2	1	4	4	3	3	1
Instability	0	0	0	0	0	0	0	0
Special	Asphyxiant gas			Asphyxiant gas	Asphyxiant gas			

HFO: Heavy Fuel Oil, MGO: Marine Gas Oil, MeOH: Methanol, EtOH: Ethanol.

Table 2: Comparison of hazardous characteristics between the currently prevailing fuels and the potential alternatives [9].

Table 2 reveals that LNG and LPG are the most hazardous fuels; hence this is one of the reasons they are not included as the most favoured options in Table 1. Ethanol follows as the fuel with hazard implications on both health and flammability, while methanol is similar though with a lower health risk. On the other hand, liquid hydrogen is highly flammable and can be an asphyxiant gas, whereas ammonia is can be very dangerous towards health but its flammability is very low. It can be concluded that the hazard concerns of the alternative options support the pre-selected carriers as the safest ones.

2.2 PROPERTIES OF INTEREST

The significance of this chapter lies in identifying the fuel properties relevant to the early stage of design for the chosen alternative options. These properties will lay the foundation on which the Sustainable Ship Design Generator (SSDG) will be built. The considered properties are listed below:

- **Energy density**: The measure of the amount of energy (MJ) that is contained in a certain amount of space (m^3) and mass (kg) by a fuel.
- **Storage**: Refers to the required conditions (temperature and pressure) at which a fuel is stored in a specific state. This means that special tank types might be required in order to maintain the appropriate conditions effectively and safely.
- **Regulations**: Official regulations regarding implementation requirements for the location and the protection of the engine room and the fuel tanks. For the purposes of this study, these are limited to the constraints impacting the general arrangement. Regulations applicable for more detailed aspects (e.g. pipe insulation or ventilation) are excluded.
- **Power generation**: Investigation of the power generation options for each fuel where the most efficient and sufficiently mature technologies will be selected for the SSDG.
- **Engine and tank rooms**: Arrangement and space occupation of the chosen power generation systems and tanks.

The mentioned properties are driving factors limited to the purposes of early-stage design. These requirements for the shortlisted fuel options deviate significantly from the conventional fuels to date; hence, they need to be addressed due to their impact on space occupation, deadweight and general arrangement of the relevant systems. By extension, they can be considered as triggers in the decision-making on trade-offs regarding the ratios of fuel storage and powerplant occupation over certain features such as autonomy, speed, cargo space or cost. This means that likely not all of these can be equally satisfied, and thus the optimal solution is derived from the problem-specific design requirements. Therefore, this direct link between the listed fuel properties and the design requirements, demands that these properties are addressed in early-stage design though in a certain level of detail [3].

2.3 BATTERIES

2.3.1 *Background*

A battery is an EPS (Energy Power System)/electrochemical system that stores electric energy and effectively distributes it upon demand. In this way, it is understandable that a fully electric battery power plant emits zero emissions. However, in order to store the electric energy in the batteries it first needs to be produced on shore. Therefore, using this type of energy system is not exactly harmless towards the environment, since the major share of electricity production is not yet sustainable. Figure 43 of Appendix A reveals that although there is diversity in sustainable options for electricity generation, more than 60% of the worldwide electricity is still being produced by coal, gas or oil. However, there are indeed sustainable options and the overall footprint of a battery power plant can have minimal impact on the environment.

2.3.2 *Energy density*

The energy density of the batteries is defined through a range of properties that mostly depend on the battery type and its energy storage properties.

Battery types

A battery consists of one or more electrochemical cells which essentially force the electrons to flow and provide electrical energy. Each cell comprises an electrolyte and two electrodes: the positive terminal (cathode) and the negative one (anode) [10]. A range of materials can be used for the electrodes and the electrolyte, and thus the different combinations in a cell can offer diversity in the resulting battery properties. The most prevailing types of batteries are presented in the table below.

Battery Type	Power Rating [MW]	Specific Energy Density [Wh/kg]	Energy Density [GJ/m^3]	Life Time [years]	Cycle Life [cycles]	Cost [$/kW]
LA	0-20	30-50	0.180-0.288	5-15	500-1000	300-600
NiCd	0-40	50-75	0.216-0.540	10-20	2000-2500	500-1500
NaS	0.05-8	150-240	0.540-0.900	10-15	2500	1000-3000
ZnBr	0.05-2	30-50	0.108-0.216	5-10	2000+	700-2500
Li-ion	0-0.1	75-200	0.72-1.8	5-15	1000-10000	1200-4000

Table 3: Summary of the properties, lifespan and cost of the considered battery options [11].

Note, as previously mentioned, the ranges of the lifetime and the cycle life shown in Table 3 above are relatively wide as they heavily depend on the operational conditions.

- **Lead-Acid (LA)**

One of the oldest rechargeable batteries with a wide range of applications in automobiles, the marine sector and home applications. Table 3 above displays how this battery can offer very high capacity, but low space and weight efficiency. It has the lowest price per kW, but also the lowest cycle life. Additionally, there is toxic waste to be disposed of once the LA battery reaches the end of its lifetime. However, lead can be recycled and reused in a range of battery types, where more than 90% is being recycled [11, 12].

- **Nickel-Cadmium (NiCd)**

Ni-Cd offers the largest capacity amongst the batteries shown in the above tables and has better space and weight efficiency, as well as cycle life compared to LA. They can operate over a wide range of temperatures (-20 to 60 ^{o}C) and have a relatively fast recharge time. On the downside, Cd is highly toxic and harmful to the environment, and thus their usage lately has been vastly limited [11, 12].

- **Sodium-Sulfur (NaS)**

NaS comprise molten sulphur and sodium as the cathode and anode, respectively. These batteries have a relatively high cycle life, with decent capacity and high energy and specific energy densities. Nonetheless, beyond the relatively high cost per kW, they require an operational temperature of around 325 ^{o}C, for which a heat source is deployed and powered by the energy stored in the battery [11, 12].

- **Zinc Bromine (ZnBr)**

ZnBr batteries are capable of providing sufficient power rating for both small and large-scale applications; however, their specific energy and energy density are the lowest amongst the five chosen types. The electrochemical reaction inside a ZnBr battery is relatively complex and the net efficiency of its operation is only about 75%. Although it has solid lifetime characteristics and average pricing, its space and weight occupation do not allow it to be a potent solution in the shipping industry [11].

- **Lithium-ion (Li-ion)**

LIBs (Lithium-ion Batteries) currently occupy more than half of the market for small-scale applications. These batteries offer the best-combined energy storage characteristics, though they have significantly lower capacity. They are capable of operating with an efficiency of nearly 100%, but in order to do so they need to be constantly monitored in order to function within the appropriate SOC and temperature conditions. This not only ensures that efficiency and lifetime are at their upper limits, but also that safety risks are limited since Li-ion batteries are prone to malfunctions [11]. LIBs are the ones currently most used in the maritime industry, specifically the NMC (Nickel Manganese Cobalt oxide - $LiNiMnCoO_2$) [13]. This battery type is mostly preferred due to its decreased hazard risk. Moreover, the combination of Ni and Mn results in high specific energy, while the composition of the battery can be adjusted and optimised for energy density, cost and safety, depending on the desired application [14]. An indicative configuration of an NMC battery offers specific energy and energy density of 174 Wh/kg and 370 Wh/L, respectively [15].

Depth of Discharge (DoD)

DoD is the measure of the ratio of the energy used from the battery over the available energy when fully charged. Ideally, the battery operates within a certain charge percentage, and never fully discharges before recharging. This is related to the optimisation of the battery's lifespan, with the trade-off of installing a battery plant of larger capacity than what is actually being used [16]. Once again, there is no ideal solution to fit all problems and the relevant manufacturers usually provide the regions of safe operation for a battery. Although this does not affect the actual energy density of the battery, it creates energy redundancy reducing the "useful" energy density.

C-rate

C-rate is another parameter that affects the sizing of a battery system and by extension its energy density. It is defined by the energy storage capacity and the power rate of the battery when storing or providing energy, and it essentially measures the speed required to discharge a battery relative to its maximum capacity. For example, when the C-rate of a battery is 1, then it can discharge from the maximum State of Charge (SoC) to the minimum within one hour. The required C-rate can be computed as in the example given by MAN for high power demand in thruster operation [13]. The problem consists of a system with two 750 kW bow thrusters, that would be required to operate for around ten minutes when manoeuvring in a port. The C-rate is computed as follows:

$$1500\ [\text{kW}] \cdot \frac{10}{60}\ [\text{hr}] = 250\ [\text{kWh}] \tag{1}$$

$$\text{C-rate} = \frac{\text{Power}}{\text{Capacity}} = \frac{1500}{250} = 6 \tag{2}$$

This is the marginal C-rate required to complete the mentioned operation, but in order to ensure high battery life it would be necessary to increase the capacity of the battery; hence reducing the

C-rate as well. An increase in capacity of approximately 20% above the demanded power usually suffices in most applications. Generally, a C-rate equal to 3 is usually implemented in high-power battery systems [13].

Summary on the energy density of batteries

Based on the above analysis of this section, it is decided to integrate Li-ion batteries in the development of the SSDG. This is following the current industry trends in order to provide solutions that can be feasible at this moment. The following specifications of a Shift Clean Energy Li-ion battery can be used indicatively to finalise the scaling of a battery power plant [6].

Energy Output [kWh]	8.8
Max net Power [kW]	10
Length [m]	0.58
Width [m]	0.38
Height [m]	0.32
Energy Density [kWh/kg]	0.09
Volumetric Energy Density [kWh/m^3]	124.8

Table 4: Marine Li-ion battery specifications by Shift Clean Energy [6].

2.3.3 *Storage conditions*

It is necessary to ensure the storage conditions of the batteries are maintained within a certain range, especially during operation. The temperature will ideally be between 20 and 30 ^{o}C, preferably towards the lower end. Modern Li-ion batteries can efficiently operate at temperatures up to 35 ^{o}C; but the higher the operating temperature gets, the lower the lifetime of the battery will be. Beyond the lifetime, there are also safety concerns as it is possible for fires or even explosions to be caused, should the temperatures rise excessively. For these reasons, it is important to maintain conditions within the mentioned range using proper cooling systems [17].

2.3.4 *Regulations*

Regulatory rules regarding battery systems and their rooms are not restrictive on the arrangement. They are mostly focused on safety measures that target the limitation of risk hazards. A battery system shall consist of certain components as depicted in the following schematic provided by the Korean Register.

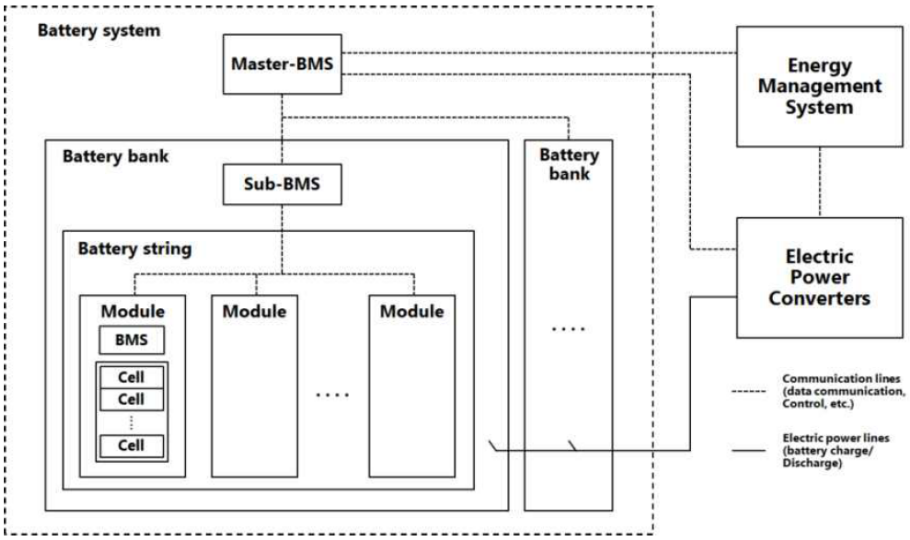

Figure 2: Block diagram for the visualisation of the components and the structure of a battery system [18].

Where BMS refers to Battery Management System, which is mandatory for handling and monitoring the battery banks, and communicating the data with the Energy Management System (EMS). Now the exact dimensions of each battery system are to be determined during the design process based on the power requirements of the application. In terms of safety regulations, the main points are listed below [19]:

- *Battery room shall be positioned aft of the collision bulkhead, and the boundaries of the battery room shall be part of the vessel's structure or enclosures with equivalent structural integrity.*
- *Battery room shall only include equipment associated with the battery system.*
- *Pipes shall not be installed inside the battery room so that it will not be endangered in the event of leaks. In case installation of pipes is unavoidable inside the battery room, then the pipes should have any flanged or screwed connections in this area.*
- *Fire hydrants shall not be located inside the battery room.*
- *Battery room shall have A-60*[3] *fire integrity towards machinery spaces of category A*[4]*. Additionally, the room shall have A-0*[5] *fire integrity towards the rest of the machinery spaces.*

2.3.5 *Power generation*

As it was previously mentioned, a battery power plant has power generation in itself, and thus it does not require a separate power generation system. Instead, it has energy stored in a chemical form, and upon demand, a conversion to electrical energy is triggered. In order then to distribute the electrical energy to the users, it is necessary to utilise a series of components in order to properly distribute the demanded electricity to all the consumers. Batteries provide DC power, but the

[3] Noncombustible, thermal insulation specifically designed and manufactured for use on ships' bulkheads and decks. The "-60" part means the *that the average temperature of the back fire side of the wall is not more than 140 °C higher than the initial temperature when it is burned for 60 minutes on one side of the wall, and the temperature at any point, including any joint, does not rise more than 180 °C from the initial temperature [20].*

[4] The machinery spaces that contain internal combustion type machinery.

[5] *The A-0 level means that there is no requirement for the temperature rise of the back fire surface. [20]*

components of the distribution system can vary depending on whether there is a DC or an AC grid installed on the ship. Both cases are provided below, along with components and total system efficiencies.

System components and efficiency

- **AC grid**

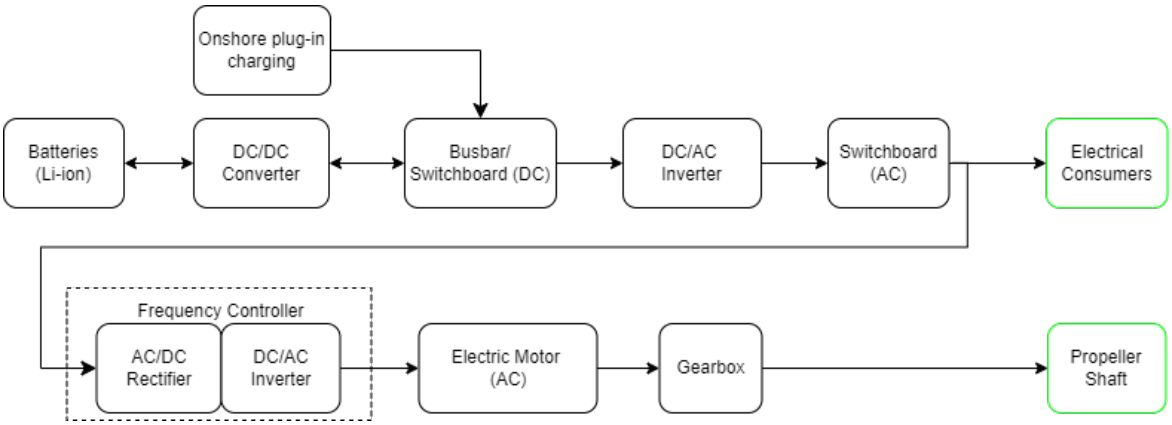

Figure 3: Schematic of the components used for a battery system in AC grid [14].

Component	Efficiency [%]
Batteries (Li-ion)	97
DC/DC Converter	99
Busbar (DC)	99
DC/AC Inverter	97
Switchboard (AC)	99
Frequency Controller	94
Electric Motor (AC)	98
Gearbox	99
Overall system efficiency	**83.3**

Table 5: Component and overall efficiencies of an AC grid battery power plant [14].

- **DC grid**

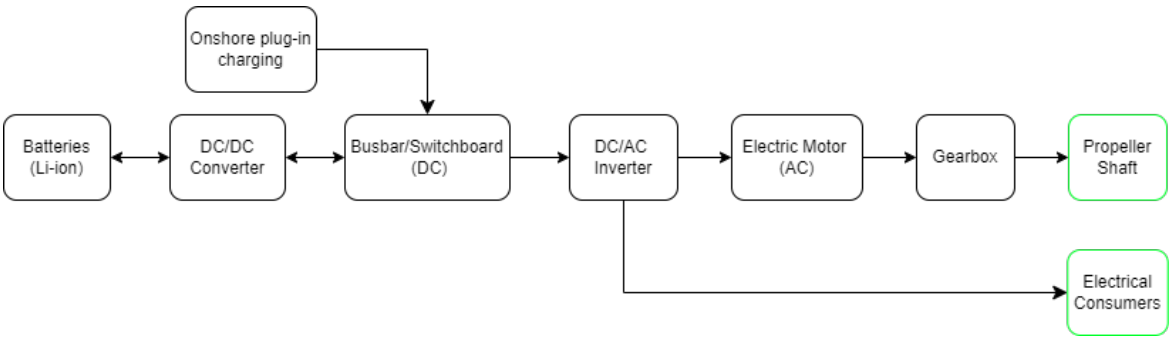

Figure 4: Schematic of the components used for a battery system in DC grid [14].

Component	Efficiency [%]
Batteries (Li-ion)	97
DC/DC Converter	99
Busbar/Switchboard (DC)	99
DC/AC Inverter	97
Electric Motor (AC)	98
Gearbox	99
Overall system efficiency	**89.5**

Table 6: Component and overall efficiencies of a DC grid battery power plant [14].

2.3.6 *Battery room*

The existing regulations do not have any dimension-specific implications on the design of the battery room. In this way, an indicative schematic of a generalised battery room design is drawn below as derived from the relevant design principles of C-Job Naval Architects by observing technical drawings of past projects.

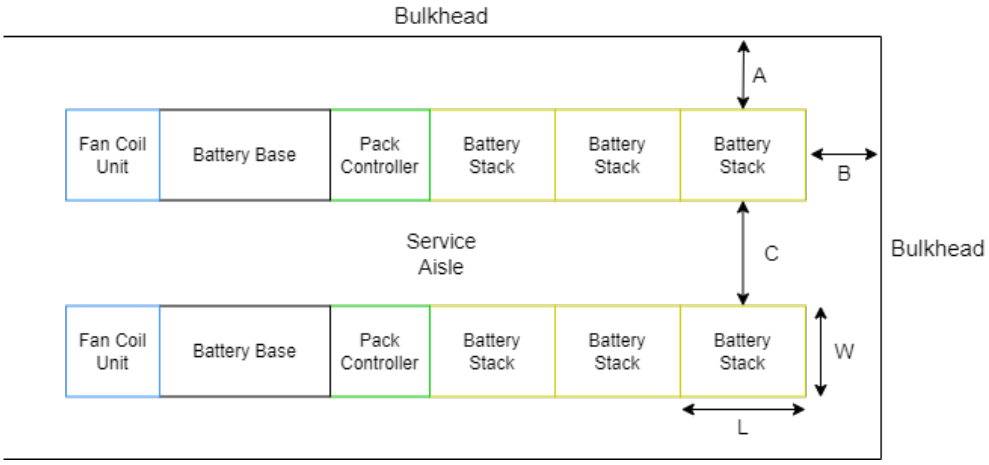

Figure 5: Top view of a battery room schematic including the battery packs and the major components of the system.

The amount and the size of the battery stacks are to be determined through the computation of the vessel's power demand. The pack controller is the system that handles its assigned battery pack, while the battery base is used for monitoring and servicing. Lastly, the fan coil unit is necessary for ensuring the operating conditions inside the room are appropriate for the safe operation of batteries. Now, the annotated dimensions of Figure 5 are tabulated in the following table. The dimensions A, B and C are indicative of the C-Job Naval Architects standards, as mentioned before.

Dimension	Size [mm]
L	Battery length
W	Battery width
A	200
B	600
C	800 or W + 200

Table 7: Dimension sizing of the battery room design shown in Figure 5.

Note, dimension C has a minimum of 800 mm, but if the battery width (W) plus 200 mm is greater, then it is also applied as the width of the service aisle. Dimensioning can be finalised once the power demand is known and the corresponding capacity of a battery system is computed.

2.4 HYDROGEN

2.4.1 *Background*

Hydrogen is one of the most popular alternatives, especially for the maritime sector. As a fuel, it is the most environmentally friendly option since it only emits water and zero GHG; though hydrogen production is not fully sustainable yet. Currently, the largest share of hydrogen is formed from fossil fuels. The hydrogen is then used directly and combined with other compounds to form other gases and liquids. However, the production of hydrogen using fossil fuels results in a very large amount of CO emissions, for which it is necessary to pursue further technological developments in order to limit the impact on the environment [21]. Of course, there are currently various developments on producing hydrogen from renewable sources by using biomass gasification, pyrolysis, aqueous phase reforming, water electrolysis, photoelectrolysis or thermochemical water splitting [22].

Establishing green hydrogen as one of the main fuels in the following years is posed with a range of obstacles. The major ones revolve around hazard risks since hydrogen is extremely flammable. It has one of the highest flammability ranges and flame temperatures, while also having one of the lowest minimum ignition temperatures amongst the popular alternatives [23].

Table 2 shows how LH_2 is the most flammable (together with LNG/LPG), without any health (non-toxic) or instability risks. It is, however, an asphyxiant gas, meaning that if it is diluted in air in high concentrations it can cause suffocation. Additionally, in order to have LH_2 under atmospheric pressure (1 bar) it needs to be at -253 ^{o}C. This temperature not only causes cold burns upon contact, but a leak can lead to the creation of a liquefied air and hydrogen mixture that is explosive [9]. For these reasons, it is crucial to ensure that all the parameters are analysed and all the risks are properly addressed, for the safe and effective implementation of the hydrogen fuel without further setbacks [24].

2.4.2 *Energy density*

The energy density properties of hydrogen depend on the state of the fuel. For hydrogen, it is possible to use it in liquid and compressed states on board ships, by adjusting its storage conditions [25]. The table below displays the properties of the two options (LH_2 and CH_2, respectively) for the fuel itself, excluding the tank implications.

Fuel state	Energy density LHV [MJ/kg]	Volumetric energy density [MJ/litre]	Volumetric energy density (fuel + tank) [MJ/litre]	Renewable synthetic production cost [MJ/MJ]
LH_2	120	8.5	3.4	1.8
CH_2	120	4.5	1.9	1.7

Table 8: Energy density and renewable production cost of liquid and compressed hydrogen [4].

It is visible that based on these properties, LH_2 is more useful due to having almost two times higher volumetric energy density, and only marginally higher production cost.

2.4.3 *Storage*

Conditions

The first aspect that needs to be addressed for the storage of hydrogen is the storage conditions that correspond to the two states. The conditions for LH_2 and CH_2 are presented in the following table.

Fuel state	Storage temperature [°C]	Storage pressure [bar]
LH_2	-253	1
CH_2	20	700

Table 9: Storage conditions for liquid and compressed hydrogen [4].

Compressed hydrogen is cheaper to install and it is usually stored in tanks under a pressure between 350 and 700 bar, in the effort of increasing its density in the range of 23.3 and 39.3 kg/m^3 (compared to the ~0.09 kg/m^3 of hydrogen in STP conditions). Nonetheless, when it is stored under such high pressures, there are issues arising when refuelling. The higher the storage pressure is, the higher the energy consumption and the smaller the tanks have to be in order for them to sustain the forces on their walls [26, 27].

Regarding the liquefied option, it requires a storage temperature of 21 K (~ −253°C), offering a density of approximately 71 kg/m^3. In this way, not only the tanks can be larger in size, but they are also lighter since in this state hydrogen is kept at ~1.4 bar. This pressure is usually applied to prevent hydrogen from initialising boiling, by slightly increasing its boiling point. It is also necessary to ensure the application of vacuum insulation for the storage tank, bunker and vent line since in case air is mixed with liquid hydrogen the supply lines will freeze. Eventually, the fuel is vaporised and used as a gas [26].

For the purposes of this study, it decided to choose the option of LH_2 in order to take advantage of the significantly higher energy density.

Tank type

Liquefied gases can be stored in integral, membrane or independent tanks [28]. The latter is usually preferred as they are not part of the hull's structure, and thus are not directly affected by the loading that the hull is subjected to. Furthermore, the independent tanks are more efficient in storing the fuels in refrigerated or pressurised conditions. The different types of independent tanks are displayed below.

Tank type	Boundary requirement	Design	Ideal for
Type A	Complete secondary barrier	Prismatic	Refrigerated fuels
Type B	Partial secondary barrier	Prismatic	Refrigerated fuels
Type C	No secondary barrier	Cylindrical or multilobe	Semi and fully pressurised fuels

Table 10: Available tank types for storing

It is preferred to use the Type C ones, as they do not require any secondary barrier, venting or re-liquefaction systems. They are, also, able to cope with pressure increases over time improving

holding time. Type C tanks are also explored in greater depth for LNG during the past few years; hence, there is an existing foundation for the safe and efficient application of this tank type [27, 29].

2.4.4 *Regulations*

It is crucial to note the regulations for the location and the required protection of LH_2 storage tanks since it can have a major effect on the design arrangements of the vessel. The following specifications are from the IGF code as released from IMO, on regulations for ships using low-flashpoint fuels of the IGF Code [30, 31, 32].

1. *Minimum distance of B/5 or 11.5 m (whichever is less) from the inboard of the ship walls at right angles to the CL (centerline) at the level of the summer load draught.*
2. *Boundaries of the fuel tanks are the extreme outer longitudinal, transverse and vertical limits of the tank structure (including valves).*
3. *For independent tanks the tank shell is used to measure the safety distance.*
4. *The boundary of the fuel tank cannot be located closer to the aft terminal or the shell plating of the ship than:*
   - **Passenger Ships**: *B/10 and in no case lower than 0.8 m, while this distance does not need to be larger than B/15 or 2 m if the shell plating is placed inboard of B/5 or 11.5 m.*
   - **Cargo Ships**:
     (i) 0.8 m, when $V_c \leqslant 1000m^3$
     (ii) $0.75 + V_c \cdot \frac{0.2}{4000} m$, when $1000m^3 \prec V_c \prec 5000m^3$
     (iii) $0.8 + \frac{V_c}{25000} m$, when $5000m^3 \leqslant V_c \prec 30000m^3$
     (iv) 2 m, when $V_c \geqslant 30000m^3$

     Where V_c shows the 100% of the gross design volume of the individual fuel tank @ 20 °C (including domes and appendages).
5. *The lowermost boundary of the tanks is to be distanced B/15 or 2 m (minimum) from the moulded line of the bottom shell plating (at the CL).*
6. *The tank to be located abaft a transverse plane* $0.08 \cdot L$ *from the forward perpendicular for passenger ships (SOLAS II-1/8.1), and abaft the collision bulkhead for cargo ships.*
7. *Ships with a hull structure of higher collision and/or grounding resistance, shall be studied on a case-by-case basis for the determination of the tank location and shall be approved if an equivalent level of safety is ensured.*

In terms of safety, only fire-related protection is considered. Hydrogen is not toxic and any asphyxiation risk would only occur if fire-related hazard are already exceeded.

- **Open decks**: *Exposed parts of* LH_2 *tanks located on open decks must be covered with water spray systems, in order to protect from heat input in case of external fire. Furthermore, since* LH_2 *is not expected to cause fires and/or explosions on open decks, it is not necessary to install water spray systems in spaces (such as accommodation) that otherwise need to be protected from fuel tank fires as per the IGF Code.*

- **Under open deck**: *Due to the risk of fire and/or explosion by* LH_2 *in closed and semi-closed spaces, it is required to protect fuel storage systems from machinery spaces of category A and other spaces with a high risk of fire as follows:*

  (i) *Protect tanks with A-60 class insulation.*

  (ii) *Separate the fuel storage systems and the mentioned spaces by a cofferdam of 0.9 m or longer. In case the Type C independent tanks are not positioned in the said spaces (category A or high fire hazard risk space) the fuel storage hold space can be considered as a cofferdam.*

Additionally, it is important to address the allowable maximum loading limit of a Type C tank carrying liquefied gases. The IGC code [28] indicates that the maximum loading of such a tank shall not be higher than 98% at the reference temperature. More specifically, the exact loading limit can be computed using the following formula:

$$V_L = 0.98 \cdot V \cdot \frac{\rho_R}{\rho_L} \tag{3}$$

Where,

- V_L = maximum volumetric level to which the tank may be filled
- V = volume of the tank
- ρ_R = relative density of fuel at the reference temperature
- ρ_L = relative density of fuel at the loading temperature and pressure

2.4.5 *Power generation*

ICE

Experimental investigation on ICEs has revealed the potential of exploiting hydrogen even as an only fuel. Both CI and SI engines have been successfully tested, while dual fuel (DF) scenarios have also been suggested and proven more feasible. Nieminen et. al compared the combustion characteristics of a specific V6 SI engine when it was fuelled by gasoline and then hydrogen. The results showed a noticeable increase in thermal efficiency when hydrogen was used; though, there was a significant decrease in power output, as well as an increase in the pressures and temperatures of the cycle [33]. Regarding CI engines, there were several attempts of operating a diesel engine with only hydrogen. One of the first ones dates back to 1979 when with small modifications it was proven possible to obtain a working CI hydrogen-only engine. The major issue that occurred was the high resistance of hydrogen in auto-ignition; hence resulting in a vastly limited operation range, even with compression ratios as high as 29:1 [34]. Similar findings were concluded in the following years on the low operational range of the hydrogen-fuelled CI engine by relevant studies from Ikegami et. al [35, 36]. In these studies, some improvements were observed with the introduction of pilot fuels. Nevertheless, it was also observed that the higher the inflow of the pilot fuels, the rougher the combustion process became.

The DF (diesel/hydrogen) CI engine scenario has been investigated in much greater depth as a more feasible and effective solution. The idea behind the exploration of dual fuel setups was to ensure decent combustion output and reduce hydrocarbon emission proportions. Early studies showed that although the combustion efficiency was similar to a diesel-only setup, there was noticeable engine knocking well before the optimal point [37]. Another approach involved

the aspiration of gaseous hydrogen at the intake of the cylinder in a naturally aspirated DI (direct injection) engine. It was observed that smoke levels were reduced up to 50% in certain operating conditions, and about 17% when the engine was running at full load. In terms of the hydrocarbon emissions, the effect was insignificant, while the formation of NO_x emissions was actually higher [38]. Further exploration and experimentation of such DF CI engines throughout the years came to the following conclusions around hydrogen enrichment [39]:

- Does not affect the SFC (Specific Fuel Consumption) or the engine efficiency
- Lowers volumetric efficiency up to 6%
- Significant reduction of CO and CO_2 emissions
- Sharp increase of NO_x emissions at high engine loads
- Smoke reduction up to 50%

Regarding the feasibility and effect of blending ratios, Zhang et al. [40] experimented on three scenarios: hydrogen enrichment of 10 and 20% in diesel operation, hydrogen substitution with 30, 60 and 90% ratios, and a relative injection timing test keeping the 90% hydrogen substitution. The most relevant is the hydrogen substitution, which proved that the higher the hydrogen content the less the CO, CO_2 and hydrocarbons (HC) emissions, where HC and CO are eliminated in all three ratios, and CO_2 can be reduced proportionally to the increase of the hydrogen content. On the other hand, NO_x showed an exponential rise, reaching almost 500% increase for the 90% content case. Similarly to ammonia in Section 2.5.5, it was demonstrated that NO_x emissions heavily depend on the operation conditions of the engine. The injection timing test proved that NO_x generation can be drastically limited to an approximately 10% increase compared to diesel-only operation.

It is clear that although hydrogen fuelled ICEs can have a positive environmental impact compared to pure fossil fuel ICEs, the effect is not sufficient to aid the energy transition in the long term and limit GHG emissions. This option could be considered as a short-term transition alternative until other more drastic and sustainable solutions become commercially available. Currently, there are available DF (diesel/hydrogen) marine engines by the leading manufacturers, for which specifications are publicly available through the relevant databases.

Fuel cell

Fuel cell systems are capable of generating electricity by triggering an electrochemical reaction using a fuel and an oxidising agent (usually air). The main difference between fuel cells and batteries is that the former requires a constant flow of the reaction components, in order to sustain the reaction. On the other hand, batteries simply store the energy in the chemical and can recycle the reaction upon demand until the end of their lifetime. Furthermore, fuel cells have a higher power density than batteries, while they can be powered with green fuels such as hydrogen, NH_3 or methanol [41].

Regarding fuel cell types, the main focus is shifted towards the Proton Exchange Membrane Fuel Cell (PEMFC) and Solid Oxide Fuel Cell (SOFC) options in the shipping industry. The PEMFC operates using platinum-based electrodes and a humidified polymer membrane as an electrolyte, which infuses hydrogen ions (H+). The operating temperature is relatively easy to maintain as it ranges between 50 and 100 ^oC, while higher temperatures are forbidding due to the membrane needing to remain humid. The system efficiency is around 50-60%, and the ideal fuel is hydrogen (H_2) since only water is emitted [42]. A simple cycle flow chart of the PEMFC operation is provided below, as presented by DNV GL.

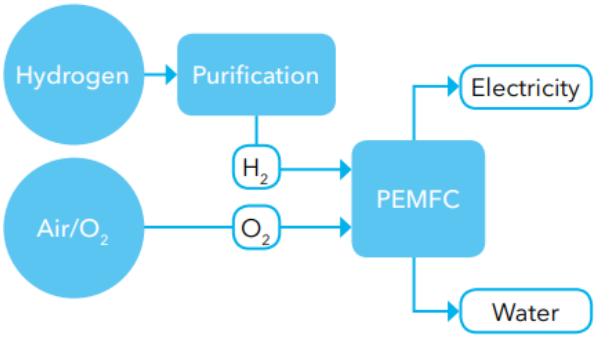

Figure 6: Operational flow chart of a PEMFC system [42].

The power output of the fuel cells depends on the manufacturer, though each fuel cell unit provides a relatively low amount of electrical power. The latest PEMFC unit that has become available from PowerCell Group has a max power output of 200 kW; hence, in order to cover the power demand for a large vessel, several units are stacked together working in parallel. The specification of these units is presented below:

Max net Power [kW]	200
Length [m]	0.7
Width [m]	0.9
Height [m]	2
Weight [kg]	700
Max system efficiency	55-60%

Table 11: Specifications of a PEMFC unit as provided by PowerCell Group [43].

Note, the displayed efficiency in Table 11 is only the highest that can be achieved by the selected PEMFC unit, but there is in fact a greater range during operation. The efficiency ranges from about 28% up to 60% depending on the output. For the purposes of this tool a fixed value can be assumed; though it is recognised as a limitation and a more elaborate model could be deployed to provide an adaptable value based on the requested output.

SOFC systems operate with an electrolyte made of a porous ceramic material, while the anode is a nickel alloy and the cathode is a lanthanum strontium manganite: a porous material that offers compatibility with the electrolyte. Operational temperatures are significantly higher than the PEMFC, as they range between 500 and 1000 °C. This means that various fuels can be used in the SOFC, including hydrogen, LNG, methanol or ammonia, without requiring any extra processes such as the previously mentioned ammonia cracking. SOFCs have a system efficiency of ~60%, but the overall power plant performance can be raised up to ~85% with the implementation of a heat recovery system [42]. The reaction flow chart of the SOFC is displayed below.

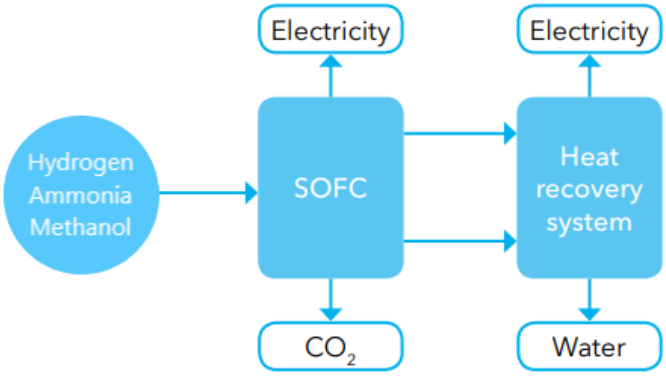

Figure 7: Operational flow chart of a SOFC system[6] [42].

The SOFC units provide a relatively low output with most manufacturers producing solutions of 1-3 kW output. Therefore, similarly to the PEMFC, it is necessary to stack multiple SOFC units to achieve the desired power output for a vessel. Indicatively, a 1.5 kW unit produced by SolydEra for small-scale onshore applications has the following specifications [44]:

Max net Power [kW]	1.5
Length [m]	1.01
Width [m]	0.55
Height [m]	1.2
Weight [kg]	250
System efficiency	55-60%

Table 12: Specifications of a SOFC unit as provided by SolydEra [44].

In this case, PEMFCs are considered more useful for this study due to having similar efficiency with SOFCs, while operating at dramatically lower temperatures. PEMFCs also have a high enough Technology Readiness Level (TRL), compared to that of SOFCs that require further development before they are implemented on board ships [45].

Summary on power generation for H_2

It is concluded that PEMFCs are the preferred power generation system for the development of the SSDG. Fuel cells are more sustainable than DF ICEs and it is expected that they will be one of the long-term solutions that aid the achievement of the GHG emissions goals.

2.4.6 *Engine and tank rooms*

This subsection provides all the necessary information on the components of the chosen PEMFC-powered propulsion system with Type C fuel tanks.

Engine room

The power plant schematic with all the essential components of a system fully powered by PEMFCs is illustrated in Figure 8:

[6] Note, the figure shows CO_2 emissions, but that is in fact only applicable for methane.

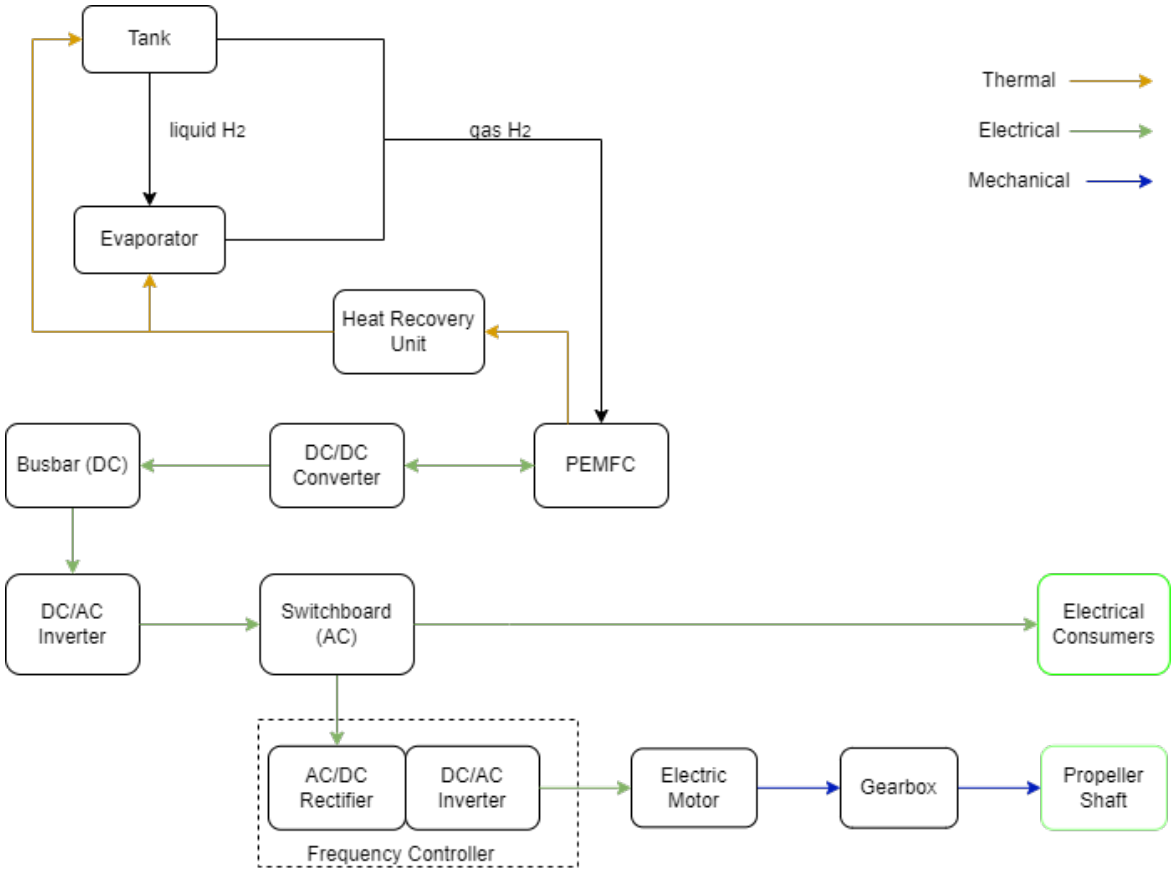

Figure 8: Power plant schematic of a LH_2 PEMFC powered vessel.

Where the efficiencies of each component, as well as the overall system efficiency, are tabulated below.

Component	Efficiency [%]
PEMFC	57.5
DC/DC Converter	99
Busbar (DC)	99
DC/AC Converter	97
Switchboard	99
AC/AC Converter	98
Electric Motor	96
Gearbox	99
Overall system efficiency	**50.4**

Table 13: Component and overall efficiencies of a PEMFC power plant [4].

The sizing of the power generation system will depend on the power demand of the design problem, for it will be necessary to stack multiple PEMFC units.

Tank room

The design of the tank room depends on the chosen type of tank and the demanded capacity. In this case, as type C tanks are deemed as the most appropriate option for liquid hydrogen, there are the options of cylindrical, bilobe or trilobe tanks [46]. The size and number of the tanks can be determined based on the needs of the vessel and can be placed in series, parallel or both (if multiple). Design solutions are acceptable as long as they comply with the regulations presented in

the above sub-section. Moreover, the wall thickness of the tanks can be simply computed by using the storage pressure and finding the required wall thickness that can withstand the pressure without breaking. The shell thickness requirements can be computed based on the IGF Code guidelines [30], but for the purposes of this study, they can be simply covered by assuming a safety margin that can later accommodate the exactly computed values. The following provisional sketch can be used to visualise the design considerations for the tank room.

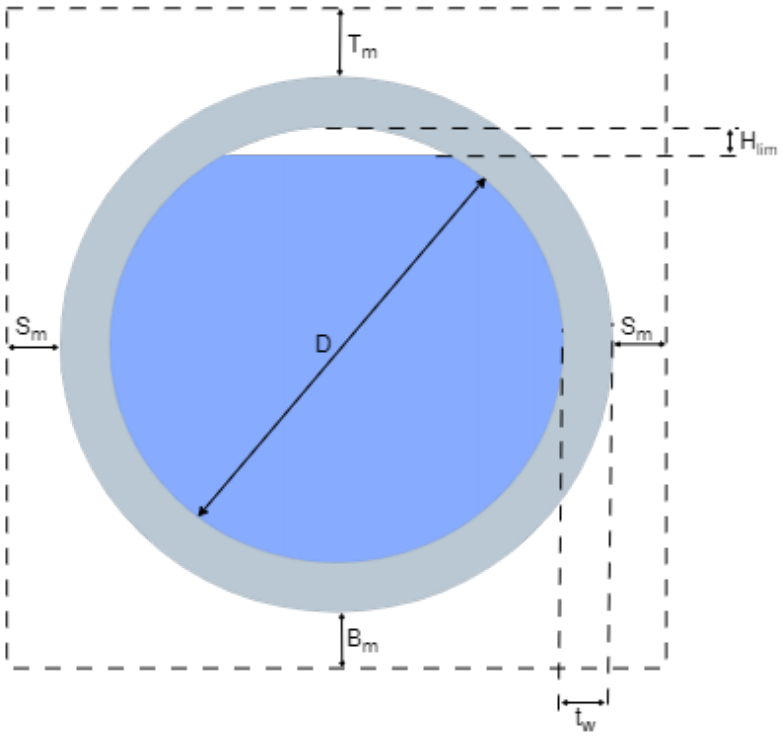

Figure 9: Schematic of the tank room using a cylindrical design of a Type C tank for LH_2 storage.

Where,

- D = Internal diameter of tank
- T_m = Top margin distance between tank and top deck
- S_m = Side margin distance between tank and inside of ship's hull
- B_m = Bottom margin distance between tank and inside of ship's hull
- H_{lim} = Filling limit of tank
- t_w = Wall thickness of tank

2.5 AMMONIA

2.5.1 *Background*

The next investigated alternative fuel option is ammonia (NH_3), a highly potent fuel for the maritime sector, that is expected to occupy a fair amount of the market in the near future. As DNV projected in their 2022 outlook, NH_3 is expected to have the highest share of the fuel mix in 2050 [47]. It is a chemical that is already being produced and used on large scale, as it is utilised in the sectors

of agriculture, plastics, pharmaceuticals and explosives production. This means there is existing knowledge and infrastructure for efficient production, storage and transportation of NH_3. One of the suggestions towards pursuing NH_3 as a fuel that can address the energy transition goals was in 2006, supporting that it is not only an environmentally friendly option but can also improve the operational efficiency [48]. This is based on the notion of NH_3 being an ideal hydrogen carrier, due to its large-scale availability and existing production foundations, as well as its cost being approximately the same as hydrogen at the time. The main drawback of NH_3 is its toxicity, which in case of a leak during transportation or storage can be highly harmful to both the environment and directly to humans. This is also the reason why advancements around establishing NH_3 as a fuel have been significantly delayed.

Additionally, NH_3 offers a wide range of options for producing it, as it can be created through gasification from fossil fuels, electricity, or even waste heat [49]. Currently, the most used method (90%) is the Haber-Bosch which utilises fossil fuels, which is not the most sustainable option with GHG emissions and high energy usage to achieve the required high temperatures (400-500 ^{o}C) [50]. It is, however, possible to establish NH_3 as a CO_2 neutral fuel if it is completely produced from either waste heat or sustainable electricity.

2.5.2 *Energy density*

Ammonia is preferable to be used in its liquid form in the shipping industry, due to its convenient storage requirements that are explored in the following subsection. The energy density properties of liquid ammonia are, therefore, the ones presented in Table 1, with LHV of 18.6 MJ/kg and volumetric densities of 12.7 and 6.6 MJ/litre, for fuel alone and fuel plus the tank's effect respectively.

2.5.3 *Storage*

Conditions

The preferred state of storing NH_3 is in its liquid form, for which there are three options for achieving it. The most commonly used ones are either fully pressurised or fully refrigerated, while the semi-pressurised/refrigerated is also a valid option [4]. The fully pressurised case requires a pressurised tank at 10 bar and a temperature of 20 ^{o}C. Alternatively, the fully refrigerated option can be achieved by maintaining NH_3 at a temperature of -34 ^{o}C (boiling point of NH_3) and at ambient pressure of approximately 1 bar [49, 51]. These specifics for the two storage conditions are tabulated as follows.

Condition	Storage temperature [^{o}C]	Storage pressure [bar]
Fully pressurised	20	10
Fully refrigerated	-34	1

Table 14: Storage conditions for ammonia in both fully pressurised and fully refrigerated states.

Tank type

Regarding the tanks, it is preferred to use the Type C ones as it was also explained in the relevant section above for hydrogen (Section 2.4.3) [52, 53]. Type C tanks are ideally used for semi and

fully-pressurised NH_3, but types A and B are expected to be further studied for onboard NH_3 storage in the future [54].

2.5.4 *Regulations*

The location, protection and filling limit regulations, for ammonia tanks, are exactly the same as the ones elaborated for hydrogen (Section 2.4.4) since they are both covered by the same IGF Code rules for low-flashpoint fuels [24].

2.5.5 *Power generation*

ICE

The first attempts to explore the feasibility of ammonia as a fuel were on ICEs. One of the oldest efforts dates back to 1966 when liquid ammonia was directly injected in the cylinder of a compression ignition (CI) engine and auto-ignition was achieved with a compression ratio of 35:1 and 150 ^oC temperature [4]. To date, there have been numerous experiments on both CI and SI (Spark Ignition) engines with success. Although many scenarios have been proven feasible, the most prevailing CI setup was found in a DF NH_3-Diesel on a TDI (Turbocharged Direct Injection) engine [55]. Efficient and feasible SI engine setups were found again in dual fuel cases with both ammonia-hydrogen and ammonia-gasoline combinations [56, 57].

It is proven that ammonia can be utilised as a combustion fuel, though it has to be in a dual-fuel (DF) combination as ammonia's combustion characteristics are not as fruitful [23] (Table 29, Appendix B).

For the blending proportions when mixing ammonia with diesel, it is claimed that a DF engine could operate with an energy share ratio of up to 95% ammonia and 5% diesel. Nonetheless, in terms of fuel efficiency, reasonable results are observed with ammonia energy ratios in the range of 40 to 80%. Additionally, in 60% or less of ammonia energy share it was shown that NO_x emissions were lower than 100% diesel operation [58]. Regarding emissions, Nadimi et al. experimented on ammonia with biodiesel blends and tested two setups with a constant flow rate of biodiesel and an increasing flow rate of ammonia for the increasing loading on the engine. $CO, CO_2 and HC$ were found to be the lowest when the ammonia energy contribution was the highest achieved at 69.4% at 100% engine load. Regarding particulate matter (PM) emissions, they were lower in biodiesel-only operation in lower engine loads, but lower in DF operation in higher loads above 70 and 85% respectively in the two setups. Lastly, NO emissions were lower for biodiesel-only operation for almost all the engine loads as expected, and the authors have noted that there are methods to limit both NO and NO_x emissions, such as mixing ammonia with a small amount of hydrogen or adjusting the timing of ammonia injection [59]. It can be summarised that the higher the ammonia content the more the reduction of $CO, CO_2 and HC$, but the effect on the rest of the emissions is highly dependent on the setup and the operation conditions of the engine [58].

Currently, the option of using NH_3 as an ICE renewable fuel in the shipping industry is claimed to become possible with the existing DF engines of the market very soon. MAN and Wartsila have set the deadlines of 2024 and 2023 respectively, for the finalisation of NH_3/diesel DF ICEs [60, 61]. Sizing specifications for such engines are readily available by the manufacturers, though without a sizing calculator tool. In this way, the available information can be used as a database and once the power demand is known, the corresponding engine and its dimensionality will also be known.

Lastly, it should be noted that there is also the potential of NH_3/H_2 DF engines, but they are still at the laboratory experimental level [62].

Fuel cell

As it was previously mentioned in Section 2.4.5 PEMFCs and SOFCs are the prevailing options for the implementation of fuel cells in the shipping industry. NH_3 can be used as a fuel in both systems; however, an extra system needs to be integrated in PEMFC in order to perform NH_3 cracking and separate it into hydrogen and nitrogen over a catalyst [63]. In this way, it is not preferred to use NH_3 as a PEMFC fuel since it increases both the cost and complexity of the system. On the other hand, NH_3 can be directly used SOFCs without the addition of further systems, as was also explained in Section 2.4.5. However, NH_3 fuelled SOFCs are still under experimentation for large-scale applications, and although feasibility has been proven, there are no readily available options for the maritime industry [41].

Summary on power generation for NH_3

It can be concluded from the above that the power generation option for the SSDG will be the DF NH_3/diesel engine. Although it is not the most future-proof solution from the sustainability perspective, it is the one with the highest TRL for the time being with a substantial reduction in harmful emissions.

2.5.6 *Engine and tank rooms*

Engine room

The main components of a DF ICE power plant can vary depending on the chosen configuration. The options may include either 2- or 4-stroke engines, the inclusion of a gearbox or not and the integration of a Power take-off (PTO) system. A simple schematic with a 4-stroke ICE is visualised in Figure 10 below:

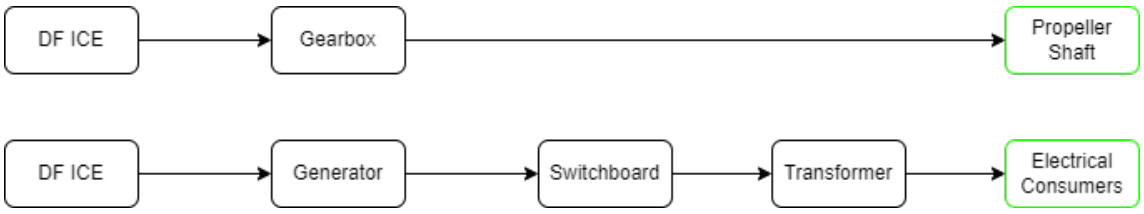

Figure 10: Power plant schematic of a DF ICE powered vessel.

Where the efficiencies for each component, as well as the overall system efficiency, are shown in the table below.

Component	Efficiency [%]
DF ICE	50[1]
Gearbox	99
Generator	96
Switchboard	99
Transformer	99
Overall system efficiency	**46.6**

Table 15: Component and overall system efficiencies of a DF ICE power plant [4].

The sizing of the power generation system can be finally computed by combining the required systems and their efficiencies shown above, with the power demand of the desired design problem.

Tank room

Regarding the tank room for ammonia liquid tanks, the relevant information has been already covered under Section 2.4.6. Type C tanks are chosen and both hydrogen and ammonia are regulated by the same IMO rules of low flash-point fuels, while the design considerations are depicted in Figure 9.

2.6 METHANOL

2.6.1 *Background*

Methanol is the last fuel that is included in this study as another promising alternative option. It is widely considered as the fuel that will make a difference in the maritime sector by playing a major role in the energy transition and the achievement of the GHG emissions reduction/elimination goals [2]. The chemical is being widely used in various sectors, such as in producing plastics, paints, furniture, pharmaceuticals and in the automotive industry; hence, similarly to ammonia, it has solid existing foundations in production, handling and storage. Methanol's yearly production keeps increasing especially in the past few years that it got involved in the energy sector [64, 65]; however, it is still far from occupying a fair amount of the energy share in shipping. The energy consumption of international shipping was as high as 8.7 EJ in 2021 [66], whereas there were only a ~ 107 millions of metric tonnes of methanol produced during the same year [67]. The latter translates to ~ 0.0021 EJ, after using the tabulated values of Table 1.

Similarly to the previously mentioned fuels, the production of methanol is not sustainable yet either. The largest production share belongs to grey methanol; i.e. methanol produced from the combustion of a fossil fuel, which is usually natural gas. It is estimated that using natural gas for methanol production has the same, or even worse than utilising natural gas as a fuel in terms of GHG emissions. There is also the possibility of producing green methanol, by using biomass or sustainable energy in general. Regarding bio-methanol (produced from biomass), the emitted CO_2 upon combustion is considered to be "climate-neutral", and thus not included in GHG. The amount of the emitted CO_2 of a biomass-produced fuel is actually absorbed from the environment during the growth of the new respective amount of biomass [64, 68].

[1] Assumed a 50% efficiency of the DF ICEs due to the vessels' size range of interest, where the (larger) size of engines offers higher efficiencies.

In terms of the hazard risks of using methanol, its main issue is its toxicity. It has a direct impact on human health if swallowed, comes in contact with skin, or is inhaled, and can cause serious illnesses to even death. Methanol also has an effect on the environment in case of a leak, though it must be in very large quantities and will still have a limited impact. This is due to the ability of a range of micro-organisms to cause an enzymatic reaction and oxidize methanol, resulting in rapid biodegradation.

2.6.2 *Energy density*

Methanol is only considered in its liquid form, the properties of which are presented in Table 1. The fuel in this state provides an LHV of 19.9 MJ/kg and volumetric energy densities of 15.8 and 15.5 MJ/litre, for fuel alone and fuel plus the tank's effect respectively.

2.6.3 *Storage*

Conditions

The storage of methanol is the simplest to safely implement on board a vessel. This is due to methanol naturally being in liquid form in ambient conditions of 1 bar and 20 ^{o}C as shown in Table 1.

Tank type

Due to the mild storage requirements of methanol, it is possible to store it in conventional integral liquid tanks that are part of the ship's hull structure. It is necessary, however, to ensure appropriate leakage precautions are taken in order to inhibit potential accidents. In this way, the whole storage and distribution system of methanol is significantly more complex than that of MGO, by being enhanced with a range of monitoring and control systems [68, 69].

2.6.4 *Regulations*

Once again, methanol is also covered by the same IGF Code guidelines for tank location, fire hazard protection and tank filling limit as ammonia and hydrogen (Section 2.4.4). However, the American Bureau of Shipping (ABS) has released guidelines specifically covering the application of methanol and ethanol application on vessels [70]. The integral tanks are specifically addressed and it is highlighted that the tanks:

- *Need to be surrounded by protective cofferdams unless the tanks are bound by shell plating under the lowest possible waterline, other fuel tanks (containing methyl/ethyl alcohol), or fuel preparation space.*
- *Should not be located closer than 0.8 m from the ship's side when they are located on the deck.*
- **Fire integrity**:
  - (i) *Should be separated by a cofferdam of 0.6 m (minimum) from category A and high fire risk spaces.*
  - (i) *Be protected with at least A-60 class insulation.*

2.6.5 *Power generation*

ICE

Power generation from methanol can be successfully achieved with ICEs in both mono- and dual-fuel setups. Ideally, methanol can be utilised in mono-fuel SI engines as it possesses a high octane[7] number, and thus a high knocking resistance. Nonetheless, the majority of the ships use CI diesel engines, for which methanol alone is not the optimal candidate. It has a very low cetane[8] number (~3), which is approximately 15 times lower than that of diesel (40-55).

Lastly, methanol's specific CO_2 emissions are rather high but still lower than those of gasoline; besides, in the case of bio-methanol, it can be considered CO_2-neutral as mentioned before [65]. The full emissions caused by the combustion of methanol are summarised in the following table.

Compound	Emissions [g/MJ]
CO_2	69
CH_4	0
N_2O	0
NO_x	0.4
SO_x	0

Table 16: Emissions from the combustion of methanol in marine engines [68].

Note, CH_4 (methane) and N_2O are in such small concentrations that can be assumed negligible. Similarly, methanol has such a low concentration of sulphur that SO_x emissions can also be assumed negligible. Tests on marine engines by the leading manufacturers showed that there are approximately 60 and 40 % reductions of NO_x compared to when the tested engines were running on HFO (Heavy Fuel Oil) and diesel, respectively [68].

For these reasons, methanol as an ICE fuel can be fruitfully implemented on board vessels in DF engines with diesel. Such engine setups are feasible in the four following scenarios [71]:

1. Fumigation concept: methanol is mixed with the charge in the intake and then the pilot fuel (diesel) is injected into the cylinder to ignite the mixture.
2. Premix the two fuels and use a single injector to pour the mixture into the cylinder.
3. Use a single dual direct injector with separate channels and inject both fuels simultaneously but individually.
4. Use two direct injectors, one for each fuel.

All of these methods are valid and can be used, or are already being used in marine engines. They differ in their advantages/disadvantages of course; hence, each can be better suited to different situations. The important part is that such ICEs are capable of offering operations and efficiencies equivalent to those of conventional fossil fuel engines, though with an evident reduction in GHG emissions. The mentioned dual-fuel solutions are ideal as a transition step for limiting the environmental impact until more sustainable solutions are available. SI engines running on bio-methanol could be one of the long-term alternatives with a proven increase in efficiencies too;

[7] The measure of a fuel's ability to resist engine knocking during combustion, which is caused by the air/fuel mixture's premature self-ignition in the engine.
[8] The measure of the performance of diesel fuel, by measuring the delay in the ignition time of the fuel; the higher the number, the better the combustion.

but such setups are not yet commercially available in the maritime industry, unlike the dual-fuel diesel/methanol ones [71]. More specifically about the commercial availability of the DF ICEs running on methanol, Wartsila has officially released the *Wartsila 32 Methanol engine* [72]. This engine is capable of running either in combination with diesel or completely on diesel. Finally, there is also the potential of using pure methanol ICEs in SI setups, that do not require a pilot fuel. Nonetheless, such engines are still under development and are currently in the early experimental stages [73].

In terms of feasible blends of methanol with diesel, the extensive review of Saxena et al. [74] showed that most experimentations have been conducted for up to 20% methanol content, while none of them has gone higher than 60%. The effects on emissions in each experiment showed great fluctuations, meaning for methanol/diesel blends the operating conditions, as well as the setup, affect the entirety of emissions. Overall, this review concluded a decrease of NO, CO and HC emissions, and NO_x that decreased in low speeds, and increased in high speeds. Furthermore, the experiment of Dierickx et al. [75] tested blends of up to 80% methanol content, and demonstrated overall reducing trends for NO and NO_x and increasing trend for NO_2 for up to 60% methanol contents.

Fuel cell

Similarly to the previous relevant sections of ammonia and hydrogen (Sections 2.4.5 & 2.5.5), once again only the PEMFC and SOFC systems are considered. It was also found that PEMFCs are ideally fuelled directly by hydrogen, or indirectly by a hydrogen carrier (such as methanol) by adding the necessary conversion systems. On the other hand, SOFCs can be directly fuelled by a range of options including methanol; hence, it is preferred to consider the SOFC as it is less complex to have a direct fuel.

Summary on power generation system for methanol

Similarly to ammonia, it is concluded that DF ICEs of methanol plus diesel will be implemented in the SSDG due to having the highest TRL and offer a significant reduction in harmful emissions. The alternatives of pure methanol engines and SOFCs [42] are highly potent and can have a greater impact on GHG emissions, but they are not yet at a sufficient TRL to be further considered.

2.6.6 *Engine and tank room*

Engine room

The engine room description for a DF ICE running on methanol can be considered the same as the one visualised in Figure 10 with the same system efficiencies as in Table 15. Once again the sizing of the power plant is finalised by combining the components and their efficiencies with the demanded power for the desired vessel.

Tank room

The tank room description for methanol is the simplest among the chosen energy carriers. It is not necessary to further define integral box-shaped tanks for early-stage design, as long as the design complies with the applicable regulations. The following schematic is used to visualise the design considerations for the integral methanol tanks.

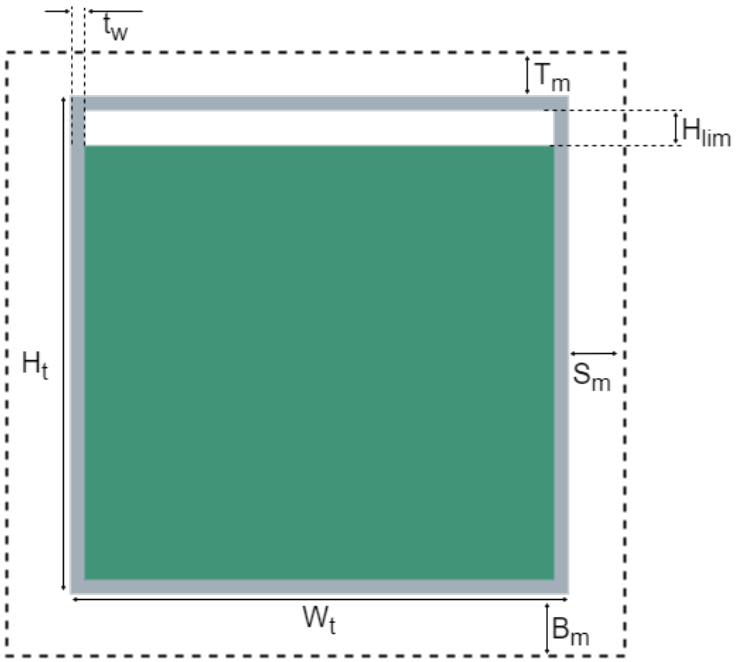

Figure 11: Schematic of the tank room for integral methanol tanks.

Where,

- H_t = Total height of tank
- W_t = Total width of tank
- H_{lim} = Filling limit of tank
- T_m = Top margin distance between tank and top deck
- S_m = Side margin distance between tank and inside of ship's hull
- B_m = Bottom margin distance between tank and inside of ship's hull
- t_w = Wall thickness of tank

It is important to remark that the above specifics for the location of the methanol tanks are not to be consistently applied for all boundaries in all cases, but only when the existing regulations (Sections 2.4.4 and 2.6.4) instruct the use of cofferdams.

2.7 SUMMARY OF DECISIONS ON ALTERNATIVE ENERGY CARRIERS

The overview of the shortlisted fuel options that are presented in this chapter contains all the relevant information on implementing them on ships. The comparisons between the fuels aided in the development of an understanding of their relevant performance, as well as justified the selection of the four options. The table below presents the decisions on implementing the chosen fuels based on performance and current technological advancements.

Energy carrier	State/Type	Tank type	Power generation
Batteries	Li-ion	-	-
Ammonia	liquid	Type C	DF ICE
Hydrogen	liquid	Type C	PEMFC
Methanol	liquid	Conventional	DF ICE

Table 17: Summary of decisions on the application of fuels in the generator.

3

SHIP DESIGN GENERATORS

This chapter aims to introduce the state-of-the-art advancements in methodologies and techniques used in ship design generators. This is achieved by exploring developed frameworks with different approaches on early stage design, but with the same goal of optimising the ship design process. The investigated frameworks include Charisi's and Kao's master theses on KBE [76, 77], design building block approach [78], Vessel.js [79], packing approach [80] and modularity approach [81]. These frameworks were shortlisted due to their deeper focus on generating general arrangements and/or parametric models. Each of them presents a different state-of-the-art approach and can trigger the development of a methodology with a combination of their key elements. At the same time, there is a lack of existing studies that integrate a range of alternative energy carriers in early-stage design generation. The chapter is concluded with a closing section highlighting the main findings of this investigation, followed by a summary of the identified literature gap.

3.1 ADVANCEMENTS IN THE FIELD

Ship design in preliminary stages can be approached by either top-down or bottom-up methods. The former consists of data derived from formulas, regressions, previous designs or parametric designs of existing design solutions such as in the work of Roh and Lee [82]. This methodology offers consistent and practical products with decent time and cost efficiency since the generation of a new solution is derived based on empirical knowledge of equivalent problems. In most cases, this approach does not promote innovation as its fundamental principles are biased toward existing designs. On the other hand, the bottom-up method is linked to certain key elements and systems that have a direct qualitative impact on different design stages. Bottom-up allows the presentation of different vessel division approaches and allows for the development of the understanding around the vessel from different perspectives. This approach was implemented in renowned methods such as the System-Based Ship Design (SBSD) [83], and the Design Building Block (DBB) [78]. On the downside, bottom-up methods lack the security of stepping on an existing foundation of empirical knowledge, hence derived solutions come with higher uncertainty and/or increased development time. It is visible that top-down methods are not useful for the purposes of this study, since the main objective relates to the lack of knowledge on the effect of the shortlisted alternative fuel option on early-stage design. However, there are also Data-Driven Ship Design (DDSD) methods as analysed by Gaspar [84], that are capable of combining top-down with bottom-up. The idea revolves around extracting data from the value chain all the way from concept to operation, which is then studied under the three distinct layers of overall standards, third-party choices and proprietary data. The commercially available DDSD-based Product Life Management (PLM) tools offer the mentioned integration of top-down and bottom-up; though their main drawback is that they mostly offer limited user freedom regarding customisation of libraries or calculations [79].

3.1.1 *Knowledge Based Engineering (KBE)*

KBE "*is a comprehensive application of artificial intelligence in engineering*" [85]. It is a method of automating repetitive design tasks of a product development process, by identifying, transforming and reusing engineering knowledge relevant to both the product and the process. The principles of KBE lie in storing the relevant engineering knowledge, before utilising it in a "*formal, well-documented, repeatable and traceable process*". A KBE-based framework comprises a dynamic network of classes and objects in which the knowledge (of both product and process) is modelled through a diverse range of rules [85, 76].

One of the identified design generators is the parametric modelling tool that was developed by Nicole Charisi as part of her thesis project [76]. The tool was developed based on KBE and High-Level Primitives (HLPs)[1] were utilised in order to apply this technique in early-stage ship design. As part of the process of creating the said tool, a series of steps were determined and formed a more generic methodology.

1. **Identification of the design requirements**: Determination of the requirements (such as DWT, speed or building cost) and lead to the corresponding input variables of the tool, which will then define the different design solutions in each scenario.

2. **Main drivers analysis**: Mostly depends on the vessel type, as it is carried out to determine how the vessel will be parametrised. This step is when the building blocks are decided and converted to the HLPs.

3. **Qualitative description of the HLPs**: Ensure space reservation for the development of the vessel's geometry, while the qualitative description is also used as the driver for the mathematical representation that follows.

4. **Mathematical representation of the HLPs**: Developed following up on the previous step, including an analysis of the relations between the HLPs, before the vessel's architecture is generated.

5. **Define the HLPs for each "total ship" architecture**: HLPs are drawn from the vessel's toolkit and are combined to form the "total ship" architecture, based on the decisions of the user. The various design combinations of the HLPs define the different design solutions and form the design space of the investigated scenario.

6. **Tuning the HLPs to fit the design problem**: The chosen HLPs are tuned to match the needs of the desired problem, where the design requirements are used as the guidelines to ensure the suitability and feasibility of the end product.

7. **Extract and evaluate the geometric model**: The end product of the mentioned framework is visualised on a 3D CAD software. Additionally, preliminary level weight and stability computations are performed in order to ensure a level of technical feasibility.

These steps were further organised into three "design process blocks" with elaborated sub-steps for each procedure. More specifically, the first block consists of the definition of inputs and HLPs, as well as accessing the available databases to introduce the relevant knowledge into the framework. The second block includes the tuning of the HLPs, where with some simple computations performance was monitored, and the model was then refined by returning the HLPs.

[1] Specifically developed classes of objects in the context of a design process [86]; i.e. educated building blocks in this context.

Lastly, the third block is where the final refinements are executed if necessary for ensuring the solution's technical feasibility. When the latter is secured, the script generates the final 3D solution. The developed generator was also tested on a case study of an LNG (Liquid Natural Gas) bunkering vessel, and one of the resulting geometries is presented below:

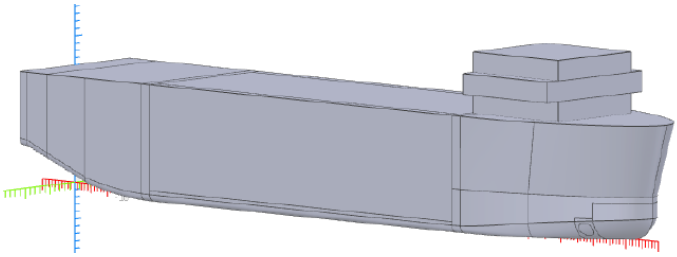

Figure 12: Resulting 3D geometry of the tested LNG bunkering vessel [76].

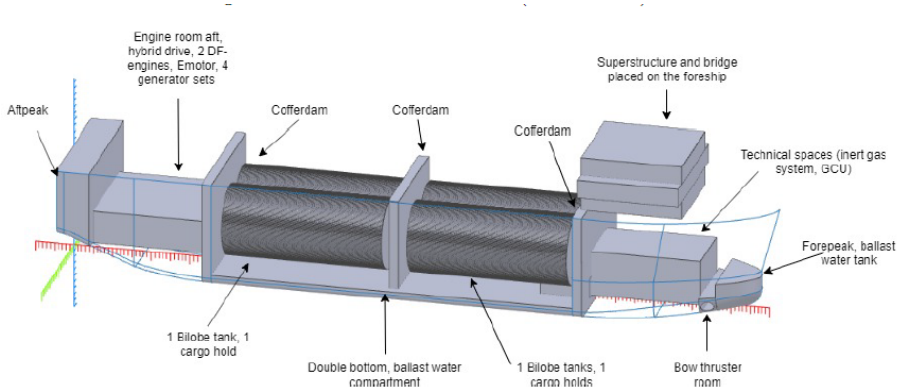

Figure 13: The resulting geometry of Figure 12 revealing the sub-components of the generated solution [76].

This methodology for the development of the said parametrisation tool was developed on Python, before integrating it with NAPA to create the 3D models that are displayed in Figure 13. The end product of this study manages to successfully create early-stage technically feasible design spaces for the desired problem and provides the user with the opportunity of analysing and comparing the 3D models before making the final decision. The presented methodology can prove highly useful towards the development of design generators with similar intents. Nonetheless, in the case of the generator that is aspired in this project, adaptations are necessary. This is mostly due to the integration of alternative energy carriers, and the desire of allowing the user to study design variants with each fuel option.

This work was mostly inspired and guided by relevant research in the aerospace field since KBE has been deployed and extensively investigated there for years. An example of this is the Multi-Model Generator (MMG) which is a KBE application and was developed as part of the Design and Engineering Engine (DEE) framework. The DEE is essentially consisted of a range of multidisciplinary tools that exchange information with each other and ultimately generate an educated design solution for an aircraft in early-stage design. The MMG is the tool that generates a design space with parametric models tailored to the desired solution, which it then feeds to the analysis tools [87].

A similar approach was studied by I-Ting Kao, as he developed a "*Parametric Multi-Modular-Ship-Model Generator*" [77]. This work was also based on KBE and was majorly inspired by DEE as well, but also integrated some modularity principles (elaborated further in subsection 3.1.5). Kao's tool was developed to generate both a parametric model of the hull and a block-based layout. This was

done in order to allow studying both simultaneously, by using the parametrised hull geometry as a boundary limit for the block layout. Additionally, the layout generator was assigned two stages: the modular section and the working deck layout. The flowchart of the generator's layout is shown below as presented by I-Ting.

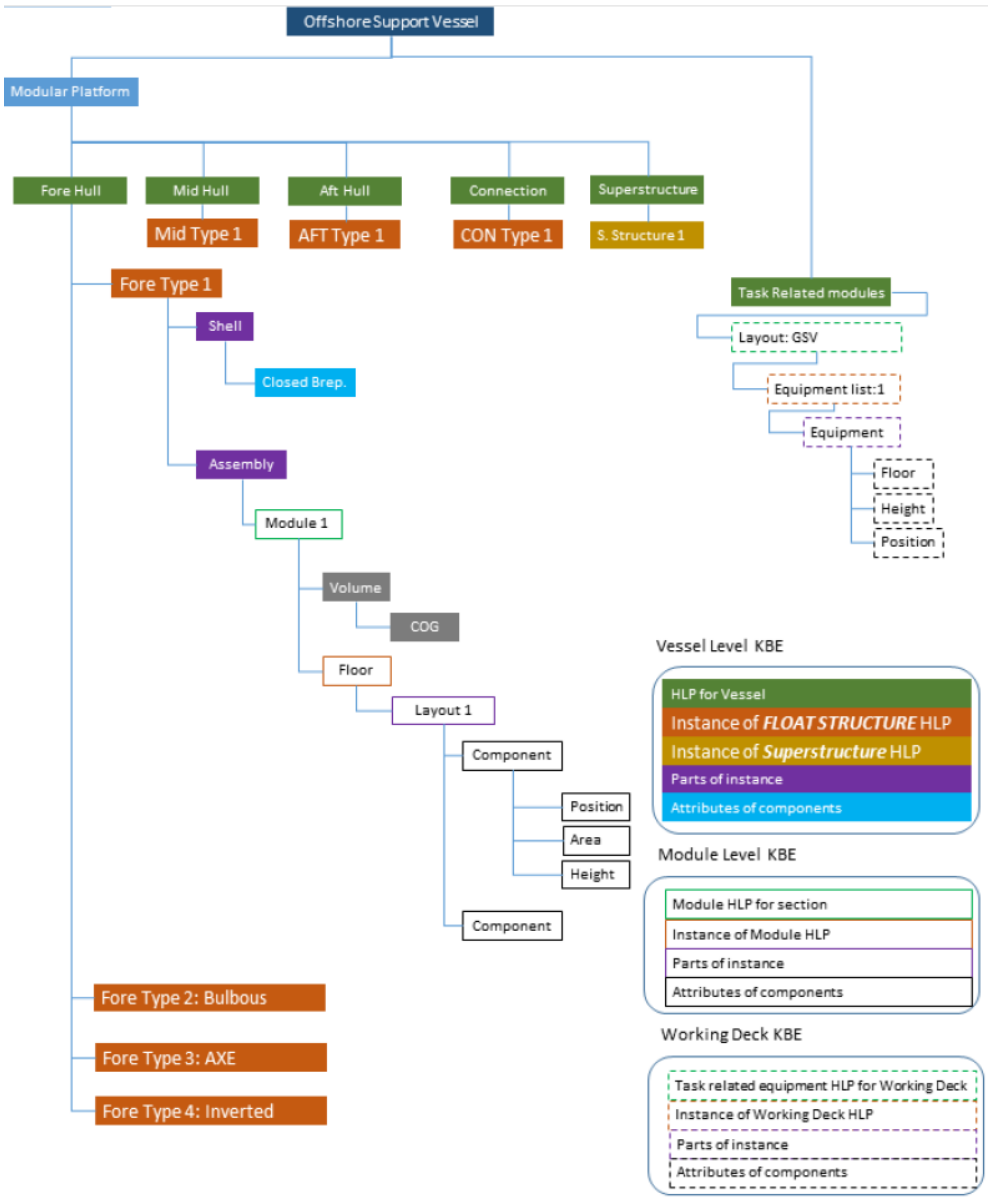

Figure 14: Resulting 3D geometry of the tested LNG bunkering vessel [77].

The branch "*Task Related Modules*" on the right side of Figure 14 refers to the layout generator, and everything else to the hull generation and parametrisation. The hull generation is performed based on the available predefined options for each section, such as the different fore types. Of course, this framework is tailored to the desired application of modular Offshore Support Vessels (OSVs); i.e. decision-making revolves around the desired role of each vessel. The user can input the type of the OSV (e.g. a Construction Support Vessel - CSV) and the generator draws from the defined database of functions and modules. Eventually, the performance of the tool is evaluated with the successful replication of some existing OSV paradigms. This evaluation was achieved by implementing the framework on Grasshopper and visualising the 3D results on Rhinoceros, with the following sample CAD results shown in Figures 15a and 15b.

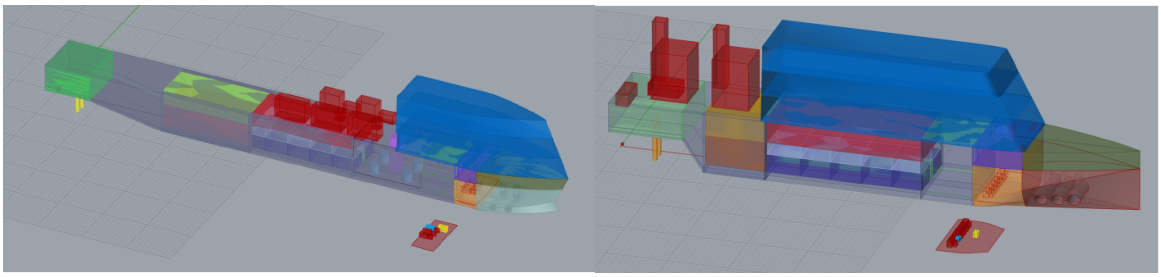

(a) Diving Support Vessel (DSV) (b) Cable Laying Vessel (CLV)

Figure 15: Final CAD models displaying the replication of two existing OSVs [77].

Although the framework of I-Ting Kao diverges from the purposes of this study with its deeper focus on modularity and OSVs, the core ideas of developing the generator can prove useful. More specifically, the main point of interest is the utilisation of KBE in both the parametric hull generation and the layout arrangements. These two "branches" of the generator are defined by the major vessel HLPs (forehull, midhull, afthull, connection, superstructure and task-related modules), which are further refined by case-specific HLPs with decision-making based on the relevant purpose of the vessel.

3.1.2 *Design Building Block (DBB)*

Another approach to early-stage design was offered by Andrews and Pawling with their implementation of the DBB approach [78]. The main feature of interest in this method is the "*functional breakdown*" of the design. This means the design is organised in functional groups that hierarchise a set of design steps each. Each step is represented by a building block and defines the components or systems of the vessel. The UCL[2]-based development of this methodology has its foundations in the inside-out (or bottom-up as mentioned earlier) designing approach. The fundamental idea was to create the design of the vessel starting with the interior spatial disposition and then iterating for ship weight and displacement, as well as hull dimensions and form. This means that an initial approximation of the interior arrangement with adjacency preferences can be generated first, before converting it into deck allocations for key components and functional systems/equipment. The said layout can be built at a preliminary level prior to having a specific hull form enclosing it. An example of such an internal layout block synthesis is provided below in, as well as an example of a finalised block design including the hull form, in Figures 16 and 17 respectively.

[2] University College London

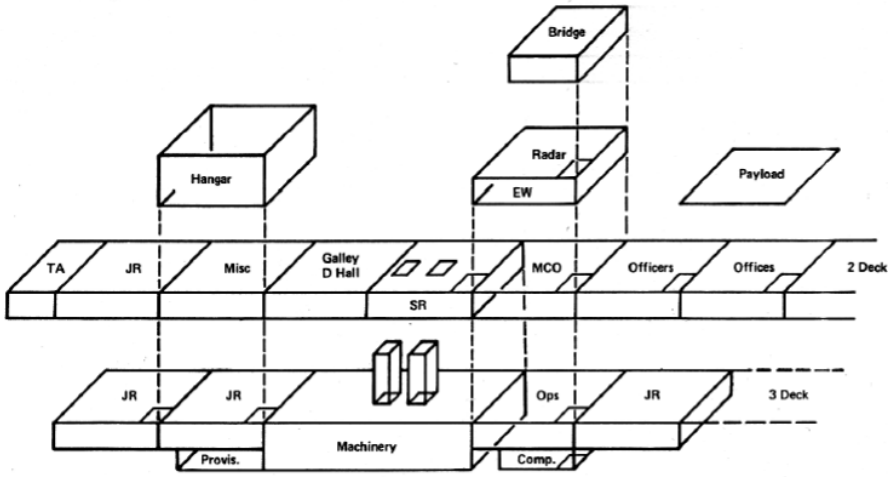

Figure 16: Block synthesis of a frigate using the DBB inside-out design approach [88].

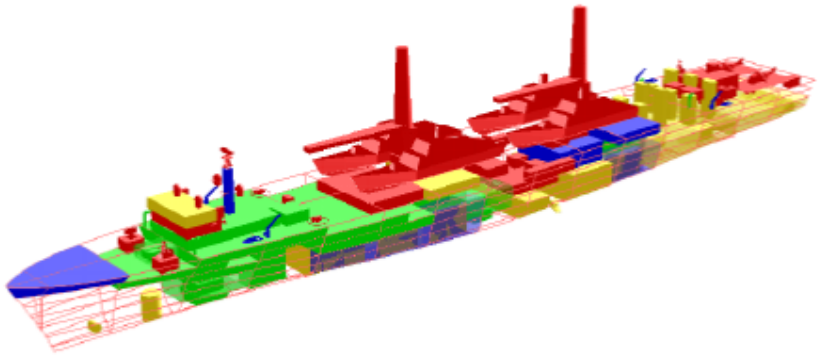

Figure 17: Resulting 3D block design of a vessel including the hull form [88].

The methodology and the respective derived tools have been extensively researched and implemented in numerous ship design cases at UCL. It is, therefore, a proven methodology that allows the naval architect to not only derive designs more efficiently but to also address wider "*Style*" decisions beyond the traditional issues (speed, stability, strength and seakeeping), as Andrews describes. Note, style in this context refers to case-sensitive topics such as sustainability, human factors or protection, that are usually studied at a later design stage. Additionally, the DBB approach allows for the integration of Simulation-Based Design (SBD) to investigate the problem on more levels before the hull geometry parameters are fixed. For example, the designer is able to study the effect of human factors such as crew comfort or efficiency, that have been traditionally overlooked at the preliminary stage. As mentioned earlier, such bottom-up approaches are lacking in the foundation of knowledge in order to avoid the bias of previous solutions. Nonetheless, this is not necessarily a drawback in the context of this study, since unbias is desired and the lack of complete empirical information around alternative fuels is a fact.

3.1.3 *Data-Driven Ship Design (DDSD)*

One of the most interesting implementations of DDSD is found in the work of Henrique Gaspar on the development of "*Vessel.js*". Vessel.js is an open-source[3] ship design library developed on JavaScript (JS). Regarding the underlying methodology, one of the fundamental pillars of this framework is the "*inheritance concept*". Object-based languages[4] like JS allow for the modelling of the vessel as an object, that inherits properties and functions from special objects, the prototypes. Moreover, in such languages it is possible to "*encapsulate*"; i.e. to assign functions in an object in a way that they cannot be accessed by other applications. In this way, certain properties and functions can be specific inside the boundaries of the object. This translates to the vessel and its subsystems being expressed as objects within objects and described by global and customised properties and methods. The global ones refer to the properties that are pre-defined within the library, while the customised ones can be adjusted to fit each problem. The appropriate definition of the object can then allow for proper analyses (computations, simulations and visualisations). A simple example of modelling the ship as an object and assigning its properties and methods is displayed in Figure 18.

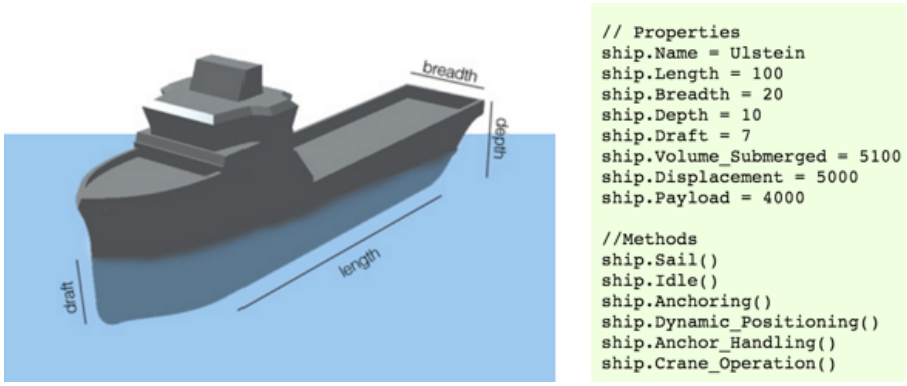

Figure 18: Example of a vessel modelled as an object, along with some basic properties and methods [79].

The above description of the object-based modelling of the vessel is based on the idea of having a virtual prototype model that is consisted of the three models of entities, states and processes. The *entities* include the physical and logical parts of the design relating to the basic structure and geometric properties of each component. Then, the *states* are reflecting on the way that each entity reacts when an internal or external change is triggered. *Processes* are responsible for integrating entities and states in the long run, where different conditions cause a number of different *states* to accumulate [89]. It is understandable that the *processes* proportion is somewhat irrelevant to this project, while it is also initially overlooked by the author; hence, the structure of the framework presented below (Figure 19) tackles the *entities* and *states* proportions.

[3] Readily available online for anyone to access, use freely and collaboratively develop further through the users' feedback and recommendations

[4] Computer programming languages that revolve around the concept of an object, where the concept of a class (description of an object) is substituted by constructs for the creation of individual objects.

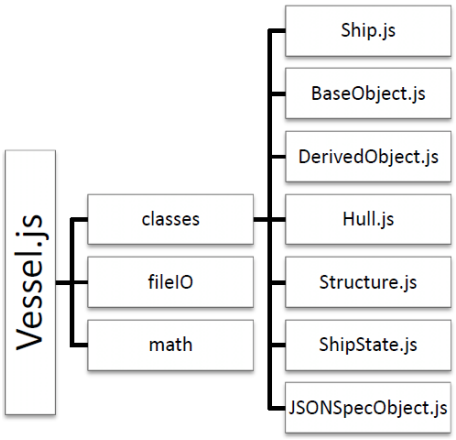

Figure 19: Structure of the vessel.js framework as presented by Gaspar [79].

It is visible that the main component of the framework is the "*classes*", which include entities and internal states and handles the majority of the vessel design information. Then, "*fileIO*" refers to the functions of file management and exchange, such as loading or downloading an existing ship file. Lastly, "*math*" consists of a library that performs all the formulas and regressions for the analysis and evaluation of the design, such as the hull resistance using the Holtrop model[5]. A further insight on the "*classes*" constituents is offered below:

- **BaseObject.js**: Constructs the library containing the systems and subsystems of a ship, excluding the hull and the structure. It may contain as a base object from a tank to a whole machinery room and serves as the foundation to derive the case-specific objects. For example, a given type of tank is defined by fixed properties for height, volume, lightweight and 3D model, and it can then be used multiple times with various content types and locations inside the vessel.
- **DerivedObject.js**: Contains the classes for each individual component that is derived from the ones in the *BaseObject.js*.
- **Hull.js**: The geometry of the ship's hull, including some standard methods to calculate significant properties such as volume, displacement and coefficients. Additionally, it carries methods of computing the metacentric height (GM) of the ship to be used in 3D rendering within a realistic environment.
- **JSONSpecObject.js**: Used to load or export objects in JSON[6] format, for objects that are derived from a literal object.
- **Structure.js**: Objects relating to the structural integrity of the vessel, such as the decks or the bulkheads. It handles the structural analyses of the model in longitudinal, transversal and local perspectives.
- **Ship.js**: Constructs the model of the ship using the definitions of the previously mentioned classes. It, then, collects and performs the analyses specifically for the defined vessel (e.g. the mentioned GM computation using both the hull (hydrostatic) and objects' (weights) properties.

[5] Holtrop and Mennen's method: A model for the computation of a ship's dimensional total resistance
[6] JavaScript Object Notation: a standard text-based format for representing structured data.

- **ShipState.js**: Implements different ship states for simulation purposes. Such states relate to either simple effects such as changing fuel levels, or complex states of using a DP system and simultaneously checking the state of tanks or the engine.

The framework of *Vessel.js* is developed on JS with the aim of being a web-based open-source library, and there are several aspects of the implemented methodology that heavily depend on it. Additionally, the generator is an all-around tool with a range of computation and simulation libraries. However, by overlooking the irrelevant material and observing the greater picture of the methodology, fruitful information can be drawn. These relate to the philosophy of which sequence is followed in order to construct the end product, as well as how the different objects are defined, refined and related to each other.

3.1.4 *Packing Design Approach (PDA)*

This part refers to the work of Bart van Oers towards his dissertation, in which he utilised the mathematical approach of "packing problems" in order to solve the problem of generating early-stage designs [80]. Geometric packing problems, such as this one, deal with positioning geometric objects in a way that all of them overlap completely with a greater positioning space (the vessel in this case), and then the said positioning prevents undesired overlap among the objects.

The study can be summarised into three main aspects: "*the parametric ship description*", "*the search algorithm*" and "*the selection approach*". The parametric ship description is the foundation of the design proportion since it defines and adjusts the systems and their configuration on the vessel. The ship is modelled using a selection of geometrical objects that cover all the necessary systems, and are organised into seven categories: envelope, subdivision, hard, soft, free space, connection and logical. These categories as well as the objects within them are pre-defined, and thus during the designing procedure, the desired objects are drawn and assigned properties based on the user's input. Once this is completed, the objects are packed in the positioning space following the category sequence that is displayed above. In this case, the positioning space is box-shaped and has dimensions large enough to fit the ship well within its walls. In addition, depending on the object type, they either adapt their shape (such as the "soft" objects) before repositioning, or they are directly repositioned.

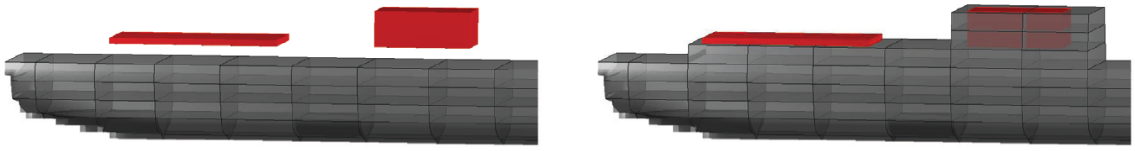

Figure 20: Adapting the envelope to support and enclose new objects [80].

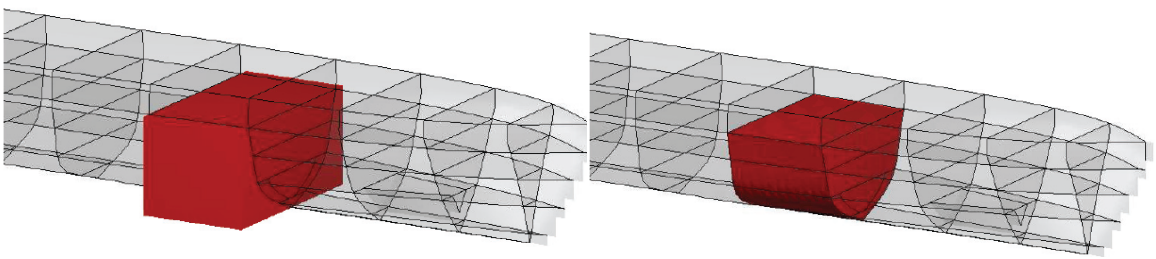

(a) Initial shape of object (b) Adjusted shape to fit in envelope

Figure 21: Adaptation of a new soft object's shape in order to fit within the envelope [80].

Figure 20 shows how two blocks, that are placed above the current shape of the hull, force the reshaping of the envelope to enclose and support them. Figures 21a and 21b demonstrate an example of a soft object that is initially box-shaped with certain properties but is then reshaped to fit within the hull, though maintaining its properties.

The last significant component of this procedure is the overlap rules, which ensure the realistic positioning of the individual objects. This is the aspect that detects infeasible positioning and determines the mandatory design changes. The packing procedure is then terminated once all objects are packed with no overlap detection, or when there is no available space left to fit everything. Eventually, the envelope shape (hull plus superstructure) is finalised by efficiently wrapping around the object arrangement and excluding redundant empty spaces. Note, the most crucial step of the process is the overlap management every time the envelope is updated. Major envelope changes affect the relevant positioning of objects; hence, the positioning space needs to be updated accordingly in order to accommodate the new feasible and prohibited areas. Complexity grows higher considering that each object has different adjacency requirements, such as access to free space, or the need to be enclosed by the envelope. Regarding the aspect of the *search algorithm*, it concerns an optimisation algorithm that is deployed for the single-objective optimisation towards packing density. It essentially converges the model generation to densely packed solutions, as long as they maintain standard technical feasibility qualities (e.g. stability or speed). Finally, the *selecting designs* part simply describes the decision-making of the designer to conclude the final solution. This comes as a product of particular case-specific features (such as manoeuvrability) combined with the engineering judgement of the user. Of course, the developed tool provides support in finalising the model's features through extensive analysis of the models within the generated design space. An example of the framework's output is depicted below.

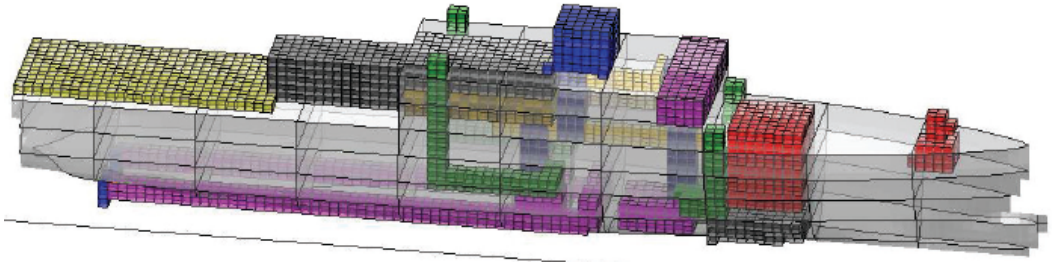

Figure 22: Sample ship design output of the packing approach, showing the first solution of a frigate design problem. [80].

The model of Figure 22 is the *original* design of the investigated case, from which a range of variations are derived. The novel ship design approach analysed in this section presents a complete tool for generating early-stage ship designs before guiding the user to reach the final decision. This is done through the chosen KPIs that are simply analysed, instead of used as optimisation objectives. The KPIs' data are plotted and provided to the designer in order to shortlist the design space. It also highlighted how the objects need to be predefined and identified as one of the existing object categories that the code knows how to handle. Although the framework touches on covering the entire procedure of early-stage design, the mentioned qualities of its methodology can prove useful towards the development of the SSDG.

3.1.5 *Modular Design Approach (MDA)*

Modularity can be summarised by the following statement of Schilling: "*The primary action of modularity is to enable heterogeneous inputs to be recombined into a variety of heterogeneous configurations.*" [90]. It is targeted to aid the analysis of systems into re-combinable parts - the modules (or blocks) - and then the said system can be reconstructed using different combinations of the existing modules. In principle, four different types of modularity have been defined, concerning the interface as well as the platform that is used. The modularity types are provided below as presented by Erikstad and Choi.

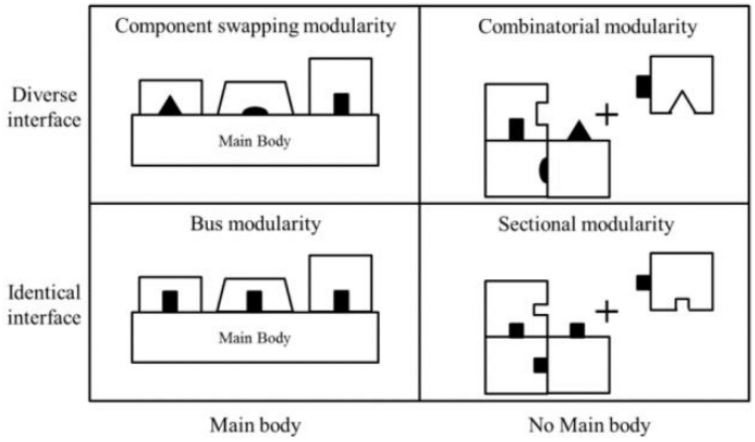

Figure 23: The four types of modularity as described by Erikstad and Choi [91].

Component-swapping modularity consists of a main body with which the modules interface independently with individual slots. Modules might share common interfaces locally, without implying any global restrictions in any way. Similarly, *combinatorial modularity* shares the same independence in interfaces, which can accidentally be locally common in some instances. However, this time there is no main body to carry the modules, and they interface with each other. Such inter-module interaction is also implemented in *section modularity*, where in this case there is a global interface to be shared by all the connections. Again, there is the option of having a main body that carries the chosen modules, though with globally applied interfaces, using the *bus modularity* alternative [92, 91]. The most fundamental method, that can be used for ship design purposes, is the *component swapping* option, as the ship serves as the main body on which a range of modules can be placed with different interfaces.

Modularity in ship design is explored in this paper through the work of Lagemann and Erikstad "*Modular Conceptual Synthesis of Low-Emission Ships*" [81]. The first step is to map the design process using the $\texttt{Requirements} \rightarrow \texttt{Functional} \rightarrow \texttt{Logical} \rightarrow \texttt{Physical}$ model. Once the end product requirements are known, the essential functions are defined in order to ensure the said requirements are satisfied. Finally, the functions are related to the physical principle systems of a ship, before being further organised in sub-systems depending on the required refinement level. An example of such a mapping is provided below, as presented in the case study of Lagemann and Erikstad.

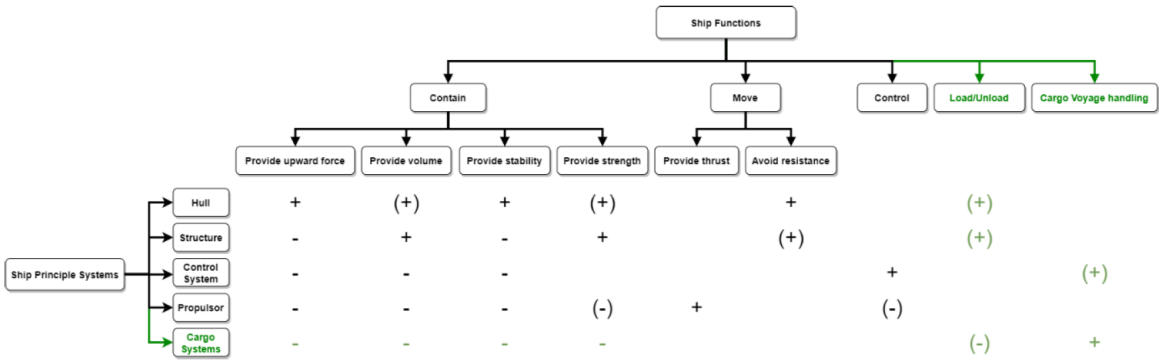

Figure 24: Proposed design process mapping for a RoRo cargo vessel [81].

Where,

- + : strong connection
- - : weak connection
- *gap* : no connection
- *()* : can be skipped for later design stages

Note, the green-coloured functions/systems are case specific, while the rest are generic for any vessel type. It can be seen that there are functions that are influenced by all the systems (upward force, stability and strength), and these interactions can be modelled using "*bus modularity*". On the other hand, there are interactions where a particular ship function is only relevant for a specific system. In the example of the "propulsor", there is a single relevant interaction to "provide thrust", which also requires secondary systems in this case. One of the potential design solutions could implement an electric motor as a prime mover, and batteries for the energy provider. However, there can be a number of different combinations for providing the said solution, which combinations eventually do not add to the value of the ship as an "*integration platform*". For this reason, *component swapping modularity* and *combinatorial modularity* can be utilised more effectively, in order to connect an overall function to appropriate logical entities (model as sub-system) and link the various logical entities on an equal hierarchical level (model as input), respectively. Additionally, the functions can be perceived as "*discrete modular entities*" with certain inputs and outputs. They can, then, be further refined by assigning *controls* (function requiring a logical entity) and *mechanisms* (logical entity specific sub-functions) at the *parent* and *child* levels, respectively [81, 93, 94]. Consequently, the concluded representation and method of combining logical systems are illustrated below.

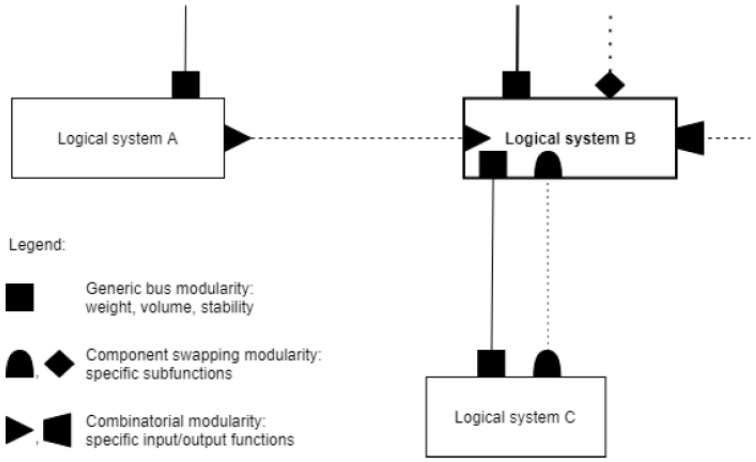

Figure 25: Proposed representation combination method of logical systems as proposed by Lagemann and Erikstad [81].

Finally, the developed logical system topology can be translated into a tangible design solution by converting the analysed logical entities into physical systems. These physical systems are essentially modules that consist of parametric descriptions and can be adapted to fit different applications.

The described principles of this study's methodology on defining a *modular synthesis model* were exploited with the aid of *Vessel.js*, which is analysed in section 3.1.3. This means that the analysed modularity framework was implemented on JS, and then coupled with *Vessel.js* to visualise the 3D models.

This framework does not suggest a methodology towards the development of a design generator, rather "*it could be a small brick within a larger, holistic design process*" as the authors state [81]. The proposed methodology triggers a different perspective compared to the previously mentioned studies; one that deals with the interaction between functions and systems as logical entities, before translating them to physical, scalable modules. These interactions are studied based on the level of relevance between a system and the defined functions. These are elements that can be definitely considered when establishing the foundations of the SSDG, adding value to the diversity of potential options. Nonetheless, the said value is limited to the relative position of modules and the general arrangement, while there is no contribution to the parametric hull generation.

3.2 SUMMARY OF FINDINGS

The summary of this chapter is presented below by tabulating the highlights of each explored methodology, focusing on the aspects most relevant towards the development of a design generator.

Study	Key takeaways
Charisi's thesis [76]	• provide minimal support regarding a given degree, smoothness, and domain partition • succinct and highly relevant steps for the development of a design generator • perceive blocks as HLPs • organise design process in greater blocks of relevant sub-tasks
Kao's thesis [77]	• KBE in both parametric hull and general arrangement generation • combine KBE with modularity principles
DBB [78]	• emphasises on bottom-up methodology • functional breakdown of design problem • spatial disposition of systems before wrapping hull around them
Vessel.js [79]	• organise design in classes with clear execution hierarchy • each class performs certain tasks and includes relevant computation methods • sequence: systems → general arrangement → hull
Packing [80]	• categorise blocks in different types • definition of overlap rules • single-objective optimisation for packing density • analysis of design space over a range of KPIs
Modularity [81]	• perceive blocks as logical entities instead of objects • modelling approach: Requirements → Functional → Logical → Physical • map relations between systems and functions with relation levels • create the layout of the logical entities and then convert to physical modules

Table 18: Key takeaways of the literature study on the design generators of Chapter 3.

3.3 IDENTIFIED LITERATURE GAP

It is evident that none of the above frameworks have directly addressed the four pre-selected energy carriers that are considered in this study in a non-biased manner. Bias in this context refers to pre-selecting a single energy carrier as the expected best fit for a problem. Instead, there is a deeper focus on the methodology of tackling the parametric hull and general arrangement generations, with standard, conventional energy carrier options. Several attempts have been made to compare and approximate the performance of the prevailing alternative carriers against the conventional ones, such as the work of Mckinlay et al. [95]. Nonetheless, this study is limited to investigating the design and cost implications for a fixed power output and was aimed to draw more generalised conclusions for long-haul shipping.

4

PROPOSED METHOD & TOOL

This chapter is aimed to merge the major findings of the two previous chapters (Chapters 2 & 3), into one generalised methodology. The method is aspired to guide the development of the SSDG or equivalent tools and will be elaborated through a series of requirements and steps. Next, the second part is focused on the specifics of the implementation of the said steps in the process of creating the SSDG.

4.1 METHOD

4.1.1 *SSDG requirements & decision making*

This section presents the defined requirements of the tool that are aimed at ensuring all the necessary goals are achieved.

1. Different design spaces are generated independently for each integrated alternative energy carrier option.
   → Each solution for the different carriers is generated and evaluated independently, before comparing the optimal solutions to each other.

2. A certain order of specifying and placing the HLPs is followed, based on the main point of interest of each study. In this case, the power generation room is configured first, then the cargo hold and the remaining space defines the energy storage room that is located between the two.
   → Hierarchy is important in order to both limit the potential general arrangement solutions and emphasise the desired aspects of the design as directed by the user inputs. This is due to having a fixed arrangement instead of exploring different variations. For this reason, firstly the cargo hold is defined and placed on the fore-side of the midhull, then the engine room is defined and placed at the aft-side of the midhull, and lastly, the energy storage room is fitted between the two.

3. The tool provides technically feasible solutions.
   → The solutions comply with certain constraints addressing stability and structural integrity, and can, therefore, be used for further analyses and simulations without any modifications.

4. Optimisation focuses on the objectives of resistance and lightship weight (LSW). Resistance is used to address the OPEX of the vessel through fuel consumption, and LSW is used for CAPEX optimisation through the building cost.
   → Aim for minimal cost and compare the optimal solutions for each energy carrier with a standard point of reference for comparison.

5. The resulting solution of each iteration is stored and analysed.
   → Observe trendlines of the relations between the energy carriers and the chosen input variables. Additionally, storing all the generated solutions will aid the development of a database with both successful and unsuccessful early-stage designs with alternative energy carriers for further studies.

6. Framework can be successfully applied to the selected case studies.
   → The applicability on cargo vessels is refined and covers the sub-categories of vessel types: Ro-Ro, bulk carriers, container ships, tankers and the default option of general cargo ships.

4.1.2 *Generalised methodology steps*

A series of steps are defined below, as derived from the requirements of Section 4.1.2. These steps can provide all the necessary directions for the development of any framework that is aimed at performing design exploration for early-stage designs.

1. Definition of input variables
   → The step of determining the inputs of cargo DWT, cargo volume, speed, autonomy and ship-type, that will manage to capture the main design requirements of the problem, by knowing the desired amount of cargo, how fast it can be shipped, and how far can it travel.

2. Determination of main design drivers
   → Definition of the main drivers of the design process in order to direct the parametrisation and general arrangement of the vessel. This depends on the general vessel type, and ultimately on the overall goals of studying the generated early-stage designs.

3. Definition of HLPs
   → Construct a library of HLPs which will include the universal blocks that are applied in all the generated solutions, as well as case-specific blocks that are chosen based on the design requirements.

4. Establish the HLPs' categories
   → The categories will be used for the organisation of the HLPs, where each category will be dealt with and processed differently. For instance, each category will be associated with information on whether a block is allowed to be reshaped, or whether certain constraints must be applied.

5. Numerical description of HLPs
   → Formulate the mathematical representation of the HLPs that can be used to derive the numerical description of each HLP for the desired solution.

6. Tuning and arrangement of HLPs
   → Tune the mathematical description of the HLPs as directed by the design requirements and the space availability of each model. The arrangement follows a predefined hierarchy, as well as a set of rules/constraints, while also aiming for neutral pitch and roll by centering along the respective axes. The HLPs are essentially re-sized to fit inside each model of the design space.

7. Technical feasibility analysis
   → Carry out standard calculations in order to check the technical feasibility of the generated solution. For the purposes of this study technical feasibility is limited to dimensional ratios.

8. Evaluation of design space
   → Evaluation of design space through a set of KPIs. The analysis will be organised and visualised in plots, in an effort to identify the areas of interest for each problem. In this study, the models are assessed on their available energy and power, as well as their LSW and total resistance.

9. Selection
   → The determination of the *optimal* solution/-s can be derived by searching for the optimal combination of the KPIs of interest. In this case, it is multi-objective optimisation for the minimisation of LSW and resistance. The said optimal solutions are eventually determined by evaluating the full design space and identifying the Pareto fronts for each energy carrier.

4.2 ARCHITECTURE OF TOOL

The focus is again shifted towards the desired function of the SSDG by combining the requirements with the generalised steps of Sections 4.1.1 and 4.1.2, respectively. The studied models are organised in five blocks: afthull, power generation, energy storage, cargo hold and forehull. The flowchart below (Figure 26) is targeted to solve the chosen case study of cargo vessels; hence the input variables of speed, autonomy, cargo DWT, cargo volume and ship type are defined. The cargo volume refers only to the amount of cargo that can be stored inside the hull. This was decided since the main point of interest is the interactions between the three main blocks (engine, energy storage and cargo hold) and how well these can fit inside the hull. This cargo hold volume is then adjusted based on the given ship type in order to include essential storage implications such as tanks, or securing mechanisms for containers. For this reason, through trial and error, it was found that the given input should be increased by a factor of 1.65 for tankers and 1.1 for the rest of the types. These are preliminary estimations to provide a suggestion to the user on how much extra space could be required in order to store the desired amount of payload. The mentioned conversion could be ignored when the user has already determined the required cargo hold space on top of the cargo volume.

In addition, a recommendation is offered for assistance in converting TEUs to the required cargo hold volume as shown in 9. These inputs are crucial for the design of a cargo vessel as they address how much cargo can be carried, how fast this cargo can travel from point A to point B, and how far apart can point A and B be. The input of the ship type was eventually included for increased accuracy in the estimation of LSW which is later explained (4.3.5). Moreover, the flowchart is adjusted for multi-objective optimisation on resistance and LSW, in order to eventually minimise both OPEX and the CAPEX of the vessel.

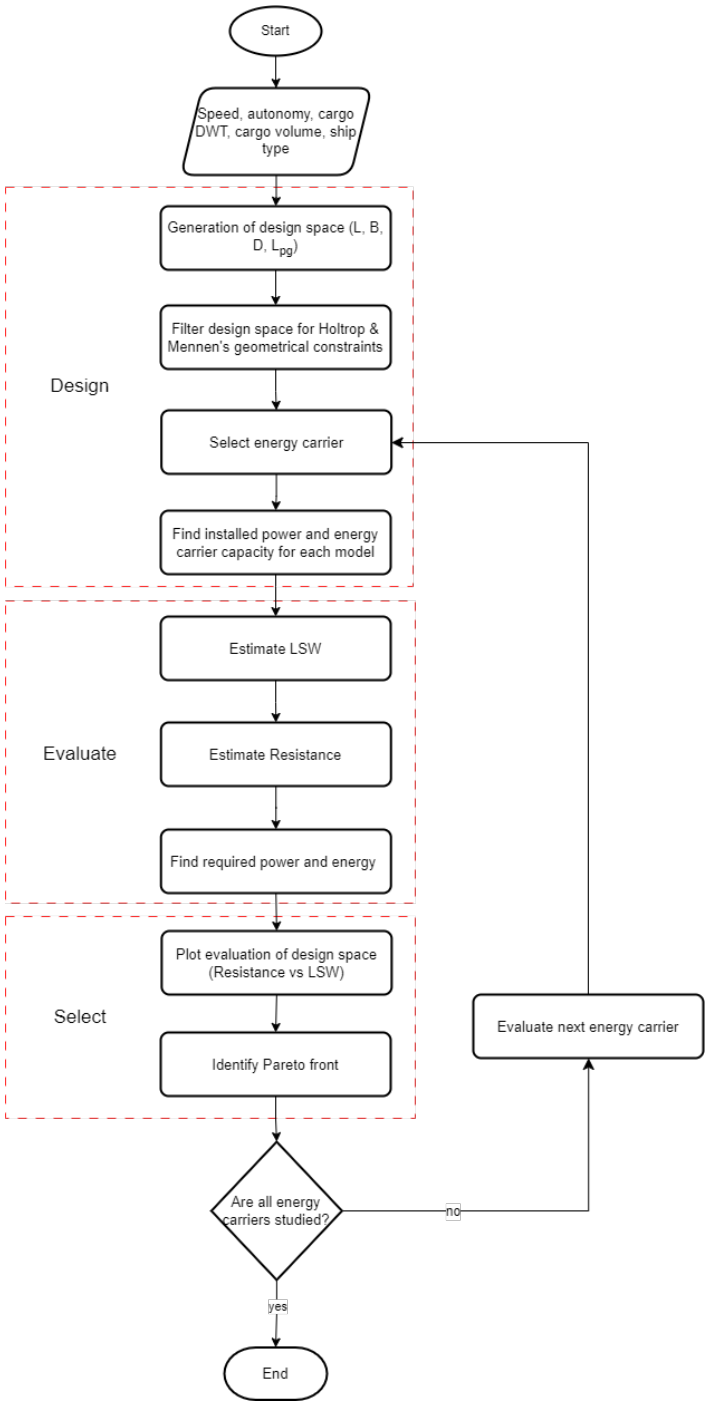

Figure 26: Flowchart of SSDG's provisional architecture for the investigation of the case study on cargo vessels.

4.2.1 *Definition of design space*

Once the user provides the desired inputs, the first step is to define the ranges of the design space for L, B, D, and $L_{eng-room}$ based on these inputs. This is because although the ranges for length (over all - LOA), beam and depth are pre-defined, the provided cargo volume affects the length of the cargo hold (L_{cargo}) block. This is calculated by dividing the requested volume by the adjusted

values[1] of depth and beam of each model's midhull. Now with LOA, L_{cargo} and length of power generation (L_{pg}) room known (drawn from a pre-defined range), the length of the energy carrier storage (L_{ecs}) room is calculated using equations 5 and 7.

4.2.2 *Filtering of design space*

The first filtering of the design space can be performed by first calculating the L/B of each model and then discarding the ones that fall out of the acceptable ranges (Table 23). In addition, the models with unreasonable cargo hold lengths are also discarded. This is addressed by only keeping the solutions with a cargo hold length greater than 15% of the total midhull length of the vessel.

4.2.3 *Analysis of models*

The next step is to determine what can each model offer with the given dimensions and sizes of the main blocks. Each block offers a certain available space which is adjusted based on regulations, while for the power generation room, there is a further space reduction to ensure other necessary components and machinery can be accommodated alongside the power generation equipment. Each room is filled with different power generation systems or energy storage methods, based on the findings reported in Table 17. These then define how much power and energy is installed in each of the models.

4.2.4 *Evaluation of design space*

LSW

Now that the available power and energy are known for each model the first optimisation objective of LSW is calculated. The estimation is performed based on a derived regression model (further elaborated on in Section 4.3.5) and it is further adjusted for the options of hydrogen and batteries an estimation of the ICE's weight is subtracted and the weight of the fuel cells (plus electric motor) and the type C tanks, as well as the batteries and the electric motor, are added respectively. In the case of ammonia, the weight of a single-fuel diesel ICE is assumed to be equal to the scaled DF ICE; hence, only the weight of the type C tanks is added. Lastly, the estimation of the methanol model's LSW is not adjusted as the energy storage in integral tanks and the DF ICE are assumed equivalent to the ones of conventional diesel-powered vessels. The mathematical relations for these are presented in equations 8. Knowing the total displacement of the vessel allows for the calculation of the models' draught as shown in Section C.4. At this point the design space is also filtered for freeboard, keeping the models' draught within the range of 0.4 to 0.8 times the models' D. These values were found in the relevant book of Papanikolaou for early-stage design [3], and it should be noted that the recommended range is 0.6 to 0.8, but the lower limit is relaxed since the vessels not yet properly loaded.

[1] The values of depth and beam are reduced by 0.6 m when less than 10m and then by 10% in order to include the double hull thickness into the calculations.

Resistance & required power and energy

Knowing the LSW of each model finally allows the computation of their total resistance. This is performed using the Holtrop and Mennen's method ([96]) for sailing at a speed equal to the user's service speed requirement. This estimation requires additional inputs revolving around the hull's geometry through coefficients and physical dimensions, which are referred to below (section 4.3.5). This step is vital towards the evaluation of each model's performance, as the total resistance allows for the calculation of the required power. A 5% is then added for the consumption of the electrical consumers on the vessel to determine the total required power of the model (equations 25).

Furthermore, in order to ensure the autonomy requirement of the user is also satisfied, it is necessary to find the required amount of energy. This is carried out by including the total system efficiency of the power plant, before converting the total power demand into energy measured in kW/h, by multiplying with the required hours of autonomy (equation 26).

4.2.5 *Shortlisting of optimal models*

Prior to the identification of the Pareto fronts, the performance of the design space is visualised by plotting all the models on a 2-D plot of LSW against resistance. On this graph, the solutions are organised into three categories based on their score. Two points are awarded for the vessels that fulfil both requirements (power and energy), one point for at least one of the two requirements, and zero for none. These are displayed as green, orange and red respectively. With this information known, the Pareto fronts are identified for the minimisation of both objectives for the fully feasible models only and are indicated on the mentioned plots. The specifications of the shortlisted models are isolated and stored separately for easier accessibility.

4.3 ANALYSIS OF IMPLEMENTATION

4.3.1 *Overview*

The applicability of the methodology as well as the functionality of the SSDG will be tested through a case study on cargo vessels. Figure 27 below shows the blocks and the provisional arrangement that will be explored. This means that the block adjacencies will be as displayed below (Figure 27).

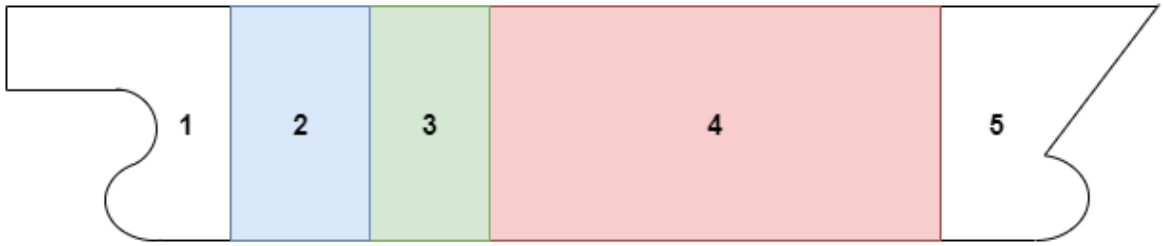

Figure 27: Schematic of a cargo vessel with the blocks and the arrangement that will be investigated.

The legend for the numbering of Figure 27, and their corresponding blocks, is visualised below.

Nr.	Block
1	Afthull
2	Power generation
3	Energy carrier storage
4	Cargo holds
5	Forehull

Table 19: Legend of Figure 27 for the numbering and respective blocks.

4.3.2 *Power generation room*

Batteries

The power generation block for the batteries is fitted with an electric motor, for which a set of regression models is derived using the equipment database of C-Job. However, before fitting the electric motor, the first step is to determine the space available for that motor to fit within. The electric motor essentially sits inside the room as depicted below in Figure 28.

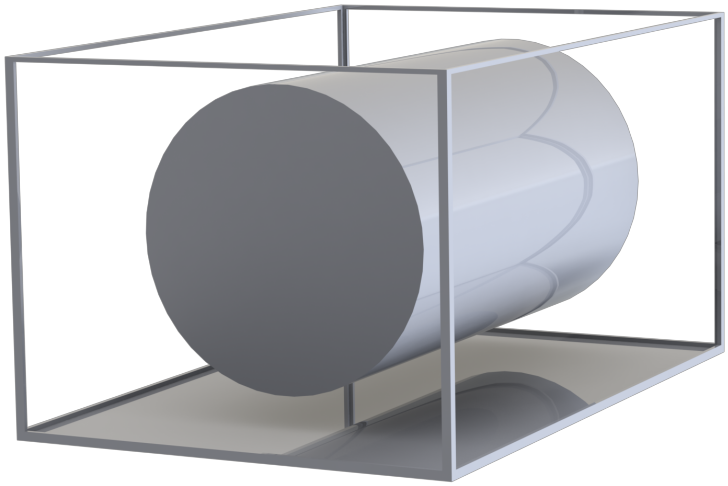

Figure 28: Power generation room for batteries-powered vessels, with a single electric motor.

This means that the provided overall dimensions of the room are reduced to make the model more realistic since the power generator (electric motor in this case) cannot occupy 100% of the room. It is essential to allow space for the gearbox at the rear side of the room, and overall allow for enough space to accommodate the rest of the necessary machinery, as well as for inspection and maintenance. The distances that amount to the mentioned spatial reduction of the room to the space available for the power generator are shown in Table 20.

Notation	Explanation	Size [m]
$d^{batt}_{er-rear}$	Distance between rear wall and gearbox	1
$d^{batt}_{er-front}$	Distance between front wall and electric motor	0.6
d^{batt}_{er-top}	Distance top of engine and ceiling	0.5
$d^{batt}_{er-side}$	Distance between engine and side walls	0.2
r^{batt}_{gb}	Length of gearbox as percentage of the available space	10%

Table 20: Distances that reduce the power generation room, for the batteries vessels, to the available space for the electric motor.

The shape of the electric motors can be approximated to be cylindrical, and thus three different models were derived, using C-Job's database for systems and components specifications. The first two were used to individually relate diameter and length with the power output, while the third was to relate power output with the mass of the motor. The first two aim to relate the available space inside the room with the power-wise size of the electric motor that can be installed inside. Since they are individually explored and two installed powers are calculated, the most limiting one is chosen, i.e. the one resulting in lower power output. Once the power is determined, the third model is utilised and the mass of the installed motor is derived. The optimal versions of the mentioned regression models were found through trial and error, from which it was found that exponential relation regression fits best the *diameter - power* and *length - power* models, while logarithmic relation was best for the *power - mass* one. The resulting regressions and their respective R^2 scores are provided below in Figure 29.

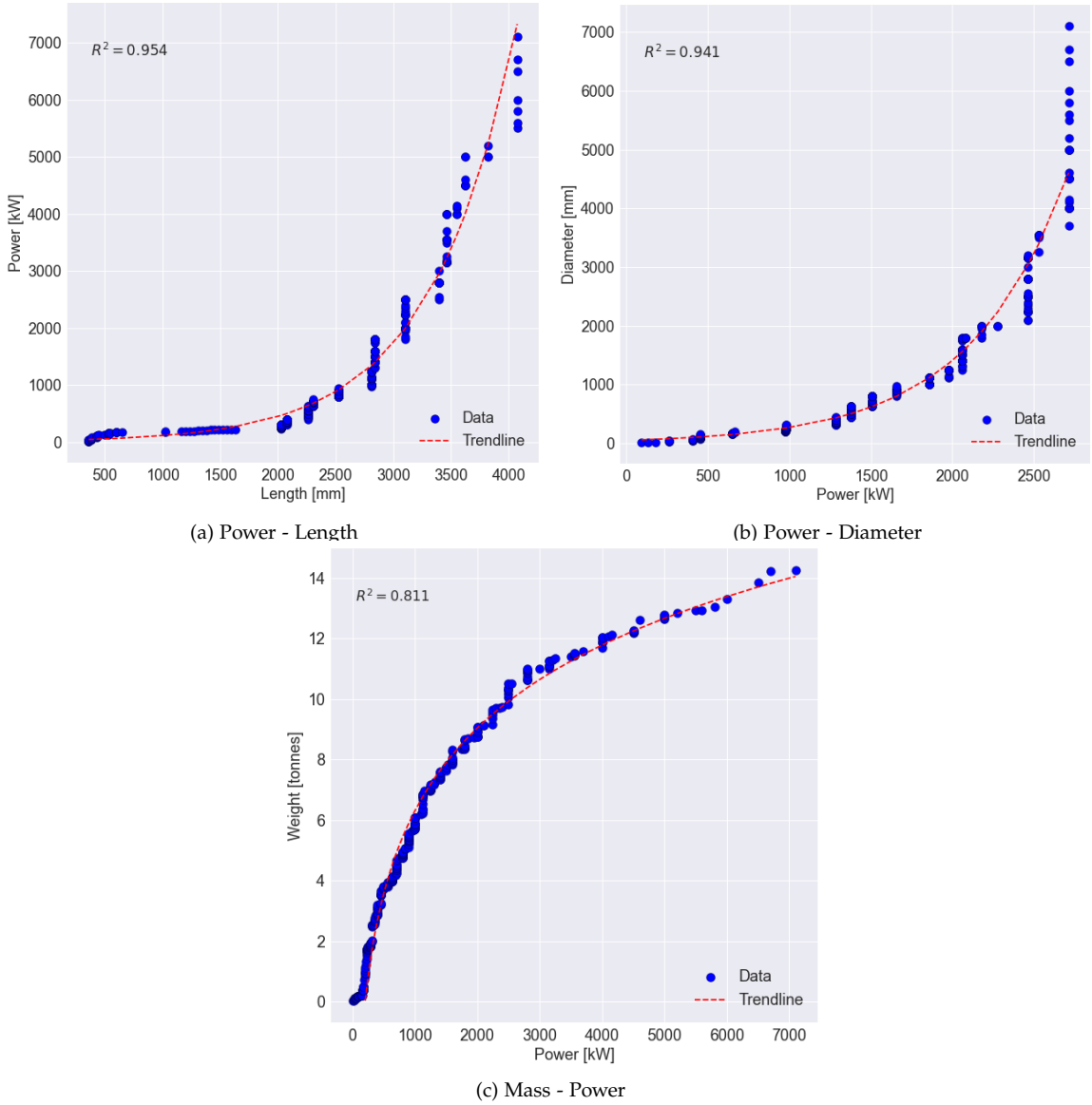

(a) Power - Length

(b) Power - Diameter

(c) Mass - Power

Figure 29: Derived regression models for fitting an electric motor in the available space of the power generation room of batteries vessels, using 488 different motors.

Hydrogen

The layout of the power generation room for the option of hydrogen is probably the most complex one, as it needs to fit both the generation of electrical energy using PEMFCs and then the conversion to mechanical energy with an electric motor. This is achieved by splitting the room into two floors: the top to stack the PEMFCs and the lower to fill with an electric motor. The split is done with a 0.6 ratio of the top floor (fuel cells) to the bottom one (electric motor). Now that the available space is known, the PEMFCs of Table 11 are stacked along the x (longitudinal) and z (vertical) axes, while the electric motor is scaled using the regressions shown in Figure 29. The resulting room configuration is visualised below in Figure 30.

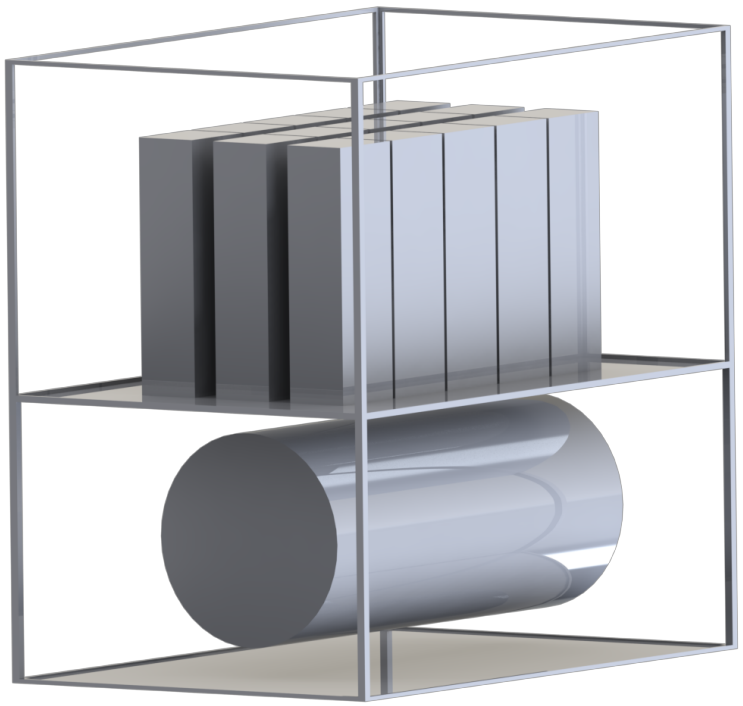

Figure 30: Power generation room for hydrogen-powered vessels, with the stacked PEMFCs at the top floor and an electric motor at the bottom.

Similarly to the *batteries* layout, there are also pre-defined distances (Table 21) that reduce the available space and the essential systems and machinery can be accommodated, but are not studied in any further detail.

Notation	Explanation	Size [m]
$d^{hydro}_{er-rear}$	Distance between rear wall and gearbox	1
$d^{hydro}_{er-front}$	Distance between front wall and PEMFCs/ electric motor	0.6
d^{hydro}_{er-top}	Distance top of engine and ceiling	0.5
$d^{hydro}_{er-side}$	Distance between engine and side walls	0.2
r^{hydro}_{gb}	Length of gearbox as percentage of the available space[2]	10%
r^{hydro}_{fc-em}	Ratio of top to bottom floors' height	0.6

Table 21: Distances that reduce the power generation room, of the hydrogen vessels, to the available space for the electric motor and the fuel cells.

[2] The length reduction of the available space to allow room for the gearbox is only applicable for the lower half of the room where the electric motor is located.

Ammonia

The ammonia-powered vessels have an engine room with a layout equivalent to one of the batteries. The major difference is that a DF ICE is installed instead of an electric motor as shown in Figure 31.

Figure 31: Power generation room for ammonia-powered vessels, with a plain box shape representing the DF ICE.

The scaling of the engine is performed using regressions developed based on existing DF ICEs by Wartsila, which are approximated to be box-shaped. However, this time there are 4 regressions in total, the three of which are relating the dimensions of length, width and height to the power output of the engine independently. Once the three different potential power outputs are estimated, the most limiting (lower) value is selected and given as an input to the fourth regression that computes the weight of the engine as a function of its power. The resulting regressions are provided in Figure 32. Lastly, it is again necessary to define the available space for the engine inside the provided room using the pre-defined distances of Table 22.

Notation	Explanation	Size [m]
$d^{amm}_{er-rear}$	Distance between rear wall and gearbox	1
$d^{amm}_{er-front}$	Distance between front wall and engine	0.2
d^{amm}_{er-top}	Distance top of engine and ceiling	0.5
r^{amm}_{space}	Ratio of width available for engine to total width of room	0.75
r^{amm}_{gb}	Length of gearbox as percentage of the available space	10%

Table 22: Distances that reduce the power generation room, for the ammonia vessels, to the available space for the DF ICE.

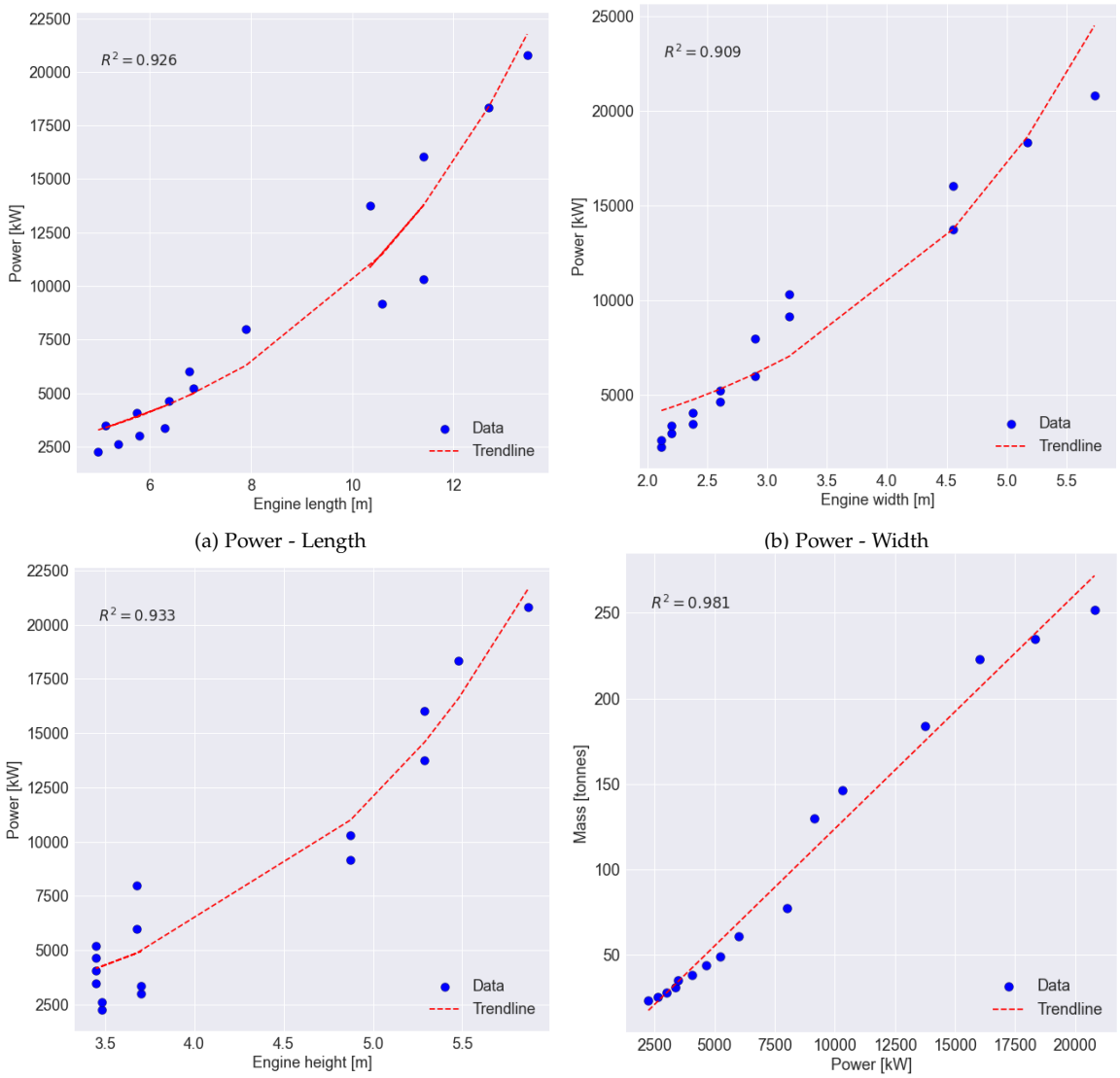

(a) Power - Length

(b) Power - Width

(c) Power - Height

(d) Mass - Power

Figure 32: Derived regression models for fitting a DF ICE in the available space of the power generation room of ammonia vessels.

The data points for these regressions are fewer (16 engines) compared to the ones in Figure 29 as a short database was created for this purpose using commercially available Wartsila DF ICEs.

Methanol

The power generation room for the methanol vessels is equivalent to the one for the ammonia vessels without any further adjustments.

4.3.3 *Energy carrier storage room*

Batteries

The battery energy carrier room shall have the layout depicted in Figure 5 and Table 7. In addition, two more distances are defined in the tool, where the one ensures clearance of 0.5 m between the ceiling of the room and the top of the last (along the vertical axis) stacked battery. The other distance is another fixed value of 1 m for the distance between the batteries and the rear-most side of the

room, since as it is displayed in Figure 5 there needs to be enough space for the management system of the batteries. Finally, using these constraints and the battery specifications shown in Table 4, the batteries are stacked in x (longitudinal) and z (vertical) directions in as many modules as are allowed by the width of the room. The room layout is visualised in Figure 33 below.

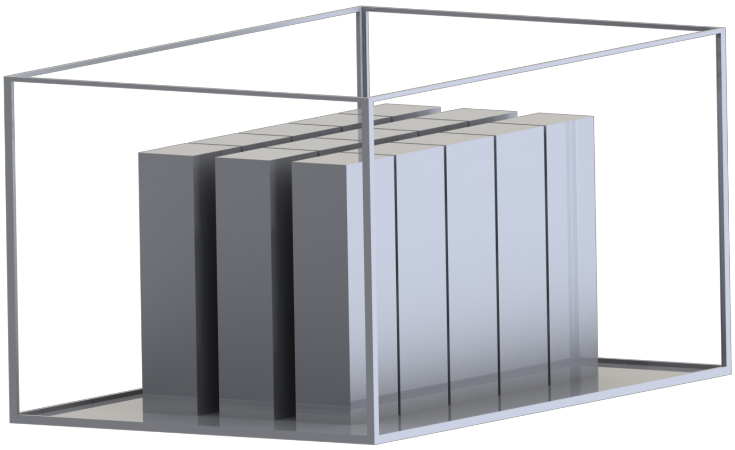

Figure 33: Energy storage room for batteries-powered vessels, showing batteries stacked in both directions (longitudinal and vertical).

Hydrogen

The energy storage room of the hydrogen vessels is fitted with two type C tanks in parallel along the longitudinal direction as visualised in Figure 34 below.

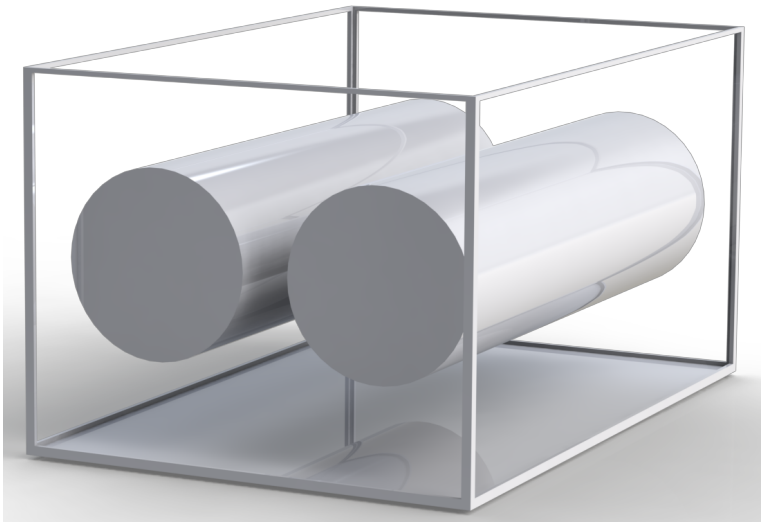

Figure 34: Energy storage room for hydrogen-powered vessels, with two Type C tanks.

The first step to determine the size of the tanks is to reduce the room to the size that is directed by the regulations explained in Section 2.4.4, and use a standard distance of 0.5 m between the tanks. Furthermore, as the shape of the tank is assumed cylindrical with flat surfaces at its ends instead of curved, a safety margin of 0.6 m is included to reduce the length of the tanks on both sides along the x (longitudinal) axis. Next, the external diameter of the tanks is calculated initially using the width of the room reduced by 0.5 m (distance between tanks) and divided by 2 (2 tanks in the energy storage room). The value is then compared to the height of the room and the smaller one is selected

as the diameter. Now the internal space available for the fuel to be stored is calculated by finding the required shell thickness to withstand the storage pressure. As advised by C-Job engineers, a double shell and a vacuum space (pre-defined thickness of 0.35m for insulation) are considered as shown in Figure44. The wall thickness of the shell is calculated using Equation 27 for computing the wall thickness of a cylinder that contains a liquid. Knowing these thicknesses finally allows the calculation of the available space for fuel storage, as well as the estimation of the tanks' weight using Equations 29 to 31.

Ammonia

The analysis of the energy storage room for ammonia is identical to the ones presented above in Section 4.3.3 for hydrogen. The only difference is found in the last calculation carried out under the energy carrier storage room analysis. That is for the required amount of the MGO for the DF operation of the vessel. For this, it was assumed that there is a 90 to 10% ratio of hydrogen to MGO and the required amount is computed using the volumetric energy density of the fuels as shown in Equations 32 and 34.

Methanol

The analysis of the energy storage room for methanol is the simplest among the four options. Type C tanks are unnecessary for the storage of methanol since it is stored in ambient conditions, and thus no thick shells and vacuum spaces are required. Instead, standard integral tanks are utilised and the room is assumed to be 100% filled with methanol. The only calculations that are performed are to reduce the initial dimensions of the room to allow for the necessary cofferdam (0.6 m on all sides) to be wrapped around the room.

4.3.4 *Technical feasibility*

The technical feasibility of the generated models was initially addressed by stability. The metacentric height (GM) was evaluated using the vessel's centre of gravity (CoG), the centre of Buoyancy (CoB) and the metacentric centre (M) as directed by Papanikolaou in his relevant book for early-stage ship design calculations [3]. For the computation of these, it was necessary to input the values of the block coefficient (C_B), the draught (T), the volumetric displacement (∇), the bilge radius (r_{bilge}) and the transverse moment of inertia (I_T). Regarding C_B, this value is pre-defined at 0.8 as this was assumed as an average value for cargo vessels. The calculation of the remaining inputs as well as the process of calculating the GM are explored in the appendix C.5. It should be, however, noted that the stability calculation and filtering (for positive GM values) were eventually excluded from the latest version of the tool. This is due to observing that many vessels of the design space were marginally excluded with negative GM values. This meant that the design space was vastly limited at a stage where ballast tanks, along with a significant amount of essential systems and machinery are not yet defined; though some space considerations to include them have already been included.

In addition, a standard set of ship design geometrical constraints is utilised, since they both address Holtrop & Mennen's applicability and are also helpful in limiting the design space with geometrically feasible models. These constraints are represented in Table 23 and were found in [97].

The provided provisional ranges are limited for applicability in cargo ships as found in relevant literature [98]. The generalised constraints shown in the last row of Table 23 were determined by

Ship type	Max F_N	C_P	L/B	B/T
Tankers, bulk carriers	0.24	0.73 - 0.85	5.1 - 7.1	2.4 - 3.2
Trawlers, tugs	0.38	0.55 - 0.65	3.9 - 6.3	2.1 - 3.0
Container ships, destroyers	0.45	0.55 - 0.67	6.0 - 9.5	3.0 - 4.0
Cargo liners	0.3	0.56 - 0.75	5.3 - 8.0	2.4 - 4.0
Ro-Ro ships, car ferries	0.35	0.55 - 0.67	5.3 - 8.0	3.2 - 4.0
Combined constraints	0.45	0.55 - 0.85	3.9 - 8.0	2.1 - 4.0

Table 23: Geometrical constraints utilised in the SSDG coming from Holtrop & Mennen's applicability found in [97].

combining the type-specific ones, and these combined ones were actually applied in the tool for simplicity.

4.3.5 *Optimisation objectives*

As mentioned earlier in Section 4.1.1, it is desired to perform multi-objective optimisation focusing on resistance and LSW.

Resistance

Resistance is calculated using the Holtrop & Mennen's method since it can be applied for vessels with relatively low L/B ratios and can include the effect of bulbous bows [96]. It should be acknowledged, however, that this model can be used to accurately estimate resistance for a certain range of vessels with geometrical constraints as presented in Table 23; hence, in order to maintain a standard level of accuracy in the design space, it is filtered to ensure all vessels fall within the combined constraints. This computation is performed by implementing the relations presented in the original Holtrop & Mennen's method paper [96]. However, in order to complete all the required computations and reach the desired total resistance output, it was necessary to define a set of parameters that fully capture the geometry of the vessel as shown in Table 24. Note, parameters such as the bilge radius, the prismatic coefficient, or the volumetric displacement of the vessel are also inputs but are not mentioned since they have already been defined for the stability calculation (Section 4.3.4).

Parameter	Notation
Length between perpendiculars	L_{BP}
Waterline length	L_{WL}
Bulbous bow transverse area	A_{BT}
Prismatic coefficient	C_P
Longitudinal Centre of Buoyancy	LCB

Table 24: Parameters that are necessary to define and input in the Holtrop & calculation script.

LSW

Regarding the computation of the LSW, individual regression models were derived using C-Job's database. This individuality refers to the ship types that are built-in and are available for the user to choose from. This was crucial to include in order to ensure higher accuracy in the estimation as it is tailored to the respective ship type. The said ship types include the options of: *tanker*, *bulk carrier*, *general cargo ship*, *tanker* and *container ship*. The models were developed to relate the main particulars of the ship with LSW, and it was determined that the most effective method was to build multivariate linear models. These are linear regression models with multiple independent variables, which in this case are the L, B, D and L^2, i.e.:

$$LSW = f\{L, B, D, L^2\}$$

This specific combination was determined after trial and error tests while performing 10-fold cross-validation and evaluating the mean R^2 score of each iteration. The resulting functions are provided in Table 25 and the predicted LSW values using the database's input are visualised in Figure 35.

Ship Type	Function	Mean R^2	No. of Vessels
Tanker	$-56.00 \cdot L + 137.42 \cdot B + 313.28 \cdot D + 0.31 \cdot L^2$	0.946	345
General cargo ship	$-49.13 \cdot L + 66.56 \cdot B + 275.16 \cdot D + 0.36 \cdot L^2$	0.918	4284
Container ship	$-60.32 \cdot L + 111.58 \cdot B + 379.43 \cdot D + 0.33 \cdot L^2$	0.931	2538
Ro-Ro	$-72.285 \cdot L + 245.61 \cdot B + 93.51 \cdot D + 0.45 \cdot L^2$	0.807	535
Bulk carrier	$-45.14 \cdot L + 165.20 \cdot B + 334.58 \cdot D + 0.20 \cdot L^2$	0.751	5520

Table 25: The functions of the developed regression models including their R^2 score.

Furthermore, the following dimensional ranges (Table 26) are provided for which better accuracy is expected by the regressions for each ship type to ensure the highest possible R^2 values. These were determined by trimming out the top and bottom 5% of the vessels included in the training data and then observing the ranges for the remaining ones.

	Bulk carriers	General cargo	Tanker	Ro-Ro	Container ship
L [m]	146 - 225	66 - 162.5	64 - 223	73 - 189	104.5 - 220
B [m]	21 - 32.5	11 - 23	10 - 32.5	13.5 - 28.5	18 - 32.5
D [m]	11.5 - 20	4 - 13.5	4 - 18.5	4.8 - 18	8 - 19

Table 26: Dimensional ranges of vessels used towards the development of the regression models per ship type.

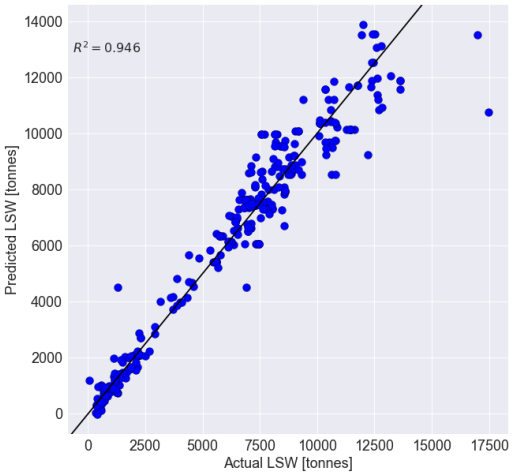

(a) Tanker

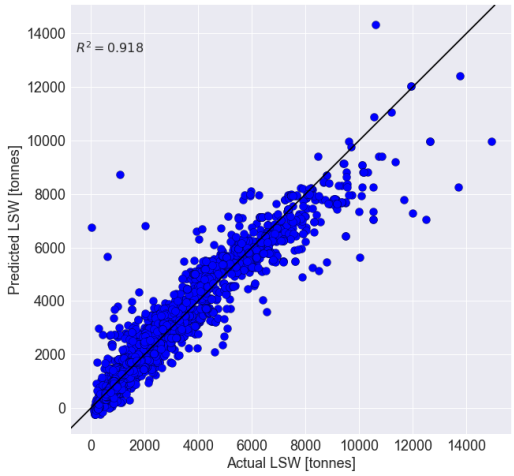

(b) General Cargo ship

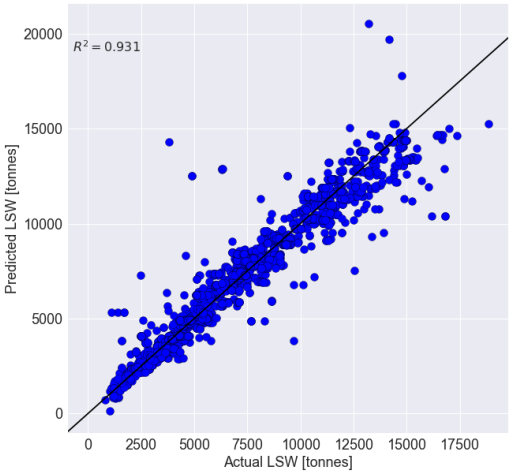

(c) Container ship

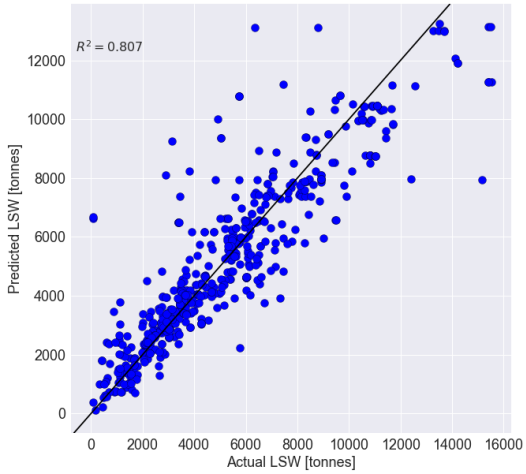

(d) Ro-Ro

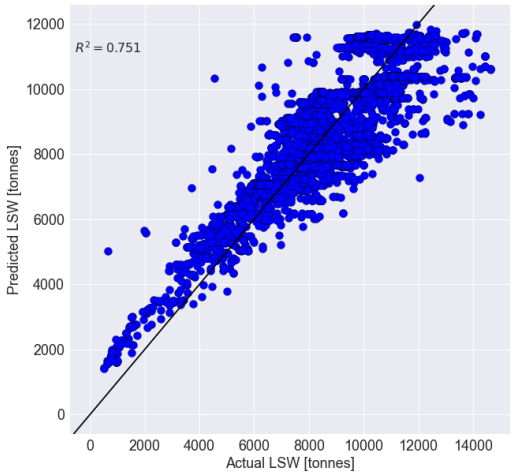

(e) Bulk Carrier

Figure 35: Graphs showing the actual LSW against the predicted LSW that is calculated using the regression models.

5

PERFORMANCE & VALIDATION OF SSDG

This chapter is aimed at exploring the accuracy and capabilities of the developed tool, and for this reason, it is split into three major parts. The first one focuses on the level of accuracy provided by the adopted methods of estimating the LSW and the total resistance of the models. Then, the second and largest part explores a set of case studies, which is further split into two subsections. The first one investigates the output's accuracy by validating results using the inputs of an existing vessel. The second part then focuses on exploring and observing how the variation of inputs affects the optimal results, focusing on service speed and autonomy. This is done to gain insight into the relationship between the inputs and the performance of the selected energy carriers. Regarding the selected vessels, they are five in total - 1 for each integrated ship type - and were chosen from the *Significant Ships* issues of the past ten years. The primary reason for the selection was the availability of information on the specifications of the ships. In the main body of this section, only the first case study of the tanker *SC Aquarius* is presented for conciseness and simplicity reasons. The rest of the case studies are provided in the appendix with a brief overview in Section 5.2.1. The last part of the chapter discusses the theoretical validation of the design method, addressed through a series of steps that aim to build confidence in the process that is followed [99].

5.1 VALIDATION OF LSW AND TOTAL RESISTANCE

This section aims to complete the proposed method by testing the level of accuracy of estimating the LSW and the total resistance of the models. This is achieved by selecting 10 vessels (2 for each ship type that is available on the tool) and comparing the actual with the estimated values. This is done using the exact geometrical variables for L, L_{BP}, B, D, T, C_B and DWT. These are also used to compute the other geometrical variables that are shown in Table 24. The result of this testing is provided below in Table 27, where average deviations of 20 and 11.3 % were found for LSW and total resistance estimations, respectively. Although it is not absolute for all cases, it can be seen that large deviations in the LSW estimation are related to increased deviation in total resistance, due to error propagation. Overall, these deviations are deemed acceptable for the purposes of this study, since it addresses solutions for early-stage design; though, it is noted that discrepancies are to be expected with respect to the accuracy of the SSDG's output.

Vessel	Ship type	LSW actual	LSW est.	% diff.	$R_t$actual	$R_t$est.	% diff.
SC Aquarius	Tanker	11146.2	9314.2	-16.4	721.3	753.8	+4.5
Gener8 Hector	Tanker	45400	32712.5	-27.9	2936.8	2284.5	-22.2
CMA CGM Argentina	Container	42907	39041.9	-9	327.7	341.8	+4.2
Valparaisso Express	Container	37061	31999.9	-13.7	3167.9	2927.7	-7.6
Da Ji	General cargo	10983	8530.6	-22.3	746.2	728.7	-2.3
Zealand Amalia	General Cargo	6954	4029.8	-42.1	417.9	384.8	-7.9
China Steel Liberty	Bulker	27500	26560.6	+3.4	1598	1691.9	+5.6
General Schmidt	Bulker	21804	18567.8	-14.8	825	1195.9	+30.6
An Ji 23	Ro-Ro	11653	7441.9	-36.1	642.1	497.3	-22.6
Shi Jiang	Ro-Ro	7410	6356.6	-14.2	514.3	541.9	+5.4
	Average Deviation			-20			|11.3|

Table 27: Validation testing for 10 vessels in total (2 per ship type) for the estimated values of LSW and R_t.

5.2 CASE STUDIES

5.2.1 *Exploration of the tool's capabilities*

The vessel that is studied here is the *SC Aquarius*, which is a chemical tanker built in 2016. The vessel as well as its main characteristics are presented in Figure 36 and Table 28, respectively.

Figure 36: Photo of the studied SC Aquarius [100].

LOA	[m]	182.8			
B	[m]	32.2			
D	[m]	15.7	Service speed	[kt]	14.5
T	[m]	9.5	Cargo volume	[m^3]	43687
DWT	[t]	32293.7	Cargo DWT	[t]	29064
LSW	[t]	11146.2	Autonomy	[days]	68
P_B	[kW]	7610			
R_t	[kN]	721.3			

Table 28: Main characteristics of the SC Aquarius (left) and its capabilities (right) used as inputs for the SSDG.

Note, the value of the *Cargo DWT* is calculated as the 90% of the provided design DWT (shown in Table 28) and not by converting the available *Cargo hold volume* into mass using an average cargo density. The latter would result in the scantling condition of the vessel since the ship is loaded to its limits. Nonetheless, the design profile is where the ship operates most efficiently without fully utilising all the available spaces.

Knowing the inputs and the main particulars of the case vessel, the next step was to define the limits of the design space by running the script for a wide range initially with large steps, before narrowing it down to the most efficient and sensible ranges with smaller steps. In this case, the following was used:

$$\text{Design space} = \begin{cases} \text{LOA} & \text{155 to 280, steps of 1 m} \\ \text{B} & \text{13 to 38, steps of 0.5 m} \\ \text{D} & \text{9 to 30, steps of 0.5 m} \\ \text{L}_{pg} & \text{5 to 15.5, steps of 0.5 m} \end{cases}$$

Upon completion of the tool's execution, the results visualised in Figures 37 were yielded. These are organised into four independent design spaces (one for each energy carrier) where the two optimisation objectives of LSW and resistance are plotted against each other. These plots indicate the performance of each solution, and eventually, the Pareto front of the optimal models fulfilling both requirements (energy and power) is also highlighted.

The vessels presented on the combined Pareto plots (Figure 37e) are further explored with the parallel coordinate plot shown below in Figure 38. This is done to obtain a deeper understanding of the solutions with insight into their main particulars and how these compare to each other as well as to the case vessel.

Interpretation of results

The first observation that can be made on the generated results is the displayed colours on each design space. The battery-powered models (37c) mostly manage to fulfil only one of the two requirements, and none of them both. This phenomenon occurs due to the low energy density of batteries and the size of the requested autonomy, meaning these vessels can achieve the requested speed, but run short on autonomy. Similarly to batteries, hydrogen-powered vessels (37b) struggle to achieve both requirements as well, but in this design space, they have marginally achieved feasibility with *green* models at the top right corner of the plot. The issue, in this case, is found in the storage requirements of hydrogen that demand unreasonable tank sizes. This is also the reason why ammonia vessels(37c) display a higher number of feasible models since the storage requirements are dramatically decreased compared to hydrogen, even though in both cases type C tanks are assumed. Lastly, the methanol design space (37d) is the one with the most fully feasible solutions with hardly any fully infeasible solutions that are slightly visible at the bottom left corner of the figure.

A reference should be also made to the different shapes of the four design spaces. These discrepancies are primarily due to the adjustments made to the estimated LSW value based on the other parts of the vessel that are counted with the LSW, such as the engine/electric motor or the fuel tanks. This also explains why the resulting design spaces of ammonia and hydrogen are similar since the greatest effect on the LSW value comes from the weight of the type C tanks. In this way, there are different contributions to the displacement of the models for different energy/power outputs for the different energy carriers and power generation systems.

The next, and greatest point of interest for these results, are the Pareto fronts. It is visible in Figure 37e that the frontier of methanol is the lowest amongst the studied energy carriers, next comes the ammonia, and last the hydrogen, while batteries are infeasible towards the fulfilment of the given inputs as mentioned in the previous paragraph. These results confirm the expectations that arise just by observing the properties of the carriers combined with their respective storage

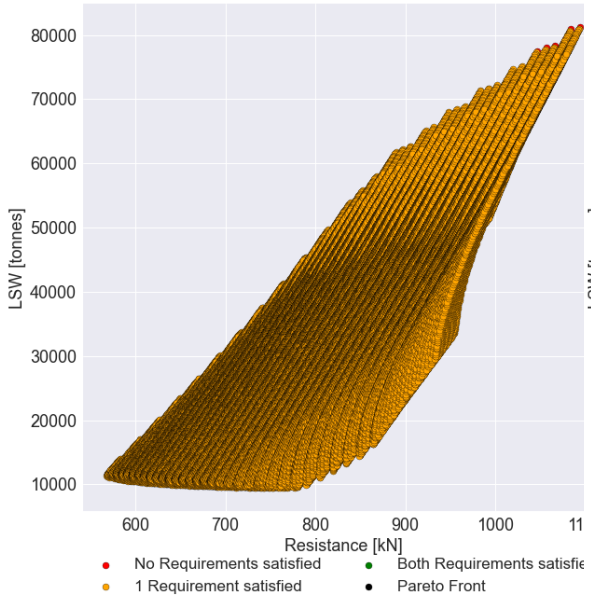

(a) Batteries

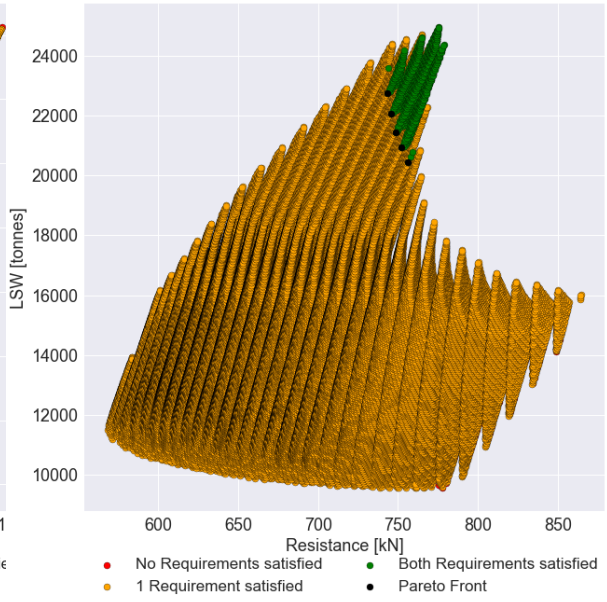

(b) Hydrogen

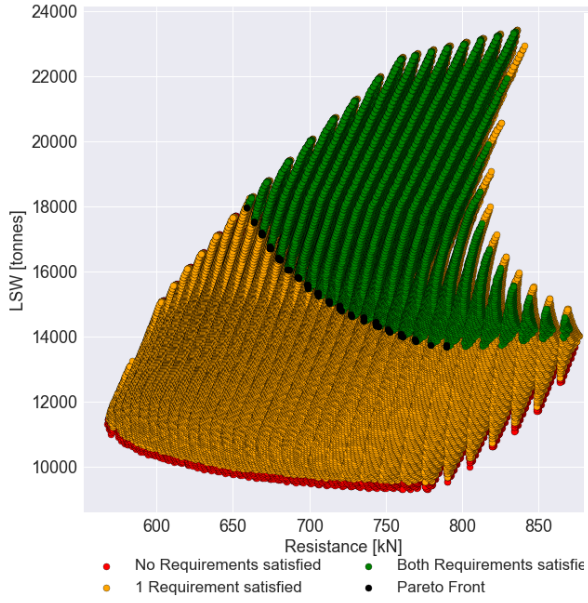

(c) Ammonia

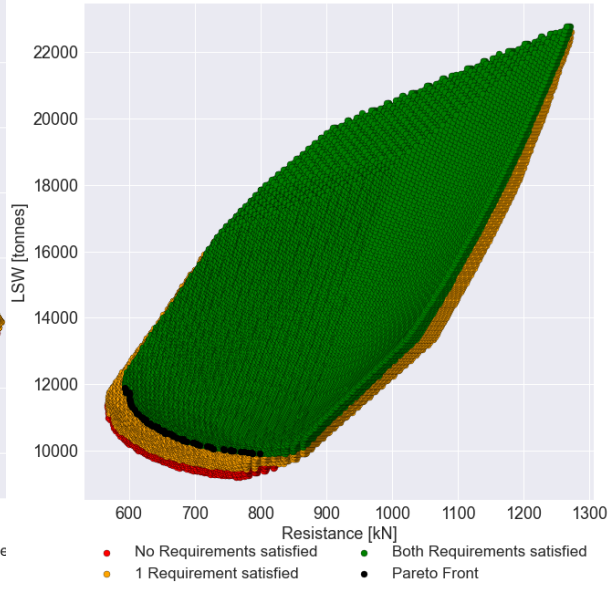

(d) Methanol

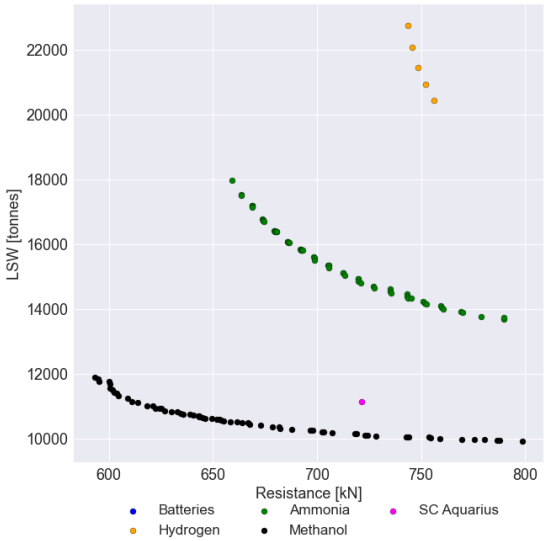

(e) Combined Pareto fronts

Figure 37: Resulting design spaces and the combined Pareto fronts plot for the case vessel SC Aquarius.

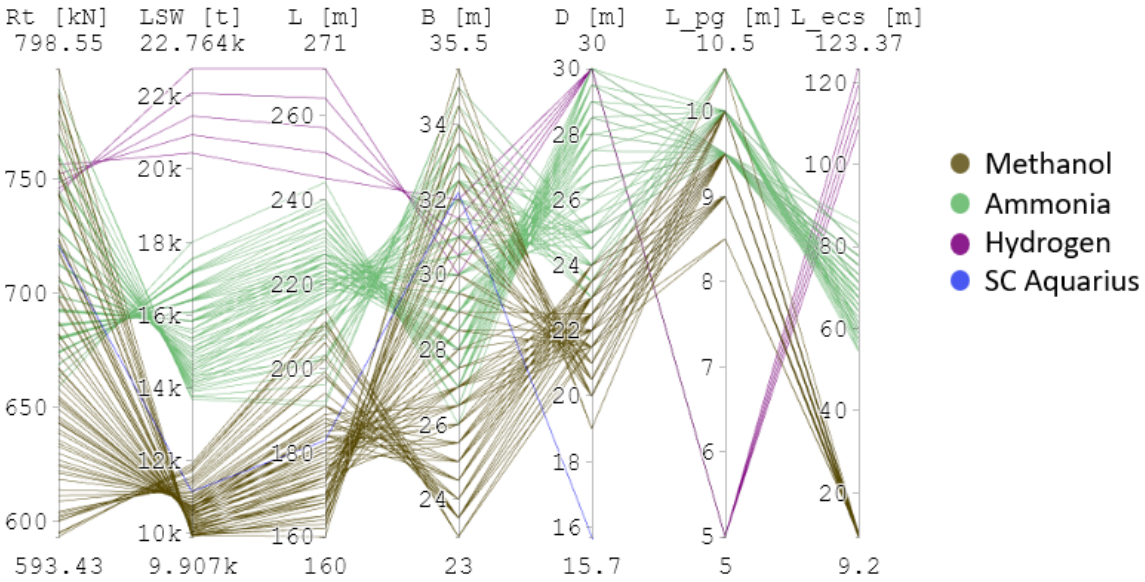

Figure 38: Parallel coordinate plot for the feasible Pareto front models.

requirements. The order of performance for the three feasible energy carriers is clearly as expected, especially for such a high autonomy (68 days). There is a significant difference that does not allow room for arguing how relative performance could be affected by other factors such as production costs that are not considered in this study. Nonetheless, for this highly demanding autonomy input, it would be expected that hydrogen vessels would be infeasible, and the ammonia ones probably marginally feasible. This seemingly extended feasibility range in the studied design space could be the result of deviating from reality due to the accuracy level of the tool, which is further elaborated upon in the following paragraphs.

The addition of the case vessel on the plot also confirms the validity of the calculations since the results are realistic and the methanol frontier is close to the actual vessel. It would be expected that there is a significantly larger distance between the two; however, it should be highlighted that this tool only attempts to fit the three major blocks and optimises the objectives for vessels that just fit them. Compared to the case vessel, there is a significant amount of tanks and other essential systems that are not addressed by the SSDG. These are expected to have a noticeable impact on the DWT of the models, affecting their total resistance as well. Therefore, it is understandable why the case vessel is marginally more efficient for the objectives of LSW and total resistance compared to the methanol solutions. Considering that the main purpose of this tool is to carry out early-stage feasibility studies and set the foundation for the relative performance of the fuels, then the assumptions made can be deemed reasonable and the level of accuracy high enough for this stage.

The mentioned differences between the resulting Pareto fronts are also captured on the derived parallel coordinate plot of Figure 38. The methanol vessels are overall smaller in size compared to the ammonia ones, and the latter are smaller than the hydrogen ones. The reason behind this is clearly demonstrated by the difference in the sizes of their energy storage rooms on the last axis (L_{ecs}) due to the different storage requirements for each fuel. Furthermore, the power generation room length (L_{pg} - second to last axis) shows how the space inside the hydrogen vessels is utilised more efficiently. This is achieved by splitting the room along its height and fitting the FCs on one floor and the electric motor on the other (explained previously in Section 4.3.2). Note, the values

of L_{ecs} and L_{pg} were not available for the case vessel; hence, the line for the case vessel stops at its depth value.

Summary of extra case studies

The purpose of the additional case studies was to provide a more complete insight into the performance of the tool by both obtaining a greater volume of results and testing the four remaining integrated options of ship types. However, due to the relatively large volume of repetitive results, the four case studies are provided in Appendix D, and their overview is provided in this subsection.

The first thing that can be observed is the overall consistency of the results. The relative performance is standard with methanol being the most efficient, followed by ammonia and hydrogen (when feasible). Similarly to the case study shown in Section 5.2, the batteries were proven unfeasible for all the studied case studies. An interesting difference that is observed is how the resulting design spaces per energy carrier differ for each vessel, shown in figures such as Figure 37. These differences are due to the different operational inputs that are fed into the SSDG. The difference in inputs translates into different models in the design space, which when filtered for the pre-defined constraints result in unique design spaces.

Regarding the differences in relative performance, it can be seen that all the case studies have feasible solutions for methanol and ammonia-powered vessels, while the bulk carrier (in D.2) has also feasible models for hydrogen. The level of feasibility also depends on how demanding the requested inputs are since the relative performance of the energy carrier is affected. It should also be highlighted how consistency is shown in the underestimation of the LSW for the generated models. This is clear by seeing all the selected case vessels being above the Pareto fronts of the methanol models and relatively close to the ammonia fronts too. The reason behind this is also addressed in the above Section 5.2.1, which relates to the fact that the tool optimises for only three major rooms, while other essential components are not properly quantified. Additionally, there is the issue of the level of accuracy in the estimation of the LSW using the regression models that were derived and presented in Section 4.3.5. It was observed in Table 27 that there is an average 20% deviation from the actual LSW values, meaning the consistency in the seemingly worse performance of the case vessels compared to the methanol vessels is to be expected.

5.2.2 *Investigation of inputs' effect*

The second part of the case study is organised into varying the different inputs sequentially, by running the tool for different speeds, autonomy and cargo DWT/cargo densities, where the latter refers to the ratio of cargo DWT to cargo hold volume. Each time one of the inputs is varied, the rest of them use the original inputs as shown on the right side of Table 28. The effect of this study is visualised solely on combined Pareto front plots, such as Figure 37e, per input to observe how the different values of the input affect the relative positions and/or the existence of the frontiers of each energy carrier.

Service speed

The investigation of the vessel's speed effect on the optimisation objectives and the feasibility of the models is carried out with the speeds of 10, 15, 20 and 25 knots. This range was assumed in order to cover service speeds for the majority of cargo vessels including the more extreme upper

and lower values of 10 and 25 knots, respectively. The rest of the inputs were kept the same as the original values of the case vessel.

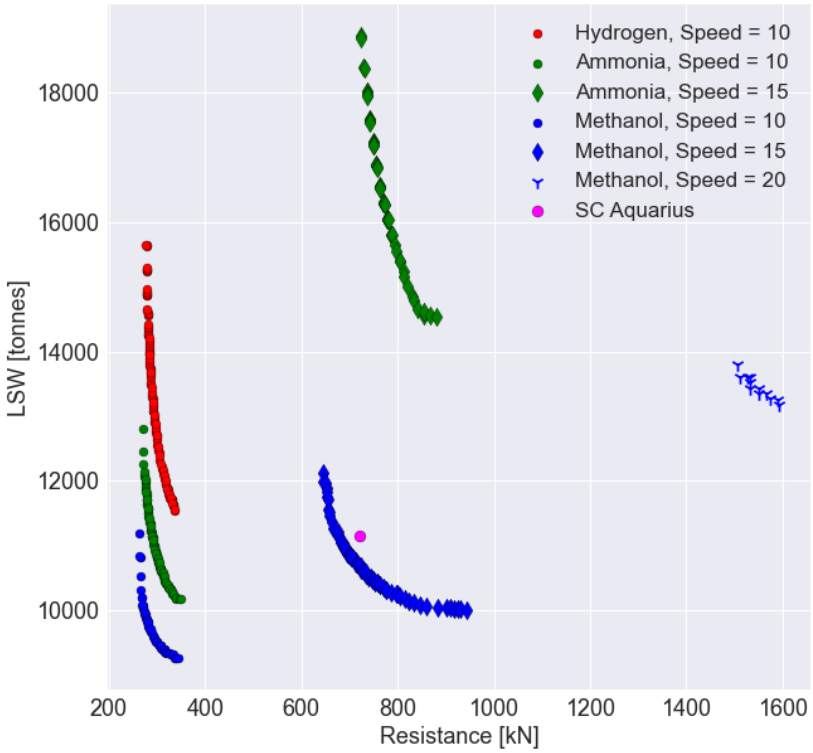

Figure 39: Combined Pareto fronts for all energy carriers for the different tested speeds.

The primary observation of these results is the complete infeasibility of batteries for the range of tested service speeds. The reason behind this is that the batteries-powered vessels do not lack the power to propel the ship at the requested speed, but instead lack the energy capacity to sail for 68 days (original autonomy input) before charging. Moreover, it can be seen that the hydrogen vessels could indeed become feasible at the lowest speed of 10 knots, with a steep Pareto front due to the small impact of the ships' displacement on their total resistance. On the other hand, ammonia provides vessels that can also sail at 15 knots, while methanol shows feasibility for 20 knots as well, with the respective expected implications. These relate to significant increases in LSW and even sharper ones in total resistances. It can also be seen that there are much fewer vessels in the front of 20 knots for methanol, meaning feasibility is highly limited. Overall, the results are reasonable and follow the results presented in Section 5.2.1. Furthermore, it is shown that the higher the velocity the greater the impact of LSW on total resistance; i.e. at the lowest speed of 10 knots there is a lower variation of resistance, while at the speed of 20 knots, the curve has a gradient projecting a sharper increase of the total resistance.

Autonomy

The effect of autonomy on the feasible Pareto fronts is explored by studying the ranges of 0.5, 1, 2, 7, 14 and 28 days, while once again the rest of the inputs were kept constant as the original values of the case vessel shown in Table 28. This range of autonomies was selected in order to study from values low enough that batteries will be feasible, up to a fairly large value for relatively longer trips. The results presented below in Figure 40 are organised in the different fuels showing the shifting of the Pareto front for the different autonomies. Additionally, the axes limits are set the same for the 4 plots in order for the curves to be comparable upon quick visual inspection.

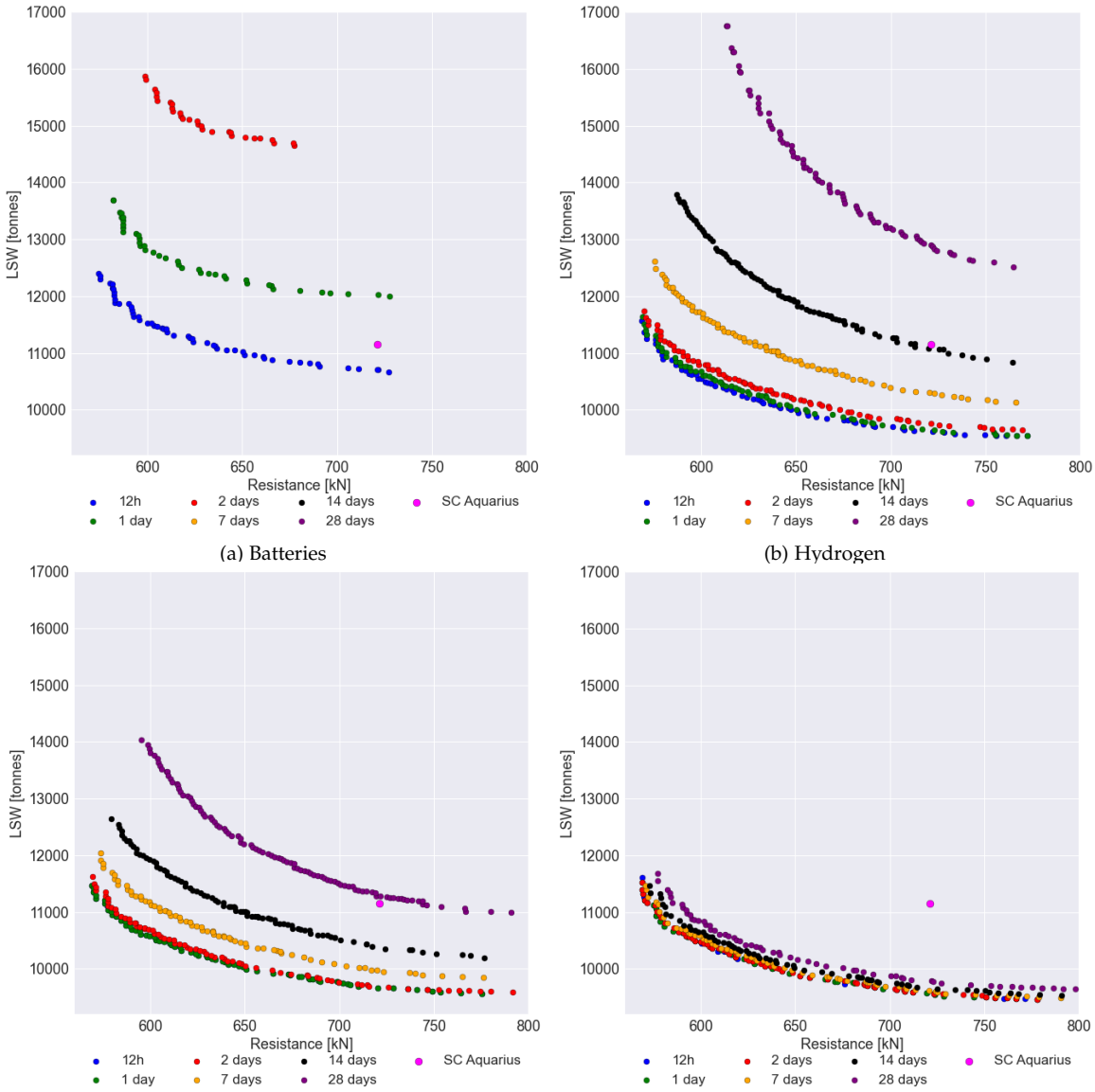

(a) Batteries

(b) Hydrogen

(c) Ammonia

(d) Methanol

Figure 40: The effect of the investigated autonomy ranges on the Pareto fronts for each fuel.

As expected, this study managed to explore the limits of the energy carriers and create a better picture of their relative performance. Starting with batteries in Figure 40a, it can be seen they are only feasible for 12, 24 and 48 hours, while the rest would require vessels of significantly greater sizes to fit the necessary number of batteries. It is also reasonable that the case vessel (with 68 days of autonomy) is marginally above the 12-hour Pareto. Next, the hydrogen Pareto-efficient models are shown in Figure 40b and there is feasibility for all the tested autonomy values. The 12 and 24-hour fronts are marginally separated as the required energy has a slight deviation between the two. After that, the distance between the fronts grows larger leading to the 28-day front barely fitting within the figure. This time, the case vessel can be seen just above the 14-day curve, validating again the expectations of the relative performance between batteries and hydrogen and also between hydrogen and diesel. Regarding the ammonia models, there is an overall higher performance compared to hydrogen as all the curves are shifted lower. In comparison, the case vessel now sits just below the 28-day front. Moreover, the 12-hour front may not be visible but is in fact covered by the 24-hour front. The reason behind this phenomenon is that the amount of requested cargo forces a certain 'minimum' vessel size in order to also allow enough space for the energy storage

room. This means that the smallest feasible vessel size provides enough energy to fulfil both 12 and 24 hours of autonomy. Lastly, the methanol results (Figure 40d) display fronts that are clustered together compared to the rest of the energy carriers; though it should be noted that the y-axis range assumed for these figures is a bit large for the methanol models. Similarly with the ammonia fronts, the 12, 24 as well as the 48-hour fronts are almost identical for the previously mentioned reason of the requested cargo forcing a certain size minimum vessel size. Overall, the performance of the methanol vessels is the highest amongst the studied energy carriers as expected, with the case vessel being clearly above the 28-day Pareto front. It should be highlighted how for lower autonomies the performance of ammonia and methanol is much more comparable, unlike in Figure 37e where methanol completely dominates the rest.

5.3 VALIDATION OF DESIGN METHOD

This part follows the approach of Pedersen et al. in [99] for the theoretical validation of design methods using the *validation square* shown in Figure 41. The said validation is vital towards providing the reader with confidence about the credibility of results and the developed method overall. Scientific research can be usually directly validated by deploying mathematical models and simulations with specific inputs and comparing the resulting outputs. However, in design research, it is not as simple to apply such an approach, and thus Pedersen et al. tackled the problem by attempting to answer the question of "*How does one validate design research in general, and design methods in particular?*". The authors state the two methods as the *Logical empiricist validation* and *Relativist validation*. The former describes an algorithmic process in which the extracted statements and information are either true or false. While this is highly dependable for areas such as algorithm development, it can only focus on the accuracy of results ignoring practical implications. On the other hand, the *Relativist validation* focuses on progressively building confidence in the way the derived knowledge can be applied and for which applications can it be used [101]. This validation process is stated as follows by the authors:

"*We define scientific knowledge within the field of engineering design as socially justifiable belief according to the Relativistic School of Epistemology. We do so due to the open nature of design method synthesis, where new knowledge is associated with heuristics and non-precise representations, thus knowledge validation becomes a process of building confidence in its usefulness with respect to a purpose.*"

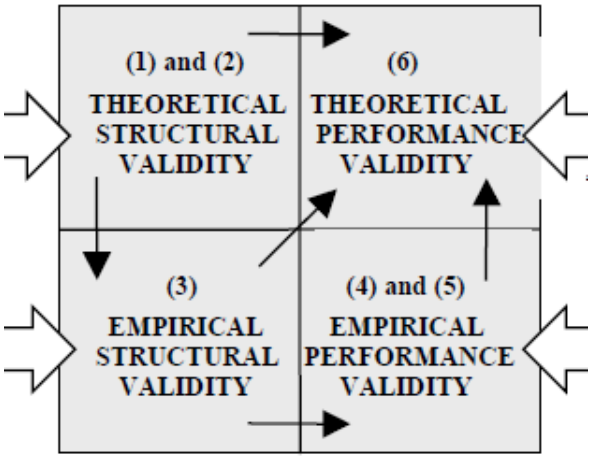

Figure 41: The validation square as presented by Pedersen et. al [99].

This approach is essentially split into two parts: the structural validation, i.e. the qualitative process, and the performance validation, i.e. the quantitative process. These are explored through three steps each as denoted in Figure 41 [99]. Therefore, the developed design method of this study will be analysed for its validity using the mentioned steps as follows.

(1) Accepting the construct's validity:

This step refers to building confidence in the validity of the components from which the design method is built. This comes through ensuring an adequate amount of credible referencing. In this work the design method is developed based on the literature findings of Chapters 2 and 3 which are thoroughly referenced throughout.

(2) Accepting method consistency:

This step suggests that in order to follow and ensure the consistency of the design method, it is recommended to present the method through flowcharts. The proposed method of this thesis is indeed presented with a flowchart, as shown in Figure 26. The framework is initialised by providing the values for the requested inputs, and then the rest is organised into three main constructs, namely "Design", "Evaluate" and "Select". Each of them is further elaborated with more detailed sub-steps that guide the reader through the main tasks that take place when the design process is deployed.

(3) Accepting the example problems:

The example problems are presented in Sections 5.2 and D. They are all cargo vessels, each of a different type, targeting one of the most important category of ships. The proposed design method intends to generate designs for ships with alternative energy carriers and by testing the developed tool with the said example problems, provide sufficient results (presented in the mentioned sections) that show how it can be used for comparing the selected energy carriers and deciding on the most suitable option.

(4) Accepting usefulness of method for some example problems:

The exploration of the case studies in Section 5.2 was aimed at observing both the way cargo vessels operating with conventional fuels would be re-designed to operate with the studied energy carriers, as well as how the requested inputs affect the relative performance of the energy carriers. The ultimate goal, following the research objective, is to aid the sustainability development of the industry by both increasing efficiency in the early-stage designs and obtaining the required knowledge to do so on a case-by-case basis. For this reason, the selected case vessels are a good match to explore the validity of the design method, since these cargo vessels represent the largest share of the shipping industry and their sustainability improvement would have a massive impact on the overall sustainability level of the world.

(5) Accepting that usefulness is linked to applying the method:

This step is explored by testing each of the individual constructs of the method separately, in order to derive whether the method as a whole is the reason for the results. The design construct uses the provided inputs and generates all the solutions that fit within a pre-defined design space. It also ensures that only useful solutions are kept by using a preliminary feasibility filter. These solutions that exit the *design* construct are indeed useful and valid, but are not yet evaluated for their performance and whether they fulfil the user requirements. Therefore, the *evaluate* construct uses the feasible solutions and assesses their performance using valid and credible (for early-stage design) estimations models. Finally, the last construct

simply selects the most efficient solutions by identifying the Pareto fronts only for the ones that fulfil all the user requirements. This construct is useful for actually being able to compare the Pareto efficient models for their relative performance between the energy carriers. It can be concluded that the *select* construct could be potentially removed without affecting the purpose of the method since the user could also explore the design space and select the most suitable solution for the problem. Nonetheless, in terms of academic contribution, it is highly useful in providing the opportunity to directly compare and analyse the shifting of relative performance when the inputs are changed.

(6) Accepting usefulness of method beyond example problems: The usefulness beyond the example problems is derived by combining the five previous steps. It is demonstrated that the targets of the said steps are adequately achieved; hence, it can be claimed that enough confidence is built for the developed design method for its validity and usefulness for problems beyond the tested ones.

6

CONCLUSIONS

This chapter presents the conclusions of this graduation research assignment, starting by answering the research questions defined in Section 1.4. The second part then focuses on recommendations, which are organised in the ones that can improve the functionality of the tool, and the ones for future research.

6.1 FULFILLMENT OF RESEARCH QUESTIONS

- 1. Which are the state-of-the-art advancements in batteries, hydrogen, ammonia and methanol?
  - (a) What are the properties of these fuels regarding energy density, energy storage, and power generation?
  - (b) What are the requirements for these fuels to be implemented on a ship?

  This question is addressed by the entirety of Chapter 2. The main properties and application specifics of the selected energy carriers are summarised in Tables 1 and 17. The information in the latter presents the summary of the decision-making after reviewing the potential options and selecting based on performance and technological readiness. In addition, in order to safely and legally implement the studied energy carriers on board ships, the current regulations were also reviewed and are presented in Section 2.3.4 for the batteries, in Section 2.4.4 for hydrogen and ammonia, and in Section 2.6.4 for methanol.

- 2. What are the state-of-the-art advancements in ship design generators?
  - (a) How have alternative fuels been addressed in early-stage design so far?

  This question is addressed in Chapter 3, in which a range of design methods and existing tools were reviewed. Overall, different approaches were found with performances varying based on the targeted applications. It is highlighted that none of the studied methods have a direct connection with automating design generation for vessels with alternative energy carriers, and only individual case studies were explored. However, the key findings from each reviewed method/tool built the foundation for the development of this thesis' proposed design method. The summary of these findings can be found in Table 18.

- 3. Which will the overall architecture of the tool be?
  - (a) Which will the input variables be?
  - (b) Which will the outputs be?
  - (c) Which will the main analysis blocks and their general arrangement be?

The architecture of the tool is elaborated on in Section 4.2, where the operational flowchart is presented (Figure 26) and each of its steps is thoroughly explained. The input variables are service speed, autonomy, cargo DWT, cargo volume and ship type. The output of the tool is the filtered design space with vessels that have a score based on their performance of achieving the user requirements of speed and autonomy, such as Figure 37d (resulting design space for methanol vessels). On top of that, the most efficient solutions that fulfil both requirements (if any) are found by identifying the Pareto fronts and also plotting them on the same graph to analyse their relative performance. The last output of the tool is a parallel coordinate plot that shows LSW, R_t, L, B, D, L_{pg} and L_{ecs} for the Pareto models of each energy carrier, as shown in Figure 38. Regarding the main blocks, these are limited to the power generation room, the energy storage room and the cargo hold, and their placed in this exact order inside the hull as visualised in Figure 27.

- 4. How will the design space be constrained and evaluated?

  This question is again addressed by Section 4.2 but also by Section 4.3. The first stage of constraining the design space is explained in subsection 4.2.2, where the models with a cargo hold length less than 15% of the total midhull length are discarded. Additionally, throughout the function of the tool, there are several geometrically limiting ranges that are applied in order to keep models that fall within the applicable range of the Holtrop & Mennen's method. These ranges are provided in Table 23.

  In terms of the evaluation of the models, the tool focuses on the estimation of LSW and R_t, using regression models derived per ship type using C-Job's database, and the Holtrop & Mennen's method, respectively. LSW and R_t were chosen in order to indirectly address and observe the impact on OPEX and CAPEX, respectively.

- 5. What are the optimisation objective/-s and how are the optimal solutions determined?

  The optimisation performed by the SSDG is multi-objective focusing on both LSW and R_t. The decision for this was easy since these were the only selected KPIs, and it was a simple task to address both. The optimisation is performed only for the fully feasible solutions (achieving both requirements of speed and autonomy), for which the Pareto fronts are identified.

- 6. How is the tool and the design method tested and validated?

  The answer to this question can be found in Chapter 5. The tool specifically is validated for its estimations of LSW and R_t by comparing the actual and estimated values for ten example vessels, as shown in Table 27. It was found that there is an average 20% underestimation of LSW, while for resistance there is an average overall deviation of 11.3%. Next, the case studies, shown in Section 5.2, aid both the performance testing and the validation of the tool. The said section only provides the findings for the first case study, while the rest can be found in Appendix D. Overall, the visualised results demonstrate the functionality of the SSDG and allow for the sanity check of whether generated models are reasonable and as close to reality as possible. Finally, the last part of the chapter (Section 5.3) focuses completely on the validation of the design method. It is explained that, unlike other research, when there is a development of a design method then it is only possible to apply a *Relativist validation* [99]. This is carried out using the validation square (Figure 41) and answering a set of steps that progressively help the reader build confidence in the credibility of the process.

- 7. What trends can be identified for the relation between the chosen energy carriers and the input variables?

This question is primarily addressed in Section 5.2.2, where the inputs of service speed and autonomy are varied while the rest of the inputs are kept the same as for the chosen case vessel. This study provided the opportunity to observe how the Pareto curves shift relative to both the different inputs for the same carrier and the different carriers for the same inputs. These results are visualised in Figure 39 for the service speed variation, and in Figures 40 for the variation of autonomy. It was concluded that for highly demanding inputs, such as the original ones coming from the case vessel (Table 28), there is a great difference in performance between the energy carriers, while battery-powered vessels are completely infeasible. However, for inputs of lower demand (especially for relatively low autonomy), there is feasibility for all the energy carriers, and the resulting Pareto fronts are much more comparable. The results still confirm the expectations of methanol being the most efficient, before ammonia, hydrogen and batteries (in that order); however, it is shown that there are ranges, where the difference can become small enough and in combination with other factors (currently not included in this study), performance could be further affected making the other energy carriers reasonable beyond just methanol.

6.2 RECOMMENDATIONS

6.2.1 *Functionality improvements*

This section provides a set of recommendations on how the tool could be improved in terms of practical applicability, and thus provide more realistic results.

- Development of an improved LSW regression model with higher accuracy and higher applicability range. This could be achieved by either improving the combination of the independent variables or by drawing training a higher volume of training data with vessels covering a wider range.
- Integrate different power plant and energy storage options configurations in order to ensure higher space efficiency. For example, instead of a single DF ICE, there could be two of them side-by-side depending on the shape/size of the room.
- Estimation of required ballast tanks will also give a better picture of the models' stability and will bring the vessels one step closer to being more realistic.
- Define a more advanced suggestion for the translation of cargo volume input to required cargo hold space for the different ship types.
- Investigation towards making the results more realistic with a focus on achieving a reasonable difference between the methanol vessels' Pareto fronts and the case vessels running on diesel. This issue is primarily due to optimising for only three blocks/rooms inside the hull, excluding all other essential systems and machinery. It is then necessary to capture such essential requirements and translate them into spatial needs in order to increase the accuracy of the vessels' dimensional estimation.
- Include a mathematical model that will provide estimations for the efficiency of a power plant (different energy carrier) based on the power demand of the model. Currently a single value of overall system efficiency is assumed for each energy carrier, but it is recognised that it can lead to noticeable deviations from reality when exploring more extreme areas of the design spaces.

- Include 3D modelling - an attempt was made to use an existing hull shape from C-Job's library, scale it for the dimensions of the desired model, and fit the three rooms inside of it. However, the current version of the tool assumes a boxed-shaped mid hull and it is also not considering the transitioning curvature from midhull to the aft and fore hulls. For this reason, the rooms ended up poking outside the hull. A simple solution to this would be to trim the rooms in the shape of the hull; nonetheless, this would result in a significant reduction in the size of the room, meaning that the requested requirements may not be fulfilled anymore. In this way, it is necessary to either iterate a few times to refine the sizes of the rooms and the overall dimensions of the vessel, or the required sizes of the rooms could be overestimated in order to still fulfil the requirements when trimmed.

6.2.2 *Future research*

The development of the presented method and the SSDG tool proved to be an important step forward towards establishing alternative energy carrier options in early-stage design. The foundation has been laid, but more research is required for the tool to be further studied. The following suggestions could be some of the potential future research on this topic, as they were identified during the development of the SSDG.

- Explore power generation and energy storage options that are not yet feasible but could have higher potential, such as lithium-sulfur batteries or ammonia-fuelled SOFCs
- Increase level of detail in essential components/systems for power generation and energy storage. This is expected to offer a better estimation of the space requirements for the desired outputs.
- Create a library of pre-defined HLPs from which standard systems and equipment can be drawn and re-sized and included in the models. This will bring the models closer to the required end product and will provide a more accurate size estimation
- Coupling the tool with a resistance solver of higher accuracy for better estimations. Although Holtrop & Mennen's is a well-established and proven method, it requires filtering of the design space in order to ensure the studied vessels fall within the method's applicable range. This could mean that computation time will be significantly increased; therefore, it may be necessary to integrate an optimisation algorithm and explore a much lower number of models in order to find the optimum.
- Addition of more KPIs and potentially more optimisation objectives, in an effort of obtaining a more complete perspective on the relative performance of the energy carriers. For example, installation costs, well-to-tank costs, energy carrier availability or even sustainable energy carrier production could be some of the potential additions.

A

ELECTRICITY PRODUCTION AND EMISSIONS

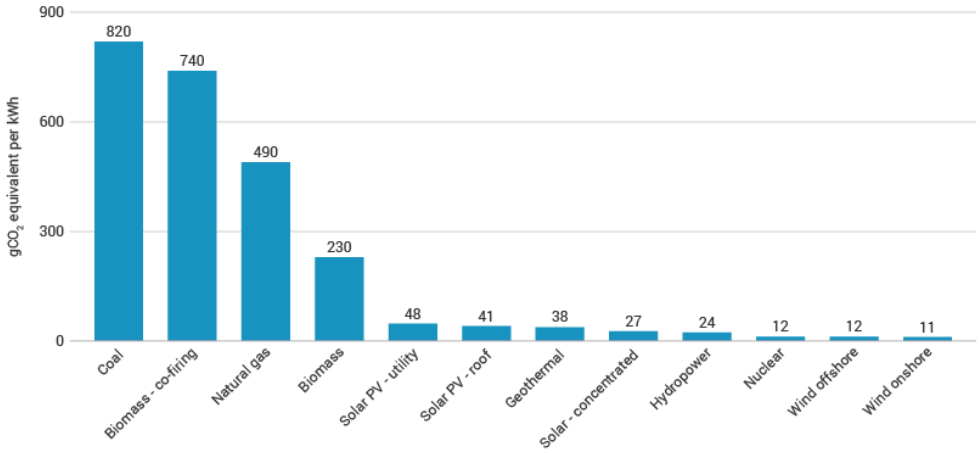

Figure 42: gCO_2 equivalent per kWh emissions when producing electricity [102].

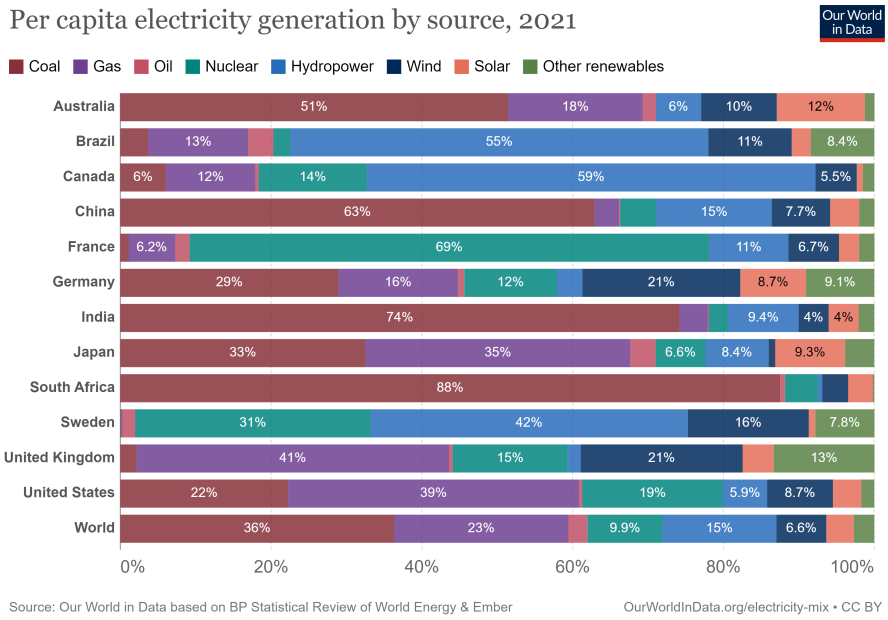

Figure 43: Per capita electricity generation distribution in 2021 [103], [104].

B

COMBUSTION CHARACTERISTICS OF ALTERNATIVE ENERGY CARRIERS

Fuel	NH_3	H_2	CH_4	C_3H_8
Boiling temperatureat 1 atm (°C)	−33.4	−253	−161	−42.1
Condensation pressure at 25 °C (atm)	9.90	N/A	N/A	9.40
Lower heating value, LHV (MJ/kg)	18.6	120	50.0	46.4
Flammability limit (Equivalence ratio)	0.63∼1.40	0.10∼7.1	0.50∼1.7	0.51∼2.5
Adiabatic flame temperature (°C)	1800	2110	1950	2000
Maximum laminar burning velocity (m/s)	0.07	2.91	0.37	0.43
Minimum auto ignition temperature (°C)	650	520	630	450

Table 29: Major combustion characteristics' comparison between ammonia, hydrogen, methane and propane [23].

C

EQUATIONS USED FOR THE CALCULATIONS OF THE FRAMEWORK

C.1 VESSEL LENGTH CALCULATIONS

$$LOA = L_{fore} + L_{aft} + L_{mid} \tag{4}$$

Where,

- L_{fore} = length of the ship's forehull section
- L_{aft} = length of the ship's afthull section
- L_{mid} = length of the ship's midhull section

$$\begin{aligned} L_{aft} &= L_{mid} \cdot \alpha_{aft} \\ L_{fore} &= L_{mid} \cdot \alpha_{fore} \\ L_{mid} &= L_{cargo} + L_{pg} + L_{ecs} \end{aligned} \tag{5}$$

Where,

- α_{fore} = fixed coefficient that scales the forehull section based on the midhull and depends on the chosen hull shape
- α_{fore} = fixed coefficient that scales the afthull section based on the midhull and depends on the chosen hull shape
- L_{pg} = length of power generation room
- L_{ecs} = length of energy carrier storage room

$$LOA = (\alpha_{fore} + \alpha_{aft} + 1) \cdot L_{mid} \tag{6}$$

$$L_{mid} = \frac{LOA}{1 + \alpha_{fore} + \alpha_{aft}} \tag{7}$$

C.2 LSW ADJUSTMENTS

$$\begin{aligned} LSW_{batteries} &= LSW_{est} - m_{ICE} + m_{batt} + m_{em} \\ LSW_{hydrogen} &= LSW_{est} - m_{ICE} + m_{fc} + m_{em} + m_{typeC} \\ LSW_{ammonia} &= LSW_{est} + m_{typeC} \\ LSW_{methanol} &= LSW_{est} \end{aligned} \tag{8}$$

Where,

- LSW_{est} = LSW estimated from the developed regression model

- m_{ICE} = estimated mass of the ICE of an equivalent-sized conventional power generation room
- m_{batt} = total mass of batteries fitted in the energy storage room
- m_{em} = mass of the scaled electric motor that is fitted in the power generation room
- m_{fc} = total mass of PEMFCs fitted in power generation room
- m_{typeC} = mass estimation of the type C tanks that are fitted in the energy storage room

C.3 CONVERSION OF TEUS TO CARGO HOLD VOLUME

The conversion to cargo hold volume is done using a ratio of 0.7 for TEUs stored below deck to TEUs stored above deck. This number is approximated based on existing vessels. In addition, the volume of a single TEU is assumed at 38.5 m^3.

$$\begin{aligned} V_{cargo} &= TEU \cdot 38.5 \\ V_{deck} &= \frac{V_{hold}}{0.7} \\ TEU \cdot 38.5 &= V_{hold} + \frac{V_{hold}}{0.7} \\ V_{hold} &= \frac{TEU \cdot 38.5}{1 + \frac{V_{deck}}{0.7}} \end{aligned} \tag{9}$$

Where,

- V_{cargo} = total cargo volume
- V_{deck} = volume of TEUs stored on deck
- V_{hold} = volume of TEUs stored in cargo hold

C.4 DRAUGHT

$$\begin{aligned} C_B &= \frac{\nabla}{L \cdot B \cdot T} \\ T &= \frac{\nabla}{L \cdot B} \end{aligned} \tag{10}$$

C.5 STABILITY CHECK

The process and calculations displayed below are extracted from the instruction presented in the relevant book of Papanikolaou [3].

C.5.1 *Calculation of required inputs*

$$\nabla = \frac{LSW + DWT}{\rho_{sea}} \tag{11}$$

$$r_{bilge} = \frac{B \cdot \frac{0.5}{0.6}}{(\frac{L}{B} + 4) \cdot {C_B}^2} \tag{12}$$

$$C_M = 1 - \frac{{r_{bilge}}^2}{2.33 \cdot B \cdot T} \tag{13}$$

$$I_T = \frac{C_{IT} \cdot L \cdot B^3}{12} \tag{14}$$

Where C_{IT} is the coefficient of specificity of form of waterplane area calculated as shown in equation 14:

$$C_{IT} = C_{WP} \cdot (0.1272 + 0.8724 \cdot C_{WP}) \tag{15}$$

C_{WP} is the waterplane area coefficient that is computed as follows (equation 16:

$$C_{WP} = \frac{1 + 2 \cdot C_B}{3} \tag{16}$$

C.5.2 *Calculation of GM*

$$GM = KM - KG \tag{17}$$

Where KM is the distance from the keel (K) to the metacentric centre (M) and KG is the distance from K to CoG.

$$\begin{aligned} KG &= \frac{B}{2} \\ KM &= KB + BM \\ KB &= T \cdot (0.9 - 0.3 \cdot C_M - 0.1 \cdot C_B) \\ BM &= \frac{I_T}{\nabla} \end{aligned} \tag{18}$$

Therefore combining equations 18 and 17 gives:

$$GM = T \cdot (0.9 - 0.3 \cdot C_M - 0.1 \cdot C_B) + \frac{I_T}{\nabla} - \frac{B}{2} \tag{19}$$

C.6 INPUTS REQUIRED FOR THE RESISTANCE CALCULATION

The relations used below are empirical formulations that can be found in the Ship Design book of Papanikolaou [3], and some are just crude estimations that are acceptable for the early-stage level.

$$\begin{aligned} L_{BP} &= LOA \cdot 0.95 \\ L_{WL} &= LOA \cdot 0.97 \end{aligned} \tag{20}$$

$$A_{BT} = 0.1 \cdot B \cdot T \tag{21}$$

$$C_P = \frac{C_B}{C_M} \tag{22}$$

$$LCB = (0.5 - \frac{L_{BP}}{L_{WL}} \cdot (0.5 - LCB_{SB})) \cdot 100 \tag{23}$$

Where,

$$LCB_{SB} = -0.135 + 0.194 \cdot C_P \tag{24}$$

C.7 REQUIRED INSTALLED POWER

$$\begin{aligned} P_{prop} &= R_{total} \cdot v \\ P_{total-req} &= P_{prop} \cdot \alpha_{ec} \end{aligned} \tag{25}$$

Where,

- P_{prop} = propulsion power demand
- R_{total} = total resistance of the vessel
- v = user-requested service speed
- $P_{total-req}$ = total required power
- α_{ec} = 1.05 = factor to increase total power demand by 5% to accommodate for the electrical consumers of the ship

C.8 REQUIRED AMOUNT OF ENERGY

$$E_{req} = \frac{P_{total-req}}{\eta_{pp}} \cdot t_{aut} \cdot \alpha_{red} \tag{26}$$

Where,

- E_{req} = required energy to power the vessel for the requested autonomy time and speed
- η_{pp} = power plant efficiency
- t_{aut} = requested autonomy time in hours
- α_{red} = 1.1 = factor to increase required energy by a 10% margin for redundancy reasons

C.9 ANALYSIS OF ENERGY STORAGE ROOMS

C.9.1 *Hydrogen*

Wall thickness of shells for type C tanks

Note, Figure 44 below represents the hydrogen tanks, while the ammonia ones are equivalent but only require a single shell; hence, the inner shell and the insulation space are still considered, removing only the outer one.

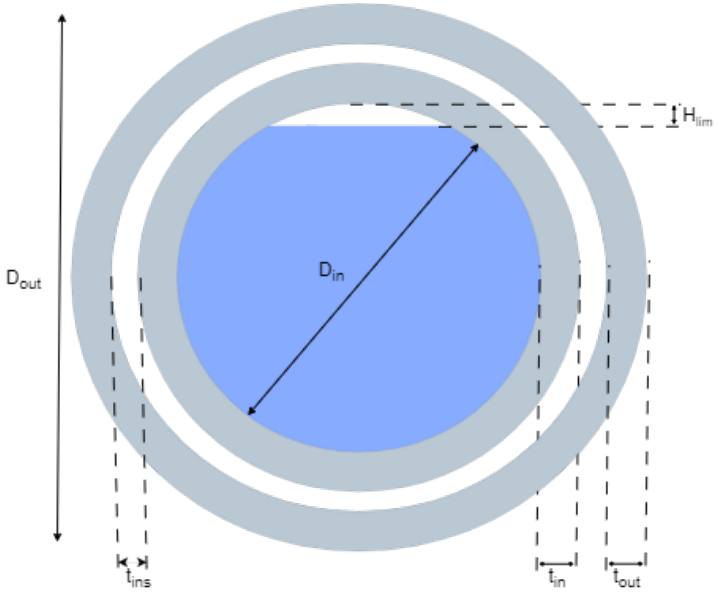

Figure 44: Schematic of the type C tank's cross-section displaying its shells and insulation thickness.

Where,

- t_{in} = Wall thickness of inner shell
- t_{out} = Wall thickness of outer shell
- t_{ins} = Vacuum thickness
- $H_{lim} = 0.05 \cdot D_{inner}$ = Allowable filling limit of the tank
- D_{out} = External diameter of the tank
- D_{in} = Internal diameter of the tank

The equation used for the wall thickness calculation of the type C tanks is as follows:

$$t = \frac{p_{fuel} \cdot D_{out}}{\sigma_y} \cdot S_f \tag{27}$$

Where,

- p_{fuel} = Pressure of stored fuel
- σ_y = Yield strength of tank's material[1]= $515 \cdot 10^6$
-

$$S_f = Safetyfactor = \begin{cases} 6 & \text{for hydrogen's inner shell} \\ 3 & \text{for hydrogen's outer shell} \\ 3 & \text{for ammonia's single shell} \end{cases} \tag{28}$$

Available volume for fuel & tank weight

$$V_{fuel} = \pi \cdot (((D_{out} - 2 \cdot t_{inner} - 2 \cdot t_{out} - 2 \cdot t_{in}) \cdot 0.5)^2) \cdot L_{tank} \cdot Lim_{fill} \tag{29}$$

Where,

- L_{tank} = Length of the tank
- Lim_{fill} = 0.95 = filling limit of the tank

In addition, the tank's weight calculation is performed as shown below in Equations 30 starting with calculating the total volume of the two shells.

$$\begin{aligned} V_{outer-shell} &= \pi \cdot L_{tank} \cdot 0.25 \cdot (D_{out}^2 - (D_{out} - 2 \cdot t_{out})^2) \\ V_{inner-shell} &= \pi \cdot L_{tank} \cdot 0.25 \cdot ((D_{out} - 2 \cdot t_{out} - 2 \cdot t_{ins})^2 - (D_{out} - 2 \cdot t_{out} - 2 \cdot t_{ins} - 2 \cdot t_{in})^2) \\ V_{total-shell} &= V_1 + V_2 \end{aligned} \tag{30}$$

Finally, the total weight of the tank is calculated using Equation 31.

$$w_{typeC} = V_{total-shell} \cdot \rho_{al-6061} \tag{31}$$

Where,

- $\rho_{al-6061}$ = the density of the tank's material (Al 6061-T6 [105]) = 2700 kg/m^3

[1] Stainless steel SS131 that was found in [105].

Required amount of MGO and total installed energy

$$\begin{aligned} E_{sust} &= \rho_{v-sust} \cdot V_{sust} = 0.9 \cdot E_{total} \\ E_{MGO} &= \rho_{v-mgo} \cdot V_{mgo} = 0.1 \cdot E_{total} \end{aligned} \tag{32}$$

Combining the two equations of 32 gives:

$$V_{MGO} = \frac{\rho_{v-sust}}{\rho_{v-MGO}} \cdot \frac{1}{9} \cdot V_{sust} \tag{33}$$

Where,

- E_{sust} = Energy from sustainable fuel
- E_{MGO} = Energy from MGO
- E_{total} = Total energy from fuels
- V_{MGO} = Volume of MGO
- V_{sust} = Volume of sustainable fuel
- ρ_{v-sust} = Volumetric energy density of sustainable fuel
- ρ_{v-MGO} = Volumetric energy density of MGO

The total energy installed on each hydrogen vessel is then calculated by simply multiplying the available amount of the two fuels with their respective volumetric energy density, as shown in Equation 34.

$$E_{total} = V_{MGO} \cdot \rho_{v-MGO} + V_{sust} \cdot \rho_{v-sust} \tag{34}$$

D

CASE STUDIES

The remaining case studies are presented in this Appendix as mentioned in Chapter 5.2. These include 4 vessels one for each of the remaining integrated ship types: general cargo vessel, bulk carrier, Ro-Ro and container ship. These case studies include only the first part presented in Chapter 5.2 which explores how an existing vessel would differ from its original design if it was operated with the studied energy carriers.

D.1 DA JI - GENERAL CARGO VESSEL

Figure 45: Photo of the studied Da Ji [106].

LOA	[m]	179.7			
B	[m]	28			
D	[m]	14.8	Service speed	[kt]	15.5
T	[m]	9.2	Cargo volume	[m^3]	35684
DWT	[t]	23772.5	Cargo DWT	[t]	21395.1
LSW	[t]	10983	Autonomy	[days]	69
P_B	[kW]	7000			
R_t	[kN]	702.3			

Table 30: Main characteristics of the Da Ji (left) and its capabilities (right) used as inputs for the SSDG.

$$\text{Design space} = \begin{cases} \text{LOA} & \text{155 to 280, steps of 1 m} \\ \text{B} & \text{13 to 38, steps of 0.5 m} \\ \text{D} & \text{9 to 30, steps of 0.5 m} \\ L_{pg} & \text{5 to 15.5, steps of 0.5 m} \end{cases}$$

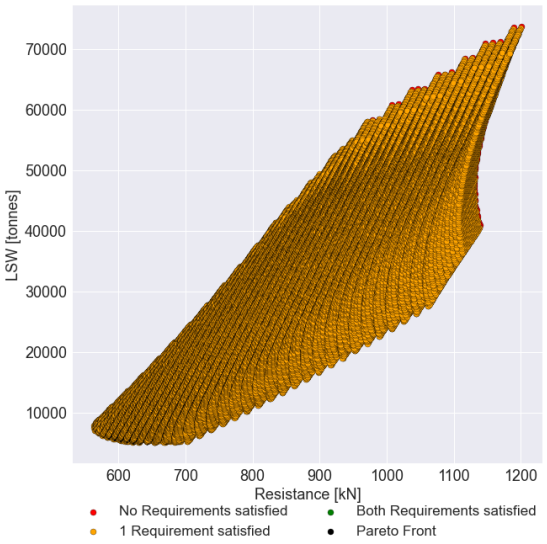

(a) Batteries

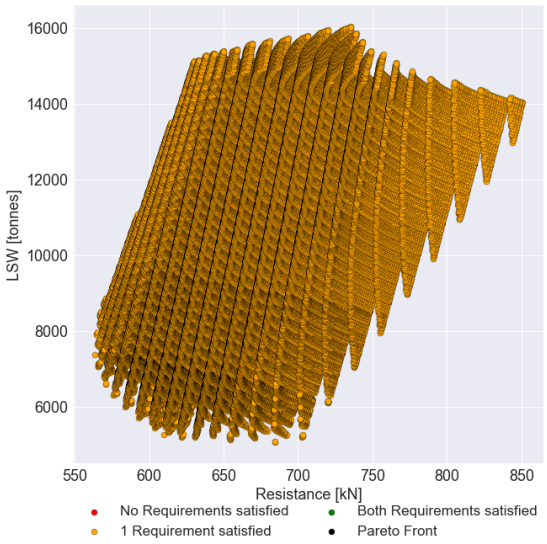

(b) Hydrogen

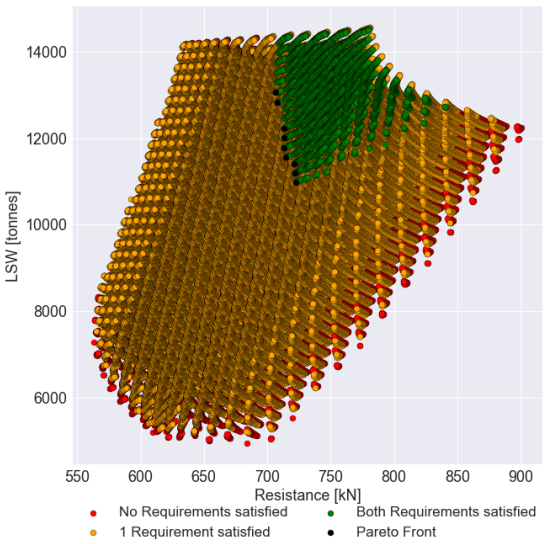

(c) Ammonia

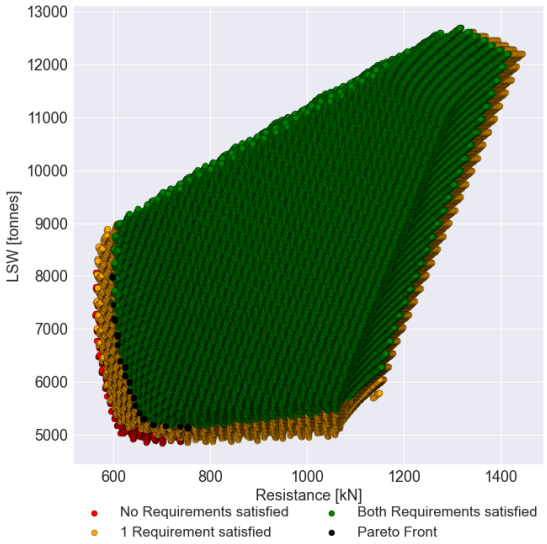

(d) Methanol

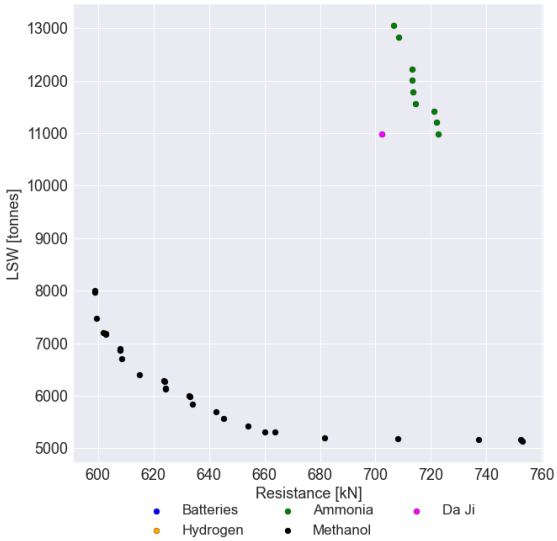

(e) Combined Pareto fronts

Figure 46: Resulting design spaces and the combined Pareto fronts plot for the case vessel Da Ji.

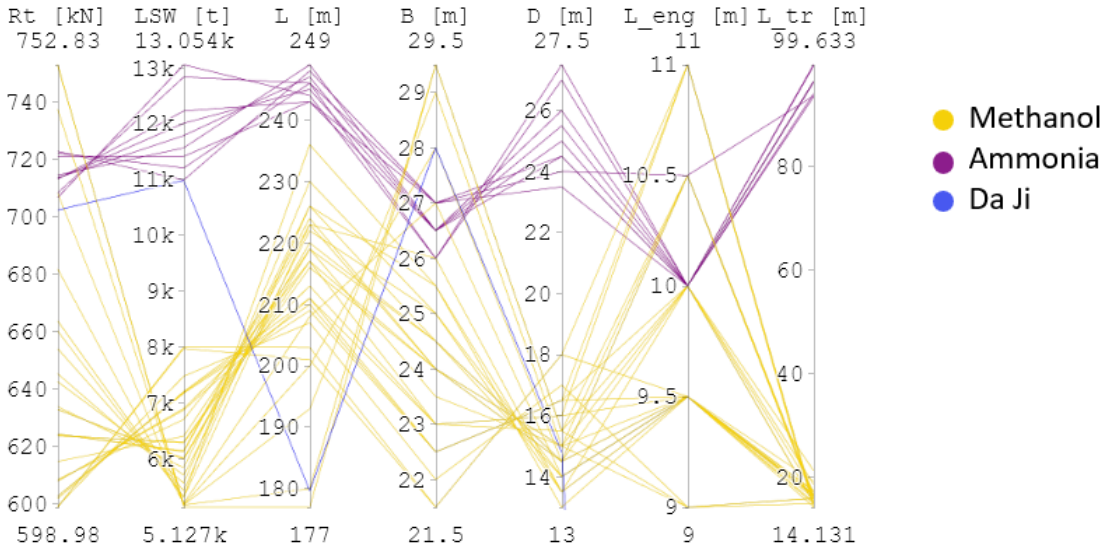

Figure 47: Parallel coordinate plot for the feasible Pareto front models.

D.2 CHINA STEEL LIBERTY - BULK CARRIER

Figure 48: Photo of the studied China Steel Liberty [107].

LOA	[m]	299.7			
B	[m]	50			
D	[m]	25	Service speed	[kt]	14.5
T	[m]	16	Cargo volume	[m^3]	210500
DWT	[t]	208600	Cargo DWT	[t]	187740
LSW	[t]	27500	Autonomy	[days]	97
P_B	[kW]	14900			
R_t	[kN]	1598			

Table 31: Main characteristics of the China Steel Liberty (left) and its capabilities (right) used as inputs for the SSDG.

$$\text{Design space} = \begin{cases} \text{LOA} & \text{250 to 380, steps of 1.5 m} \\ \text{B} & \text{30 to 70, steps of 1 m} \\ \text{D} & \text{15 to 45, steps of 1 m} \\ L_{pg} & \text{5 to 15.5, steps of 0.5 m} \end{cases}$$

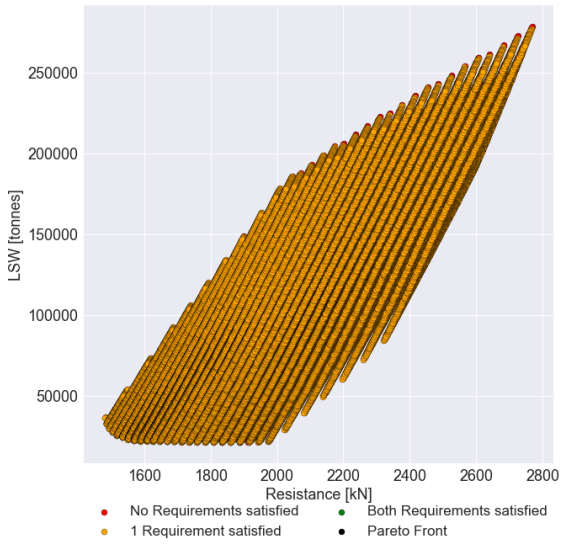

(a) Batteries

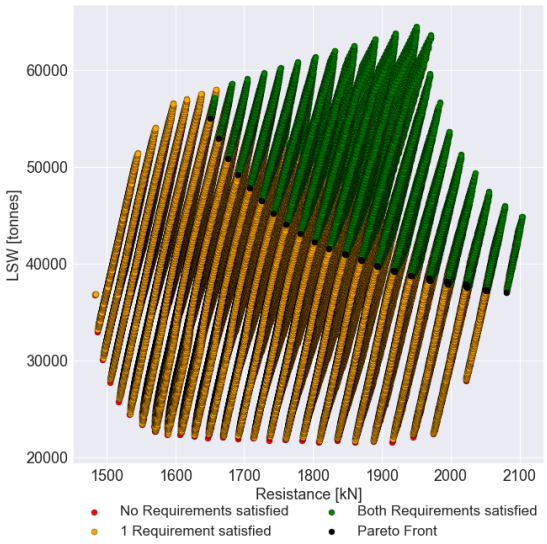

(b) Hydrogen

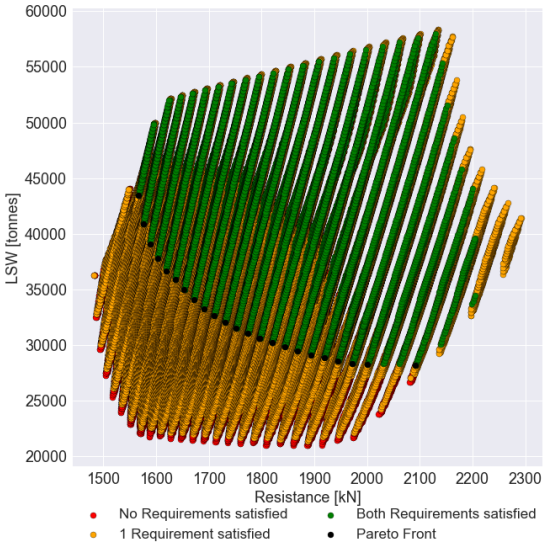

(c) Ammonia

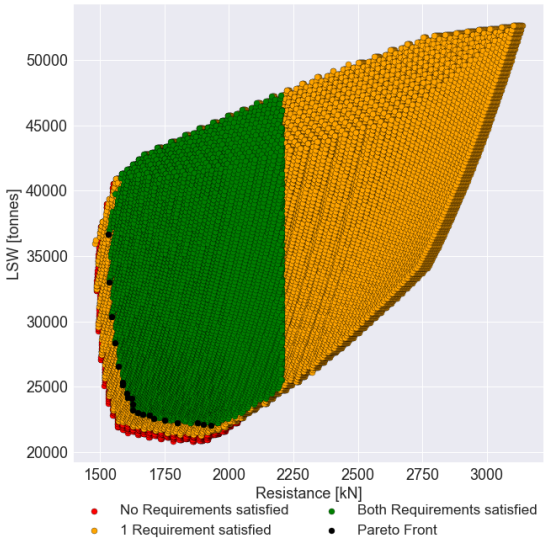

(d) Methanol

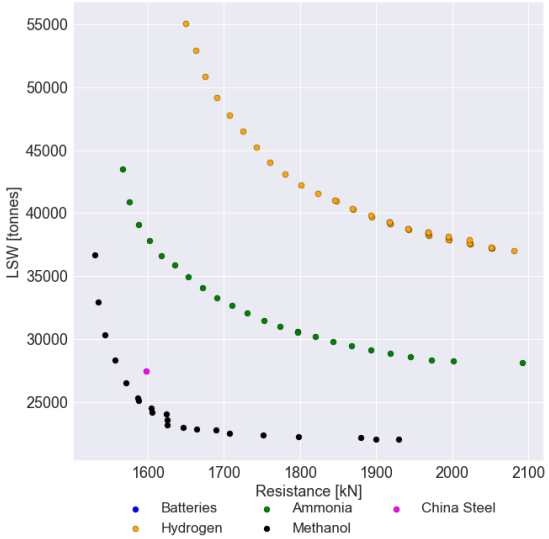

(e) Combined Pareto fronts

Figure 49: Resulting design spaces and the combined Pareto fronts plot for the case vessel China Steel Liberty.

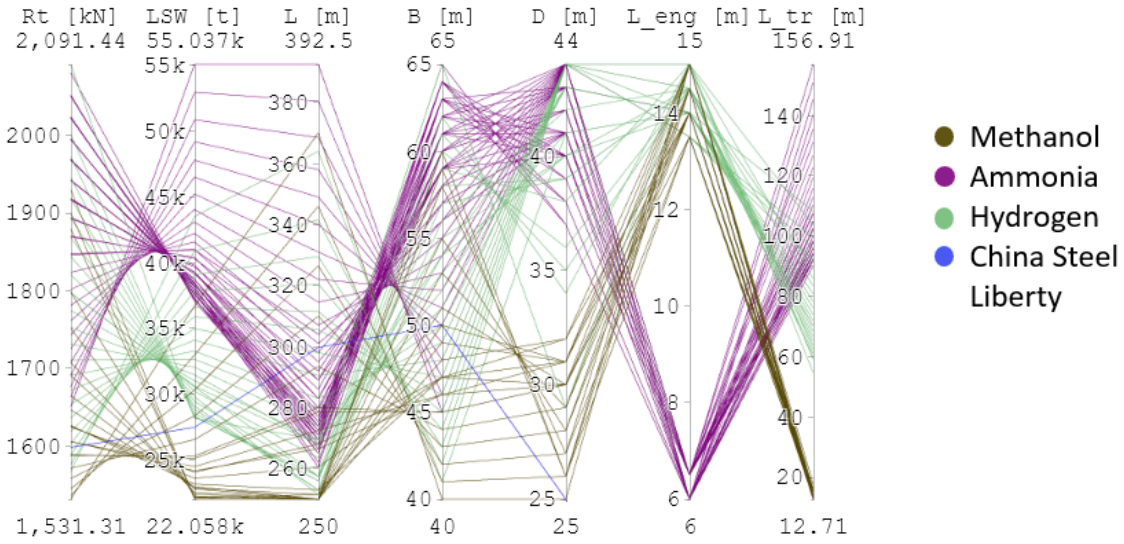

Figure 50: Parallel coordinate plot for the feasible Pareto front models.

D.3 CMA CGM ARGENTINA - CONTAINERSHIP

Figure 51: Photo of the studied CMA CGM Argentina [107].

LOA	[m]	366			
B	[m]	51			
D	[m]	29.9	Service speed	[kt]	22
T	[m]	14.5	TEU	[m^3]	15072
DWT	[t]	133607	Cargo DWT	[t]	120246.3
LSW	[t]	42907	Autonomy	[days]	80
P_B	[kW]	46360			
R_t	[kN]				

Table 32: Main characteristics of the China Steel Liberty (left) and its capabilities (right) used as inputs for the SSDG.

$$\text{Design space} = \begin{cases} \text{LOA} & \text{250 to 500, steps of 1.5 m} \\ \text{B} & \text{30 to 70, steps of 1 m} \\ \text{D} & \text{15 to 45, steps of 1 m} \\ L_{pg} & \text{5 to 25, steps of 0.5 m} \end{cases}$$

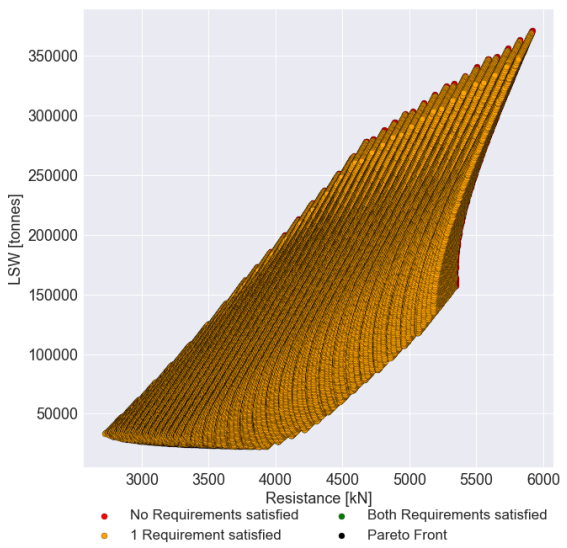

(a) Batteries

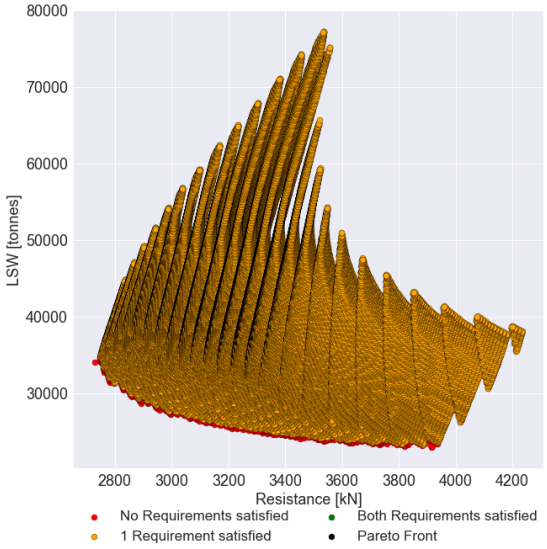

(b) Hydrogen

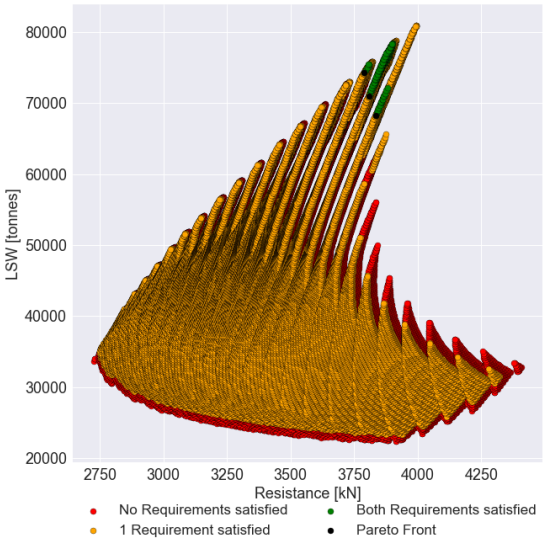

(c) Ammonia

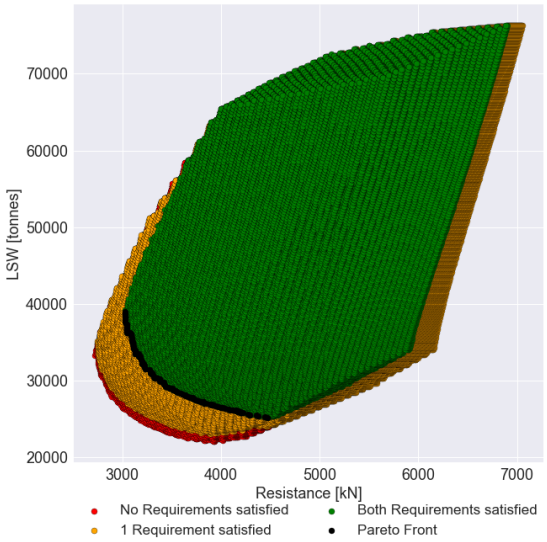

(d) Methanol

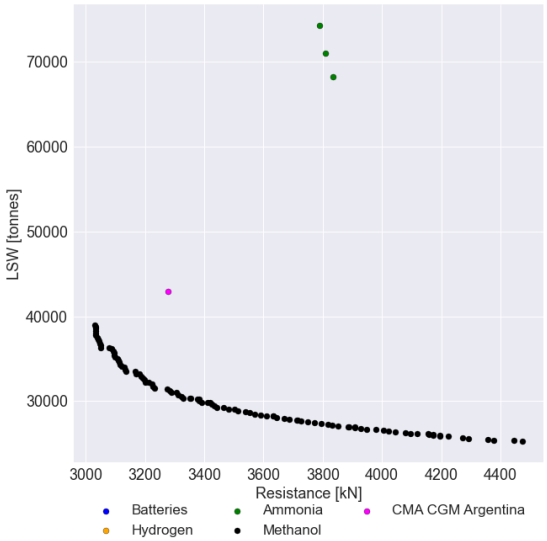

(e) Combined Pareto fronts

Figure 52: Resulting design spaces and the combined Pareto fronts plot for the case vessel CMA CGM Argentina.

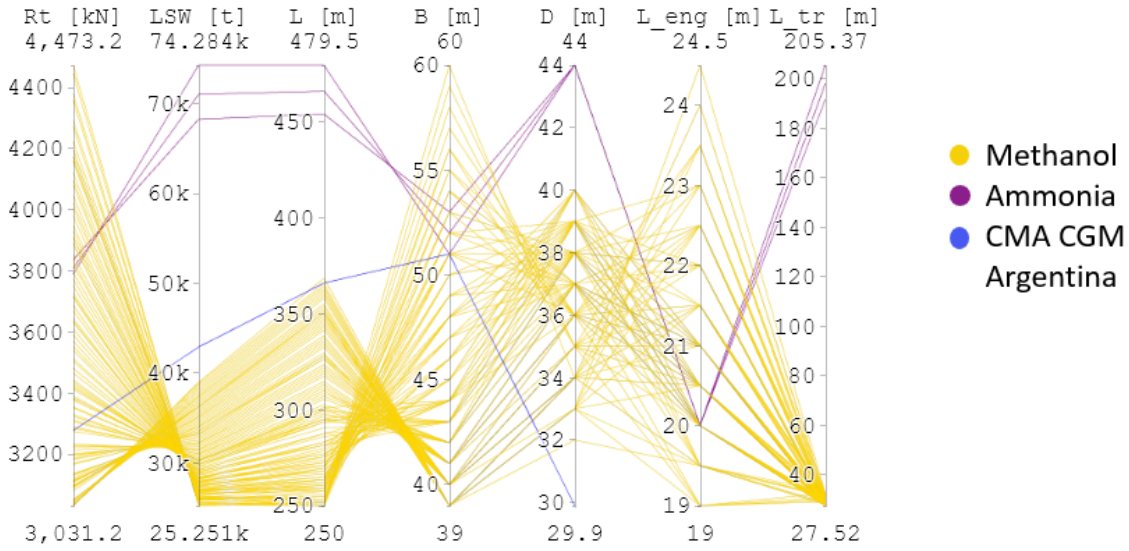

Figure 53: Parallel coordinate plot for the feasible Pareto front models.

D.4 AN JI 23 - RO-RO

Figure 54: Photo of the studied An Ji 23 [108].

LOA	[m]	169.1			
B	[m]	28			
D	[m]	13	Service speed	[kt]	16
T	[m]	7.6	Cargo volume	[m^3]	31370
DWT	[t]	8235	Cargo DWT	[t]	4940
LSW	[t]	11653	Autonomy	[days]	64
P_B	[kW]	7550			
R_t	[kN]	642.1			

Table 33: Main characteristics of the China Steel Liberty (left) and its capabilities (right) used as inputs for the SSDG.

$$\text{Design space} = \begin{cases} \text{LOA} & \text{140 to 250, steps of 1 m} \\ \text{B} & \text{15 to 45, steps of 0.5 m} \\ \text{D} & \text{15 to 45, steps of 0.5 m} \\ L_{pg} & \text{5 to 15, steps of 0.5 m} \end{cases}$$

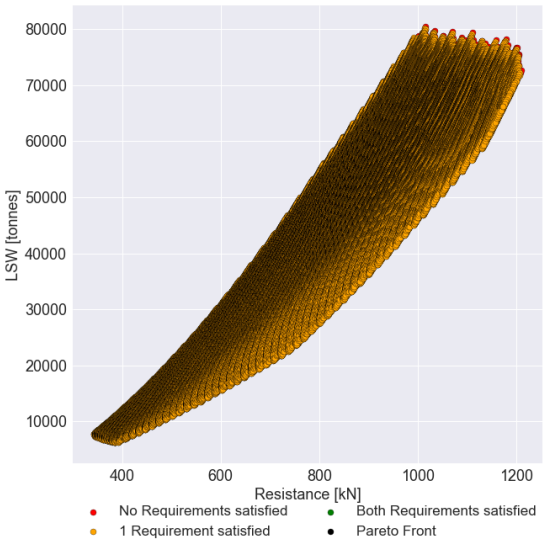

(a) Batteries

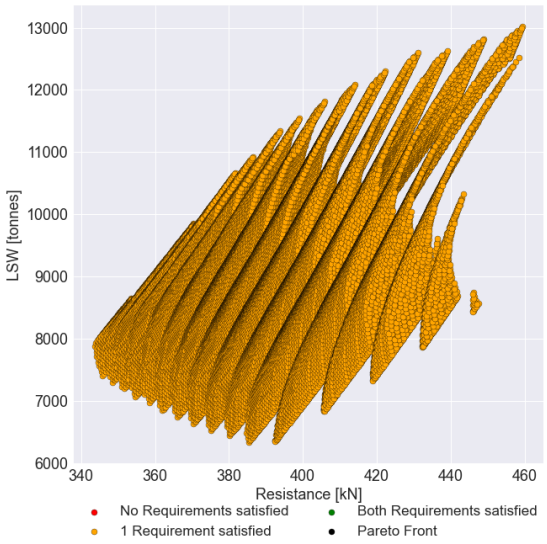

(b) Hydrogen

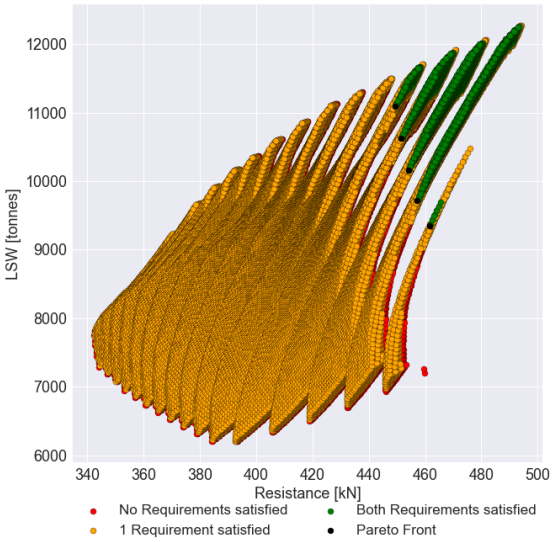

(c) Ammonia

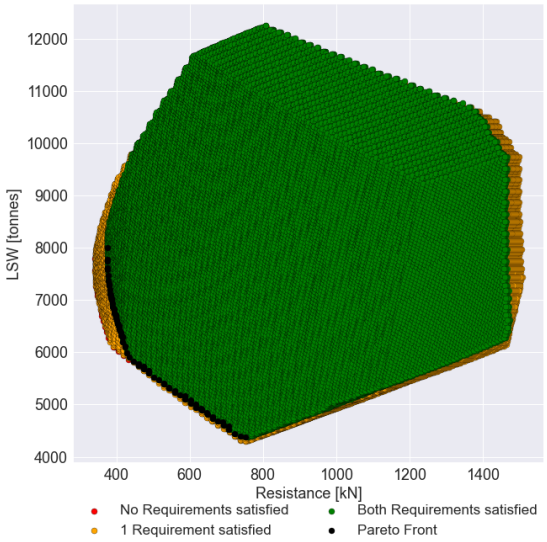

(d) Methanol

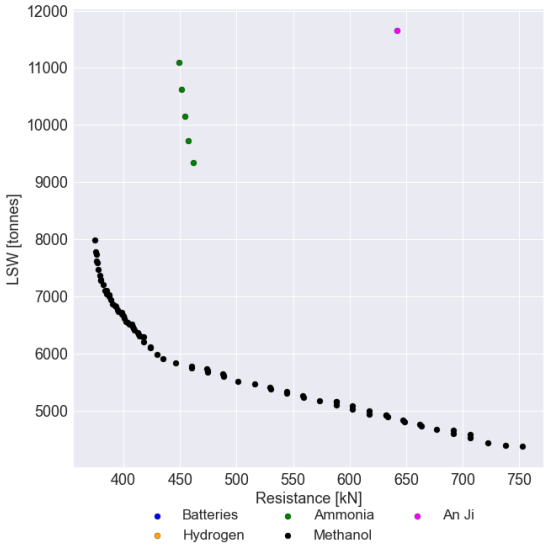

(e) Combined Pareto fronts

Figure 55: Resulting design spaces and the combined Pareto fronts plot for the case vessel An Ji 23.

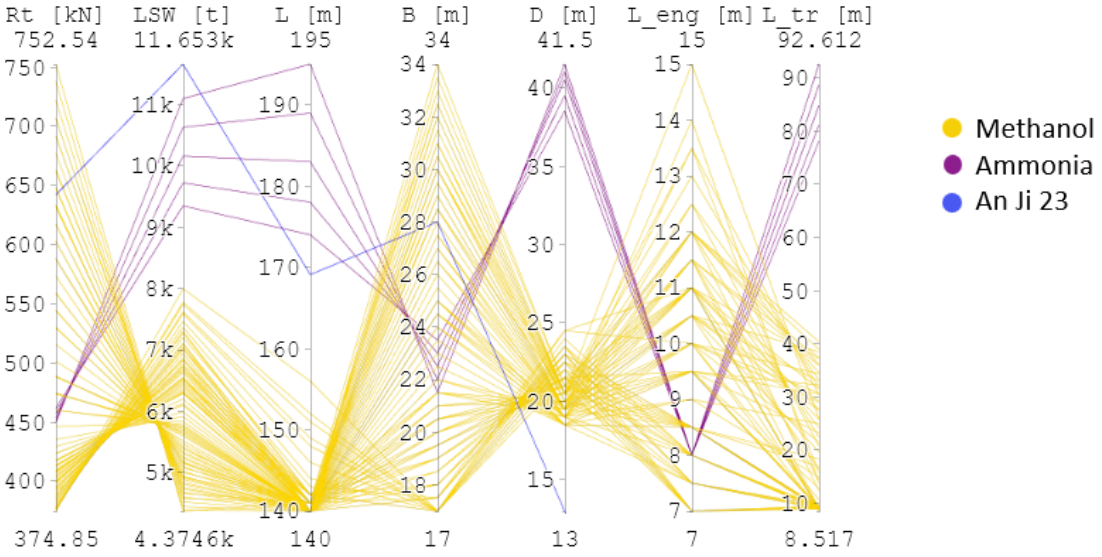

Figure 56: Parallel coordinate plot for the feasible Pareto front models.

BIBLIOGRAPHY

[1] IMO, "IMO's work to cut GHG emissions from ships," 2018. [Online]. Available: https://www.imo.org/en/MediaCentre/HotTopics/Pages/Cutting-GHG-emissions.aspx

[2] DNV, "MARITIME FORECAST TO 2050: Energy Transition Outlook 2022," 2022.

[3] A. D. Papanikolaou, *Ship design: Methodologies of preliminary design*. Springer, 2014.

[4] N. d. Vries, "Safe and effective application of ammonia as a marine fuel," Master's thesis, TU Delft, 2019. [Online]. Available: https://repository.tudelft.nl/islandora/object/uuid%3Abe8cbe0a-28ec-4bd9-8ad0-648de04649b8

[5] M. Placek, "Energy density of maritime fuels," Feb 2023. [Online]. Available: https://www.statista.com/statistics/1279431/energy-density-of-maritime-fuels/

[6] ShiftCleanEnergy, "Shift clean energy," Jan 2022. [Online]. Available: https://shift-cleanenergy.com/

[7] D. Nelissen, J. Faber, R. v. d. Veen, A. v. Grinsven, H. Shanthi, and E. v. d. Toorn, "Availability and costs of liquefied bio- and synthetic methane: The maritime shipping perspective," 2020.

[8] J. Ellis and K. Tanneberger, "Study on the use of ethyl and methyl alcohol as alternative fuels in shipping," 2016.

[9] S. Atilhan, S. Park, M. M. El-Halwagi, M. Atilhan, M. Moore, and R. B. Nielsen, "Green hydrogen as an alternative fuel for the shipping industry," *Current Opinion in Chemical Engineering*, vol. 31, p. 100668, Feb 2021. [Online]. Available: https://doi.org/10.1016/j.coche.2020.100668

[10] M. T. T. Abelleira, "Batteries for marine applications," Master's thesis, NTNU, 2013. [Online]. Available: https://ntnuopen.ntnu.no/ntnu-xmlui/bitstream/handle/11250/238654/649652_FULLTEXT01.pdf?sequence=1

[11] H. Chen, T. N. Cong, W. Yang, C. Tan, Y. Li, and Y. Ding, "Progress in electrical energy storage system: A critical review," *Progress in Natural Science*, vol. 19, no. 3, p. 291–312, 2009. [Online]. Available: https://doi.org/10.1016/j.pnsc.2008.07.014

[12] D. Kaur, M. Singh, and S. Singh, "Lithium–sulfur batteries for marine applications," *Lithium-Sulfur Batteries*, p. 549–577, 2022. [Online]. Available: https://doi.org/10.1016/B978-0-323-91934-0.00019-3

[13] M. E. Solutions, "Batteries on board ocean-going vessels," Sep 2019. [Online]. Available: https://www.man-es.com/docs/default-source/marine/tools/batteries-on-board-ocean-going-vessels.pdf?sfvrsn=deaa76b8_14

[14] N. Mjos, S. Eriksen, A. Kristoffersen, G. P. Haugom, A. Huser, B. Gully, D. Hill, R. Stoiber, L. O. Valoen, and E. Mollestad, "DNV GL Handbook for Maritime and Offshore Battery Systems," Dec 2016.

[15] A. Nikolian, Y. Firouz, R. Gopalakrishnan, J.-M. Timmermans, N. Omar, P. van den Bossche, and J. van Mierlo, "Lithium ion batteries—development of advanced electrical equivalent circuit models for Nickel Manganese Cobalt Lithium-ion," *Energies*, vol. 9, no. 360, May 2016. [Online]. Available: https://doi.org/10.3390/en9050360

[16] W. Waag and D. Sauer, "Secondary batteries – lead– acid systems | state-of-charge/health," *Encyclopedia of Electrochemical Power Sources*, p. 793–804, 2009.

[17] DNV, "STUDY ON ELECTRICAL ENERGY STORAGE FOR SHIPS: BATTERY SYSTEMS FOR MARITIME APPLICATIONS – TECHNOLOGY, SUSTAINABILITY AND SAFETY," 2020.

[18] KoreanRegister, "Guidance for Battery Systems on Board of Ships 2022," 2022.

[19] DNV, "Rules for classification of Ships: Part 6 Additional class notations, Chapter 2 Propulsion, power generation and auxiliary systems," 2022.

[20] D. M. F. Co., "What does A-0 in fire rating mean?" 2020. [Online]. Available: https://www.deyuanmarine.com/Marine-Hydraulic-Watertight-Fire-Sliding-Door-With-Hydraulic-Operating-System-pd426434.html

[21] I. S. Seddiek, M. M. Elgohary, and N. R. Ammar, "THE HYDROGEN-FUELLED INTERNAL COMBUSTION ENGINES FOR MARINE APPLICATIONS WITH A CASE STUDY," *Study of optimum design features of marine diesel engine*, vol. 66, no. 1, Feb 2015.

[22] C. M. Kalamaras and A. M. Efstathiou, "Hydrogen production technologies: Current State and future developments," *Conference Papers in Energy*, vol. 2013, p. 1–9, Mar 2013. [Online]. Available: http://dx.doi.org/10.1155/2013/690627

[23] H. Kobayashi, A. Hayakawa, K. Somarathne, and E. Okafor, "Science and Technology of Ammonia Combustion," *Proceedings of the Combustion Institute*, vol. 37, no. 1, p. 109–133, Nov 2018. [Online]. Available: https://doi.org/10.1016/j.proci.2018.09.029

[24] DNV, "HANDBOOK FOR HYDROGEN-FUELLED VESSELS," Jun 2021.

[25] M. G. Sürer and H. T. Arat, "Advancements and current technologies on hydrogen fuel cell applications for marine vehicles," *International Journal of Hydrogen Energy*, vol. 47, no. 45, p. 19865–19875, Jan 2022. [Online]. Available: https://doi.org/10.1016/j.ijhydene.2021.12.251

[26] H. T. ARAT and M. G. SÜRER, "State of art of hydrogen usage as a fuel on aviation," *European Mechanical Science*, vol. 2, no. 1, p. 20–30, Mar 2018. [Online]. Available: https://doi.org/10.26701/ems.364286

[27] C. Raucci, J. Calleya, S. Suarez De La Fuente, and R. Pawling, "Hydrogen on board ship: a first analysis of key parameters and implications," Nov 2016.

[28] DNV, "Rules for classification of ships: Part 5 Ship types, Chapter 7 Liquefied gas tankers," 2022.

[29] ABS, "HYDROGEN AS MARINE FUEL," *SUSTAINABILITY WHITEPAPER*, 2021.

[30] IGF, "ADOPTION OF THE INTERNATIONAL CODE OF SAFETY FOR SHIPS USING GASES OR OTHER LOW-FLASHPOINT FUELS (IGF CODE)," 2015.

[31] KoreanRegister, "Guidelines for Ships Using Ammonia as Fuels," 2021.

[32] ——, "Rules and Guidances for the Classification of Ships Using Low-flashpoint Fuels," 2022.

[33] J. Nieminen, N. D'Souza, and I. Dincer, "Comparative combustion characteristics of gasoline and hydrogen fuelled ices," *International Journal of Hydrogen Energy*, vol. 35, no. 10, p. 5114–5123, Oct 2009. [Online]. Available: https://doi.org/10.1016/j.ijhydene.2009.08.098

[34] H. Homan, R. Reynolds, P. Deboer, and W. Mclean, "Hydrogen-fueled diesel engine without timed ignition," *International Journal of Hydrogen Energy*, vol. 4, no. 4, p. 315–325, 1979. [Online]. Available: https://doi.org/10.1016/0360-3199(79)90006-5

[35] M. Ikegami, K. Miwa, M. Shioji, and M. Esaki, "A study on hydrogen-fueled diesel combustion," *Bulletin of JSME*, vol. 23, no. 181, p. 1187–1193, Jun 1980. [Online]. Available: https://doi.org/10.1299/jsme1958.23.1187

[36] M. Ikegami, K. Miwa, and M. Shioji, "A study of hydrogen fuelled compression ignition engines," *International Journal of Hydrogen Energy*, vol. 7, no. 4, p. 341–353, Jun 1981. [Online]. Available: https://doi.org/10.1016/0360-3199(82)90127-6

[37] G. Gopal, B. S. Murthy, K. V. Gopalakrishnan, and P. Srinivasa Rao, "Use of hydrogen in dual-fuel engines," *International Journal of Hydrogen Energy*, vol. 7, no. 3, p. 267–272, May 1981. [Online]. Available: https://doi.org/10.1016/0360-3199(82)90090-8

[38] K. Varde and G. Frame, "Hydrogen aspiration in a direct injection type diesel engine-its effects on smoke and other engine performance parameters," *International Journal of Hydrogen Energy*, vol. 8, no. 7, p. 549–555, 1983. [Online]. Available: https://doi.org/10.1016/0360-3199(83)90007-1

[39] P. Dimitriou and T. Tsujimura, "A review of hydrogen as a compression ignition engine fuel," *International Journal of Hydrogen Energy*, vol. 42, no. 38, p. 24470–24486, Aug 2017. [Online]. Available: https://doi.org/10.1016/j.ijhydene.2017.07.232

[40] B. Zhang, H. Wang, and S. Wang, "Computational investigation of combustion, performance, and emissions of a diesel-hydrogen dual-fuel engine," *Sustainability*, vol. 15, no. 4, p. 3610, 2023. [Online]. Available: https://doi.org/10.3390/su15043610

[41] M. Cheliotis, E. Boulougouris, N. L. Trivyza, G. Theotokatos, G. Livanos, G. Mantalos, A. Stubos, E. Stamatakis, and A. Venetsanos, "Review on the safe use of ammonia fuel cells in the maritime industry," *Energies*, vol. 14, no. 11, May 2021. [Online]. Available: https://doi.org/10.3390/en14113023

[42] T. Tronstad, H. H. Astrand, G. P. Haugom, and L. Langfeldt, "STUDY ON THE USE OF FUEL CELLS IN SHIPPING," Jan 2017.

[43] PowerCell, "PowerCellution Marine System 200," 2022.

[44] SolydEra, "BLUEGEN FUEL CELL TECHNOLOGY," 2022.

[45] N. Sachdeva, "Techno-Economic feasibility analysis of Solid-Oxide Fuel Cell-Gas Turbine based hybrid propulsion system fueled by Hydrogen," Master's thesis, TU Delft, 2022. [Online]. Available: https://repository.tudelft.nl/islandora/object/uuid%3Ab82355fb-da87-4884-9c85-1e35c65266b6

[46] F. Hongjun, "IMO type C tank and FGSS solution for a retrofitted 10,000 TEU LNG-fuelled container ship," *C-LNG Solutions Pte. Ltd - Technical report*, Feb 2021. [Online]. Available: https://10.13140/RG.2.2.24463.92321

[47] DNV, "Energy transition outlook 2022: A global and regional forecast to 2050," 2022.

[48] C. H. Christensen, T. Johannessen, R. Z. Sørensen, and J. K. Nørskov, "Towards an ammonia-mediated hydrogen economy?" *Catalysis Today*, vol. 111, no. 1-2, p. 140–144, 2006. [Online]. Available: https://doi.org/10.1016/j.cattod.2005.10.011

[49] C. Zamfirescu and I. Dincer, "Using ammonia as a sustainable fuel," *Journal of Power Sources*, vol. 185, p. 459–465, Jul 2008. [Online]. Available: https://doi.org/10.1016/j.jpowsour.2008.02.097

[50] S. Ghavam, M. Vahdati, I. A. G. Wilson, and P. Styring, "Sustainable Ammonia Production Processes," Mar 2021. [Online]. Available: https://www.frontiersin.org/articles/10.3389/fenrg.2021.580808/full

[51] EngineeringToolBox, "Liquid ammonia - thermal properties at saturation pressure," 2011. [Online]. Available: https://www.engineeringtoolbox.com/ammonia-liquid-thermal-properties-d_1765.html

[52] ABS, "Ammonia as marine fuel," 2020.

[53] ——, "Requirements for Ammonia Fueled Vessels," 2021.

[54] ClassNK, "Part C "Guidelines for the Safety of Ships Using Ammonia as Fuel" of Guidelines for Ships Using Alternative Fuels," 2022.

[55] A. Boretti, "Novel dual fuel diesel-ammonia combustion system in advanced tdi engines," *International Journal of Hydrogen Energy*, vol. 42, no. 10, p. 7071–7076, Jan 2017. [Online]. Available: https://doi.org/10.1016/j.ijhydene.2016.11.208

[56] M. Comotti and S. Frigo, "Hydrogen generation system for ammonia–hydrogen fuelled internal combustion engines," *International Journal of Hydrogen Energy*, vol. 40, no. 33, p. 10673–10686, Jul 2015. [Online]. Available: https://doi.org/10.1016/j.ijhydene.2015.06.080

[57] S. Liu, Z. Lin, H. Zhang, N. Lei, Y. Qi, and Z. Wang, "Impact of ammonia addition on knock resistance and combustion performance in a gasoline engine with high compression ratio," *Energy*, vol. 262, p. 125458, Sep 2022. [Online]. Available: https://doi.org/10.1016/j.energy.2022.125458

[58] J. van Duijn, "Modelling diesel-ammonia two-stroke engines," Master's thesis, TU Delft, 2021. [Online]. Available: https://repository.tudelft.nl/islandora/object/uuid%3A2be63cac-85e7-4367-99a8-e811e3248936

[59] E. Nadimi, G. Przybyła, D. Emberson, T. Løvås, Ziółkowski, and W. Adamczyk, "Effects of using ammonia as a primary fuel on engine performance and emissions in an ammonia/biodiesel dual-fuel ci engine," *International Journal of Energy Research*, vol. 46, no. 11, p. 15347–15361, 2022. [Online]. Available: https://doi.org/10.1002/er.8235

[60] N. Lindstrand, "The case for two-stroke ammonia engines," 2022. [Online]. Available: https://www.man-es.com/discover/two-stroke-ammonia-engine

[61] Wärtsilä, "Wärtsilä coordinates eu funded project to accelerate ammonia engine development," 2022. [Online]. Available: https://www.wartsila.com/media/news/05-04-2022-wartsila-coordinates-eu-funded-project-to-accelerate-ammonia-engine-development-3079950

[62] B. Wang, C. Yang, H. Wang, D. Hu, B. Duan, and Y. Wang, "Study on injection strategy of ammonia/hydrogen dual fuel engine under different compression ratios," *Fuel*, vol. 334, p. 126666, 2023. [Online]. Available: https://doi.org/10.1016/j.fuel.2022.126666

[63] R. Nielsen, P. Han, R. M. Lopez, and J. B. Hansen, "The future of ammonia cracking," Nov 2021. [Online]. Available: https://www.ammoniaenergy.org/paper/the-future-of-ammonia-cracking/

[64] J. M. Rozendaal, "Methanol Hybrid Offshore Working Vessels A technical, environmental and economic assessment," Master's thesis, TU Delft, 2021. [Online]. Available: https://repository.tudelft.nl/islandora/object/uuid:75cbd24c-8b27-4472-a935-abde91b652a4?collection=education

[65] S. Verhelst, J. W. Turner, L. Sileghem, and J. Vancoillie, "Methanol as a fuel for internal combustion engines," *Progress in Energy and Combustion Science*, vol. 70, p. 43–88, Oct 2018. [Online]. Available: https://doi.org/10.1016/j.pecs.2018.10.001

[66] E. Connelly and B. Idini, "International shipping – analysis," Sep 2022. [Online]. Available: https://www.iea.org/reports/international-shipping

[67] L. Fernández, "Global methanol production 2022," May 2022. [Online]. Available: https://www.statista.com/statistics/1323406/methanol-production-worldwide/

[68] S. Lasselle, H. Hustad, J. Vedeler, and H. Abusdal, "Methanol as marine fuel: Environmental benefits, technology readiness, and economic feasibility," Jan 2016. [Online]. Available: https://www.methanol.org/wp-content/uploads/2020/04/IMO-Methanol-Marine-Fuel-21.01.2016.pdf

[69] K. Anderson and C. M. Salazar, "Methanol as a marine fuel report," Oct 2015.

[70] ABS, "Requirements for Methanol and Ethanol Fueled Vessels," 2022.

[71] Dierickx, J. and Beyen, J. and Block, R. and Hamrouni, M. and Huyskens, P. and Meichelböck, C. and Verhelst, S., "Strategies for introducing methanol as an alternative fuel for shipping," in *7th Transport Research Arena TRA 2018 (TRA 2018)*. Ghent University, 2018, pp. 1–10. [Online]. Available: http://dx.doi.org/10.5281/ZENODO.1456425

[72] Wartsila, "Wärtsilä 32 methanol engine," 2022. [Online]. Available: https://www.wartsila.com/marine/products/engines-and-generating-sets/wartsila-32-methanol-engine

[73] Z. Zhu, Z. Mu, Y. Wei, R. Du, and S. Liu, "Experimental evaluation of performance of heavy-duty SI pure methanol engine with EGR," *Fuel*, vol. 325, p. 124948, 2022. [Online]. Available: https://doi.org/10.1016/j.fuel.2022.124948

[74] M. R. Saxena, R. K. Maurya, and P. Mishra, "Assessment of performance, combustion and emissions characteristics of methanol-diesel dual-fuel compression ignition engine: A Review," *Journal of Traffic and Transportation Engineering (English Edition)*, vol. 8, no. 5, p. 638–680, 2021. [Online]. Available: https://doi.org/10.1016/j.jtte.2021.02.003

[75] J. Dierickx, J. Verbiest, T. Janvier, J. Peeters, L. Sileghem, and S. Verhelst, "Retrofitting a high-speed marine engine to dual-fuel methanol-diesel operation: A comparison of multiple and single point methanol Port Injection," *Fuel Communications*, vol. 7, p. 100010, 2021. [Online]. Available: https://doi.org/10.1016/j.jfueco.2021.100010

[76] N. Charisi, "Parametric Modelling Method based on Knowledge Based Engineering," Master's thesis, TU Delft, 2019. [Online]. Available: https://repository.tudelft.nl/islandora/object/uuid%3A5321df04-39e6-4128-9eec-c3adcac8a68a

[77] I.-T. Kao, "Knowledge Based Engineering (KBE) automatic layout generation framework for modular offshore wind service vessels," Master's thesis, TU Delft, 2021. [Online]. Available: https://repository.tudelft.nl/islandora/object/uuid%3A34162956-baa5-49b6-984a-719cfd5d833a

[78] D. Andrews, "THE SOPHISTICATION OF EARLY STAGE DESIGN FOR COMPLEX VESSELS," *International Journal of Maritime Engineering*, vol. 160, no. SE 18, 2018. [Online]. Available: https://10.3940/rina.ijme.2018.se.472

[79] H. M. Gaspar, "VESSEL.JS: AN OPEN SOLUTION FOR DATA-DRIVEN SHIP DESIGN," 2018. [Online]. Available: https://www.researchgate.net/publication/325361495_VESSELJS_AN_OPEN_SOLUTION_FOR_DATA-DRIVEN_SHIP_DESIGN

[80] B. J. v. Oers, *A packing approach for the early stage design of service vessels*. VSSD, 2011. [Online]. Available: https://repository.tudelft.nl/islandora/object/uuid%3A6be7582c-63b1-477e-b836-87430bcfb43f

[81] B. Lagemann and S. O. Erikstad, "Modular Conceptual Synthesis of Low-Emission Ships," *High-Performance Marine Vehicles (HIPER) 2020*, Oct 2020. [Online]. Available: https://www.researchgate.net/publication/344624959_Modular_Conceptual_Synthesis_of_Low-Emission_Ships

[82] M.-I. Roh and K.-Y. Lee, *Computational Ship Design*, 1st ed. Springer Nature Singapore, 2018.

[83] S. O. Erikstad and K. Levander, "System Based Design of Offshore Support Vessels," *IMDC12*, Jan 2012. [Online]. Available: https://www.researchgate.net/publication/276958126_System_Based_Design_of_Offshore_Support_Vessels

[84] H. M. Gaspar, "Data-Driven Ship Design," 2018. [Online]. Available: http://www.shiplab.hials.org/wpcontent/uploads/2019/05/40_Gaspar.pdf

[85] S. Josip, N. Wognum, and J. W. Verhagen, *Concurrent engineering in the 21st Century foundations, developments and challenges*. Springer International Publishing, 2015.

[86] G. La Rocca and M. van Tooren, "A Modular Reconfigurable Software Modelling Tool to Support Distributed Multidisciplinary Design and Optimisation of Complex Products," 2010. [Online]. Available: https://www.researchgate.net/publication/228866963_A_Modular_Reconfigurable_Software_Modelling_Tool_to_Support_Distributed_Multidisciplinary_Design_and_Optimisation_of_Complex_Products

[87] G. La Rocca, "Knowledge Based Engineering Techniques to Support Aircraft Design and Optimization," Ph.D. dissertation, TU Delft, 2011. [Online]. Available: https://repository.tudelft.nl/islandora/object/uuid%3A45ed17b3-4743-4adc-bd65-65dd203e4a09?collection=research

[88] D. J. Andrews, "A Creative Approach To Ship Architecture," *The International Journal of Maritime Engineering*, vol. 145, no. a3, 2003. [Online]. Available: https://10.3940/rina.ijme.2003.a3.9031

[89] B. He, Y. Wang, W. Song, and W. Tang, "Design Resource Management for Virtual Prototyping in product collaborative design," *Proceedings of the Institution of Mechanical Engineers, Part B: Journal of Engineering Manufacture*, vol. 229, no. 12, p. 2284–2300, Oct 2014. [Online]. Available: https://doi.org/10.1177/0954405414551106

[90] M. A. Schilling, "Toward a general modular systems theory and its application to Interfirm product modularity," *Academy of Management Review*, vol. 25, no. 2, p. 312–334, 2000. [Online]. Available: https://10.5465/amr.2000.3312918

[91] M. Choi and S. O. Erikstad, "A module configuration and valuation model for operational flexibility in ship design using contract scenarios," *Ships and Offshore Structures*, vol. 12, no. 8, p. 1127–1135, 2017. [Online]. Available: https://10.1080/17445302.2017.1316559

[92] F. Salvador, C. Forza, and M. Rungtusanatham, "Modularity, product variety, production volume, and component sourcing: Theorizing beyond generic prescriptions," *Journal of Operations Management*, vol. 20, no. 5, p. 549–575, Mar 2002. [Online]. Available: https://10.1016/s0272-6963(02)00027-x

[93] G. Pahl, W. Beitz, and J. Feldhusen, *Engineering design: A systematic approach*. Springer, 2014.

[94] G. Esdras and S. Liscouet-Hanke, "Development of Core Functions for Aircraft Conceptual Design: Methodology and Results," *Canadian Aeronautics and Space Institute AERO 2015 Conference*, May 2015. [Online]. Available: https://www.researchgate.net/publication/277021129_Development_of_Core_Functions_for_Aircraft_Conceptual_Design_Methodology_and_Results/citations

[95] C. J. McKinlay, S. R. Turnock, and D. A. Hudson, "A Comparison of Hydrogen and Ammonia for Future Long Distance Shipping Fuels," 2020.

[96] J. Holtrop and G. Mennen, "AN APPROXIMATE POWER PREDICTION METHOD," 1982.

[97] H. Rashidul, "IMPLEMENTATION OF ENERGY EFFICIENCY DESIGN INDEX & ITS IMPACT ON THE DESIGN OF OIL TANKER," *International Conference on the Influence of EEDI on Ship Design*, Sep 2014. [Online]. Available: https://www.researchgate.net/publication/339974671_IMPLEMENTATION_OF_ENERGY_EFFICIENCY_DESIGN_INDEX_ITS_IMPACT_ON_THE_DESIGN_OF_OIL_TANKER

[98] A. F. Molland, *Chapter 9 - Ship design, construction and operation*. Butterworth-Heinemann, 2008, p. 638–727.

[99] K. Pedersen, J. Emblemsvåg, R. Bailey, J. K. Allen, and F. Mistree, "Validating design methods and research: The validation square," *Volume 4: 12th International Conference on Design Theory and Methodology*, 2000. [Online]. Available: https://doi.org/10.1115/detc2000/dtm-14579

[100] S. Speares and R. Grisbrook, "Siginificant Ships of 2016," *Significant Ships of 2016*, 2016.

[101] E. Scherpenhuijsen Ro, "Iron Powder as a fuel on Service Vessels," Master's thesis, TU Delft, 2023. [Online]. Available: https://repository.tudelft.nl/islandora/object/uuid%3A2e46edbd-7a41-4841-a341-1a069b65d48f

[102] W. N. Association, "Carbon Dioxide Emissions From Electricity," Oct 2022. [Online]. Available: https://www.world-nuclear.org/information-library/energy-and-the-environment/carbon-dioxide-emissions-from-electricity.aspx

[103] O. W. in Data, "Per capita electricity generation by source, 2021," 2021. [Online]. Available: https://ourworldindata.org/grapher/per-capita-electricity-source-stacked?country=OWID_WRL~CHN~IND~USA~JPN~DEU~GBR~BRA~FRA~CAN~SWE~ZAF

[104] B. Jeong, H. Jang, W. Lee, C. Park, S. Ha, D. K. Kim, and N.-K. Cho, "Is electric battery propulsion for ships truly the lifecycle energy solution for Marine Environmental Protection as a whole?" *Journal of Cleaner Production*, vol. 355, Apr 2022. [Online]. Available: https://doi.org/10.1016/j.jclepro.2022.131756

[105] A. B. of Shipping, "Guidance notes on: Strength assessment of independent type c tanks," Jan 2022.

[106] R. Halfhide, J. Stewart, and N. Stuart, "Siginificant Ships of 2018," *Significant Ships of 2018*, 2018.

[107] R. Halfhide, S. Collingwood, M. Latarche, and N. Stuart, "Siginificant Ships of 2019," *Significant Ships of 2019*, 2019.

[108] R. Halfhide, J. Stewart, and N. Stuart, "Siginificant Ships of 2017," *Significant Ships of 2017*, 2017.